Dissertation

submitted to the

Combined Faculties for the Natural Sciences and for Mathematics

of the Ruperto-Carola University of Heidelberg, Germany

for the degree of

Doctor of Natural Sciences

presented by

Diplom Biologist Tiago Ferreira

born in Porto, Portugal

Oral-examination:

Serotonin 1A receptor functions during development to refine the dendritic arbor of principal hippocampal neurons

Referees: Prof. Dr. Walter Witke
Prof. Dr. Thomas W. Holstein

À tia Lina, à mãe Laura,
ao pai Manuel e às manas...
... por tudo

Abstract

Mice lacking the serotonin receptor 1A (Htr1a) display increased anxiety behavior, a phenotype that depends on the expression of the receptor in the forebrain during the third through fifth postnatal weeks. Within the forebrain, Htr1a is prominently expressed in the soma and dendrites of CA1 pyramidal neurons of the hippocampus that during this period undergo rapid synapse formation and dendritic growth. Consistent with a possible role of Htr1a in synaptic maturation, CA1 pyramidal neurons in the Htr1a knockout mice show increased ramification of oblique dendrites and increased excitability to Schaffer collateral inputs. These findings suggest that Htr1a may shape hippocampal circuits by directly modulating dendritic growth.

The experiments here described show that *in vivo* pharmacological blockade of the receptor during the third through fifth postnatal weeks is sufficient to reproduce the increased branching of oblique dendrites seen in Htr1a knockout mice. Using dissociated hippocampal cultures we demonstrate that serotonin functions through Htr1a to attenuate the motility of dendritic growth cones and reduce their content of filamentous actin.

All together, these findings suggest that serotonin modulates actin cytoskeletal dynamics in hippocampal neurons during a limited developmental period to restrict dendritic growth and achieve a long-term adjustment of synaptic inputs.

Zusammenfassung

Mäuse, denen der Serotoninrezeptor 1A (Htr1a) fehlt, zeigen erhöhtes Angstverhalten, ein Phänotyp, der von der Expression des Rezeptors im Vorderhirn während der dritten bis fünften Woche nach der Geburt abhängt. Innerhalb des Vorderhirns ist Htr1a stark in den Somata und Dendriten der CA1 Pyramidalneuronen des Hippocampus exprimiert, die in dieser Periode schnelle Synapsenbildung und Dendritenwachstum durchmachen. Übereinstimmend mit einer möglichen Rolle von Htr1a im Reifungsprozess von Synapsen zeigen CA1 Pyramidalneuronen in den Htr1a Knockoutmäusen verstärkte Verzweigung apikaler somanaher Dendriten und erhöhte Erregbarkeit durch Inputs über die Schaffer-Kollaterale. Diese Ergebnisse weisen darauf hin, dass Htr1a Hippocampus-Schaltkreise formen könnte indem es direkt das Dendritenwachstum moduliert.

In dieser Studie zeigen wir, dass pharmakologische *in vivo* Blockade des Htr1a Rezeptors während der dritten bis fünften Woche nach der Geburt ausreicht, um die verstärkte Verzweigung apikaler somanaher Dendriten, die in Htr1a Knockoutmäusen gesehen worden war, zu reproduzieren. Durch Verwendung dissoziierter Hippocampus-Kulturen zeigen wir, dass Serotonin über Htr1a wirkt, um die Bewegungsfähigkeit dendritischer Wachstumskegel zu vermindern und deren Gehalt an filamentösem Aktin zu reduzieren.

Diese Ergebnisse weisen darauf hin, dass Serotonin die Dynamik des Aktinzytoskeletts in Hippocampusneuronen während einer begrenzten Entwicklungsperiode moduliert, um das Dendritenwachstum einzuschränken und eine Langzeitanpassung synaptischer Inputs zu erreichen.

Acknowledgments

I would like to thank my supervisor Dr. Cornelius Gross for careful design and revision of these experiments and the Portuguese Foundation for Science and Technology for financial support of this work.

I would like to thank all members of the Gross laboratory, specially: Luisa Lo Iacono for sharing EM data and help with osmotic minipumps implantation; Amaicha Depino with whom I performed cd3ζ^{KO}/β2-m^{KO} behavioral experiments and with whom I set up tissue culture protocols; Valeria Carola, co-responsible of the behavioral analysis of HDAC4^{KO} mice – her help and expertise were critical for this experiment; Enrica Audero, main author of the Camk2a-GluClαβ project, for permanent assistance; Olivier Mirabeau for crucial advices on motility analysis; Theodoros Tsetsenis for setting up fear conditioning protocols; Rosa Paolicelli to whom I owe several hours of manual time-lapse videotracking and Olga Ermakova for ES cells protocols.

I am extremely grateful to Prof. Walter Witke for his generosity and proficient guidance. This work would not have be possible without his valuable suggestions. My gratitude is extended to Giancarlo Bellenchi, Pietro Pilo Boyl, Friederike Jönsson, Marco Rust and Christine Gurniak, past members of the Witke laboratory at the EMBL.

A very special thank you to Prof. Jean-Pierre Hornung and Dr. Carsten Schultz for sharing their unpublished work, to Dr. Emilio Hirsch for providing the Dbl^{KO} mice and Dr. Joshua Sanes/Dr. Thomas Deller for providing the Thy1-GFP-M mice.

I thank Prof. Dusan Bartsch and Dr. Andreas Ladurner, my thesis advisories, for their care and suggestions and Professor Holstein for accepting the chairmanship of this thesis Defense Committee.

In addition I would like to acknowledge: Alen Piljič (FRET protocols involving CY-CamK2a); Dr. Wenbiao Gan and Katie Helmin at NYU (diOlistics troubleshooting); Daniel Bilbao (help with FACS genotyping); Friederike Jönsson and Valeria Berno (help with Axiovert's maintenance); Teresa Ciotti (tissue culture troubleshooting); Laura Maggi, Davide Ragozzino and Mario Barbieri (intra-cellular biotin fillings); Emerald Perlas (β-gal stainings); Sylvia Badurek (german translations); EMBL's transgenic facility (Jakki Kelly-Barrett for blastocyst injections, Simone Santanelli and Francesca Zonfrillo for aminal care) as well as all the colleagues at the EMBL–Heidelberg, EMBL–Monterotondo and CNR—IBC.

Finally, I want to mention my family and closed friends that in a not-so-obvious manner did contribute to this thesis.

Table of Contents

List of Figures

List of Tables

List of Abbreviations, Acronyms and Symbols

5–HT ..... serotonin (5-hydroxytryptamine);

8-OH–DPAT ... 8-hydroxy-2-(di-n-propylamino)tetralin;

L ..... liter;

lx ..... lux;

ACh ..... Acetylcholine;

AChRs ..... acetylcholine receptors;

ACTH ..... adrenocorticotropic hormone;

AMPA ..... α-amino-3-hydroxy-5-methyl-4-isoxazolepropionic acid;

ANOVA ..... analysis of variance;

bp ..... base pair;

BSA ..... bovine serum albumine;

CA1–3 ..... *Cornu Ammonis* areas 1–3;

CaMKII ..... Ca^{2+}/calmodulin-dependent protein kinase II ;

cAMP ..... cyclic adenosine monophosphate;

cDNA ..... complementary DNA;

CMTMR ..... CellTracker™ Orange-fluorescent tetramethylrhodamine;

CNS ..... central nervous system;

Cre ..... Cre recombinase;

CREB ..... cAMP response element binding;

DAG ..... diacilglycerol;

DAPI ..... 2-(4-amidinophenyl)-1H-indole-6-carboxamidine;

°C ..... degree Celsius;

DG ..... dentate gyrus;

DIC ..... differential interference contrast;

DiI ..... Ditetradecylindocarbocyanine, $DiIC_{18}(3)$;

DiO ..... 3,3'-dipropyloxadi-carbocyanine, $DiOC_{18}(3)$;

DIV ..... days *in vitro*;

DNA ..... deoxyribonucleic acid;

dNTP ..... deoxyribonucleotide triphosphate;

E ..... embryonic day;

EC ..... entorhinal cortex;

EDTA ..... 2-[2-(bis(carboxymethyl)amino)ethyl-(carboxymethyl)amino]acetic acid;

EGTA ..... glycol-bis(2-aminoethylether)-N,N,N',N'-tetraacetic acid;

EPSPs ..... evoked excitatory postsynaptic potentials;

ER ..... endoplasmic reticulum;

Erk ..... extracellular signal-regulated kinase;

F ..... phenylalanine;

F-Actin ..... filamentous actin;

FBS ..... fetal bovine serum;

FITC ..... fluorescein isothiocyanate;

fMRI ..... functional magnetic resonance imaging;

fpm ..... frames per minute;

FRET ..... Förster (also fluorescence) resonance energy transfer;

G-actin ..... globular actin;

G-proteins ..... guanine nucleotide binding proteins;

GABA ..... γ-aminobutyric acid;

GDP ..... guanosine diphosphate;

GEF ..... GDP–GTP exchange factor;

GFAP ..... glial fibrillary acidic protein;

GFP ..... green fluorecent protein;

GIRK ..... G protein inward-rectifying K^+ channel (Kir);

GTP ..... guanosine triphosphate;

h ..... hour;

halothane 2-bromo-2-chloro-1,1,1-trifluoro-ethane;

HBSS ..... Hanks' buffered salt solution;

HEPES ..... 4-(2-hydroxyethyl)-1-piperazineethanesulfonic acid;

het ..... heterozygous;

HPA ..... hypothalamic–pituitary–adrenal;

Htr1a ..... serotonin 1A receptor;

Htr1b ..... serotonin 1B receptor;;

Htr2a ..... serotonin 2A receptor;

Hz ..... hertz;

IGEPAL ..... tert-Octylphenoxy poly(oxyethylene)ethanol;

IP3 ..... inositol triphosphate;

KIF17 ..... kinesin superfamily member 17;

KO ..... knockout;

LGN ..... lateral geniculate nucleus;

lpm ..... liter per minute;

LTD ..... long term depression;

LTP ..... long term potentiation;

M ..... Molar;

m ..... meter;

Map2 ..... microtubule associated protein 2;

MAPK ..... mitogen-activated protein kinase;

$\tilde{x}$ ..... median;

MEM ..... Eagle's minimum essential medium;

MHC ..... major histocompatibility complex;

min ..... minute;

mRNA ..... messenger RNA;

N ..... Normal;

NA ..... numerical aperture;

NAN-190 ..... 1-(2methoxyphenyl)-4-[4-(2phthalimido]-butyl]piperazine;

NF-KB ..... nuclear factor κ-light-chain-enhancer of activated B cells;

NFAT ..... nuclear factor of activated T cells;

NMDA ..... N-methyl-D-aspartic acid;

OCD ..... obsessive-compulsive disorder;

Oprm1 ..... opioid receptor, μ1;

P ..... postnatal day;

PAK ..... p21 activated kinase;

PBS ..... phosphate buffered saline;

PCA ..... parachloroamphetamine;

PCR ..... polymerase chain reaction;

PDB ..... p21 binding domain;

PET ..... polyethylene terephthalate;

PFA ..... (para)formaldehyde;

PFC ..... prefrontal coretx;

PH ..... pleckstrin homology;

PHEM ..... PIPES, HEPES, EGTA, $MgCl_2$;

PI3Ks ..... class I phosphoinositide 3-kinases;

PIPES ..... 1,4-piperazinediethanesulfonic acid;

PKA ..... protein kinase A;

PKC ..... protein kinase C;

PLC ..... phospholipase C ;

psi ..... pound-force per square inch;

PTSD ..... post-traumatic stress disorder;

PVP ..... polyvinylpyrrolidone;

ROI ..... region of interest;

rpm ..... revolutions per minute;

RT ..... room temperature;

SAP-1 ..... serum response factor accessory protein 1;

sc. ..... subcutaneous;

SD ..... standard deviation;

SEM ..... standard error of the mean;

SDS ..... Sodium dodecyl sulfate;

SDS-PAGE ..... SDS polyacrylamide gel electrophoresis;

Ser ..... Serine;

SSRIs ..... selective serotonin reuptake inhibitors;

SYK ..... spleen tyrosine kinase;

TBS ..... tris buffer saline;

TCR ..... T cell receptor;

Tefzel ..... ethylene tetrafluoroethylene (ETFE);

Thr ..... Threonine;

TIRF ..... total internal reflection fluorescence;

Tph ..... tryptophan hydroxylase;

Tris 2-amino-2-hydroxymethyl-propane-1,3-diol;

TTX ..... tetrodotoxin;

Tween 20 ..... 4-bis(2-hydroxyethoxy)oxolan-2-yl]-2-(2-hydroxyethoxy)ethoxy]ethyl dodecanoate;

TX-100 ..... 2-[4-(2,4,4-trimethylpentan-2-yl)phenoxy]ethanol;

U ..... unit;

V ..... volt;

VBA ..... Visual Basic for Applications;

WAY100635 .... N-[2-[4-(2-methoxyphenyl)-1-piperazinyl]ethyl]-N-(2-pyridyl)cyclohexanecarboxamide trihydrochloride;

WT ..... wild type;

XFP ..... GFP or any of its spectral variants;

Y ..... tyrosine;

ZAP70 ..... ζ-chain-associated protein kinase 70.

Aim and Foreword

The aim of this thesis was to assess the developmental role of Htr1a in the dendritic remodeling of hippocampal circuitry. This dissertation is divided as follows:

Chapter 1 Provides a short overview on the contribution of the serotonergic system and hippocampal circuitry to anxiety-related behaviors. Secondly, it summarizes what is know about the regulation of dendritic morphology by serotonin and the serotonin receptor 1A.

Chapter 2 Describes how pharmacological blockade of Htr1a during the third through fifth postnatal weeks is sufficient to reproduce the increased branching of oblique dendrites seen in knockout mice. It also explains how serotonin functions through Htr1a to attenuate the motility of dendritic growth cones and reduce their content of filamentous actin in dissociated hippocampal cultures.

Chapter 3 Discusses the above findings, concluding that serotonin may regulate cytoskeletal dynamics in hippocampal neurons during a short developmental time-window to restrict dendritic growth, and speculating on how Htr1a may control the synaptic circuitry of the hippocampal formation.

Appendices The last part of this thesis is subdivided in four chapters. The first describes a histological approach for single-cell resolution staining in the nervous system. The second and third chapters describe preliminary experiments carried out to assess the contribution of other molecular/cellular substrates involved in the regulation of innate anxiety-related behaviors. Finally, the last chapter concludes by detailing protocols and tools developed during this thesis preparation.

Chapter 1

Introduction

Serotonin (5-hydroxytryptamine, 5–HT) is a monamine neurotransmitter synthesized from the essential amino acid tryptophan by means of tryptophan hydroxylase, Tph. In mammals, two Tph genes have been identified, *Tph1*, expressed outside the central nervous system (CNS) and *Tph2*, expressed in a subset of neurons of the midbrain: the serotonergic neurons of the raphe nuclei, the exclusive producers of serotonin in the brain [85, 184]. Serotonergic neurons are generated early in development (second embryonic week in the mouse) and extend exuberant axonal projections to the majority of neurons in the brain where they regulate, through 5–HT release, a wide range of behaviors (i.e., anxiety and fear, aggression, feeding, locomotion, thermoregulation and sleep [rev. in 4, 72]).

Fourteen serotonin receptors have been identified in the mammalian brain, all of them encoded by distinct genes. With the exception of 5–HT-gated ion channel 5–HT3 receptors (5–HT_{3A} and 5–HT_{3B}, cation channels with relatively high permeability to NA^{+} and K^{+} and low permeability to Ca^{2+} [222]), all serotonin receptors are G-protein-coupled receptors (GPCRs) as they couple to and transduce signals via guanine nucleotide binding proteins (G-proteins) [rev. in 72]. These receptors can be clustered into four sub-types according to their second messenger coupling pathways: 1) the 5–HT type 1 receptors (5–HT_{1A}, 5–$HT_{1B–1C}$ and 5–$HT_{1D–1F}$) which are coupled to G_i proteins; 2) the 5–HT type 2 receptors (5–$HT_{2A–2C}$), which are coupled to G_q proteins and 3) the 5–HT type 4–7 which are coupled to G_s proteins (5–HT_4, 5–$HT_{5A–5B}$, 5–HT_6 and 5–HT_7). Among theses, the 5–HT_{1A} receptor (Htr1a) has been prominently associated with mood and anxiety-related disorders.

1.1 Htr1a And Anxiety Regulation

Htr1a has been strongly implicated in the regulation of anxiety. First, buspirone, an anxiolytic used clinically, is a partial agonist of Htr1a. Second, a deficit in Htr1a binding has been associated with panic disorder [151]. Third, association studies have correlated a functional polymorphism in Htr1a's promoter with both anxiety and depression [44, 114, 202]. Fourth, selective serotonin re-uptake inhibitors (SSRIs), a class of antidepressant drugs that also have anxiolytic properties, seem to achieve their anxiolytic effect, at least partially, via postsynaptic Htr1a receptors [183]. Finally, genetic and pharmacological inactivation of Htr1a leads to mice with increased anxiety-like behavior [83, 91, 94, 158, 170, 207].

Behavioral Phenotype Of *Htr1a*$^{\mathrm{KO}}$ Mice

In 1998 three laboratories independently reported the generation of mice lacking Htr1a receptors [91, 158, 170]. Even if bred into different genetic backgrounds all lines displayed increased avoidance in spacial conflict tests, a pharmacologically–validated hallmark of rodent anxiety-like behavior [rev. in 58, 168]. In detail, Htr1a knockout mice spent less time in the aversive center of an open field arena, avoided the unprotected areas of an elevated plus or zero maze, exhibited higher latency to feed in the novelty-suppressed feeding test and explored less frequently the lit part of a light/dark box [83, 91, 107, 158, 170]. Importantly, altered arousal (increased heart rate and body temperature in response to mild stressors) has also been reported in *Htr1a*$^{\mathrm{null}}$ mice [160] as well as enhanced fear conditioning to ambiguous conditioned stimuli, a distinctive feature of human anxiety [207].

At least in one genetic background (129S6/SvEvTac) the anxiety-like phenotype of *Htr1a*$^{\mathrm{KO}}$ mice is also resistant to pharmacological treatment with anxiolytic drugs such SSRIs, compounds that block the re-uptake of 5–HT from the synaptic cleft, increasing the power of serotonergic neurotransmission [183]. In addition, chronic treatment with SSRIs, including fluoxetine, can increase neurogenesis in the dentate gyrus of adult animals [132, 183] but not in *Htr1a*$^{\mathrm{KO}}$ mice, suggesting that Htr1a receptors are required for fluoxetine-induced neurogenesis [183].

On the other hand, *Htr1a*$^{\mathrm{KO}}$ mice from a Swiss-Webster genetic background (but not 129/Sv or C57BL/6) were also unresponsive to treatment with the benzodiazepine diazepam [161, 195]. Benzodiazepines agonize $\mathrm{GABA_A}$ receptors and augment the inhibitory actions of GABA (see Chapter C) which suggested background-dependent perturbations in the GABAergic system of these mice. Indeed, reductions

in $GABA_A$ receptor expression is exclusive to knockout mice from a Swiss-Webster background [30, 195] suggesting that GABAergic deregulation is not a prerequisite for the behavioral phenotype of *Htr1a*^{KO} mice.

1.2 Physiological Consequences Of Htr1a Activation

In general, the electrophysiologic effects of 5–HT correspond well to the G-protein and second messenger coupling of the various receptor subtypes. For example. while all members of the G_i/G_o-coupled 5–HT1 receptor family tend to mediate inhibitory effects on neuronal firing, the G_q-coupled 5–HT2 family of receptors generally mediates slow excitatory effects. The ionic basis for Htr1a-mediated inhibition is mediated by its coupling to G protein inward-rectifying K^+ channels (GIRKs) that results in membrane hyperpolarization and decreased neuronal excitability [128].

Htr1a Expression

The serotonin 1A receptor was one of the first G protein-coupled receptors to be cloned [3]. This gene is intronless, and its mRNA is expressed mainly in the brain, spleen, and neonatal kidney [109]. In the brain, the highest density of Htr1a binding sites is found in the midbrain raphe nuclei (autoreceptors) and in several cortical and limbic forebrain regions (heteroreceptors), with the highest levels in the hippocampal CA1 field, dentate gyrus and entorhinal cortex [83]. In the forebrain Htr1a is first detected at embryonic day 17 (E17), after which expression gradually increase to near adult levels around postnatal day 21 (P21) [83]. Immunohistochemical studies have shown that Htr1a is localized to the somatodendritic compartment of pyramidal neurons in the hippocampus and cortex as well as granular cells of the dentate gyrus with no particular enrichment at synaptic sites [177].

Activation Of Autoreceptors In The Raphe Nuclei

Serotoninergic neurons of the raphe nuclei are inhibited by the local microiontophoretic application of 5–HT to their cell body region, and effect mediated by Htr1a [162]. Htr1a kockout animals display decreased serotonin autoinhibition and increased firing of serotonergic neurons. Recently, extracellular single-unit recordings have confirmed increased serotonin autoinhibition in mice overexpressing the Htra specifically in the raphe nuclei [10]. Indeed, *in vivo* electrophysiological recordings have shown that Htr1a autoreceptors along with $5–HT_B$ terminal autoreceptors

are responsible for serotonergic feedback inhibition, exerting a tonic inhibitory influence on serotonergic firing [63, 86].

Htr1a Activation In The Hippocampus

Similar 5–HT induced inhibition is obtained via Htr1a in intracellular recordings of both CA1 and CA3 pyramidal cells of the hippocampus [154, 191]. Relatively high concentrations of 5–HT cause a reduction in electrically evoked excitatory postsynaptic potentials (EPSPs) in CA1 pyramidal cells [189], an effect that is mimicked by the specific Htr1a agonist 8-OH–DPAT. In addition to this direct effect on pyramidal cells, it is thought that 5–HT can depress both excitatory and inhibitory synaptic potentials in the hippocampus. Htr1a-mediated inhibitory effect on putative inhibitory interneurons of the hippocampus have been described [188, 190]. Functionally, the Htr1a-mediated inhibition of GABAergic interneurons in the hippocampus would lead to disinhibition of pyramidal cells in CA1 which illustrates how the effects of 5–HT release in the hippocampus can be complex, involving both presynaptic and postsynaptic actions that may be, to varying degrees, inhibitory or disinhibitory [rev. in 46].

Transient Postnatal Expression Of Htr1a In The Forebrain Is Critical To Establish Normal Anxiety-Related Behavior In Adulthood

By means of a conditional rescue strategy that allowed restoration of the expression of Htr1a in knockout mice in a tissue-specific and reversible manner, it was demonstrated that Htr1a has a critical role in the regulation of anxiety during early postnatal development, but not in adulthood [83]. This study brought two major findings. First, postsynaptic expression of the receptor in the forebrain is sufficient to restore normal levels of anxiety-related behavior of knockout animals. Second, the absence of the receptor in the forebrain during postnatal development, but not in the adulthood, is sufficient to increased anxiety-related behaviors in the adult mouse. Together, these findings suggest that the anxiety-like phenotype of *Htr1a*$^{\mathrm{KO}}$ mice is correlated with developmental deficits and defects during the maturation of neuronal circuits in the forebrain.

1.3 Signal Transduction Pathways Activated By Htr1a

Htr1a is a $G_{i/o}$ protein-coupled receptor[1]. Heterotrimeric G proteins are compose of a GTPase α subunit and a $\beta\gamma$ dimer, and their function as molecular switches depends on the ability of the G protein α-subunit (G_α) to cycle between an inactive GDP-bound conformation that is primed for interaction with an activated receptor, and an active GTP-bound conformation that modulates the activity of downstream effector proteins [rev. in 155]. The $G_{i/o}$ family of G proteins is composed of α_i/α_o subunits and Htr1a–$G_{i/o}$ coupling has been implicated in the regulation of adenylyl cyclase while the primary Htr1a–$G_{\beta\gamma}$ coupling is linked to the activation of GIRK channels.

Inhibition Of Adenylyl Cyclase

By means of the G_α coupling, the best described function of Htr1a receptors is the inhibition of adenylyl cyclase, resulting in a reduction in cyclic AMP (cAMP) levels. This function has been reported in purified hippocampal, striatal and cortical neurons in primary cultures [48, 209] and in several neuronal and non-neuronal cell lines [rev. in 174]. Although the list of downstream signal transduction pathways triggered by the inhibition of cAMP synthesis is quite extensive, only a few have been confirmed in neuronal systems.

A well-described pathway results in the physiological inhibition of glutamatergic signaling via downregulation of Ca^{2+}/calmodulin-dependent protein kinase II (CaMKII) activity, and downregulation of both AMPA and NMDA glutamate receptor functionality. In cultured pyramidal neurons of prefrontal cortex (PFC), activation of Htr1a and the subsequent inhibition of cAMP is able to reduce the amplitude of AMPA-evoked currents, an effect mediated by the inhibition of CaMKII. Thus, Htr1a activation by deregulating the cAMP-PKA pathway, reduces CaMKII autophosphorylation at Thr286 resulting in a reduced phosphorylation at Ser831 of the GluR1 subunit of AMPA receptors [35]. Indeed, in rat hippocampus, the specific Htr1a antagonist WAY100635 produces a rapid increase in phosphorylated CaMKII and PKA enzyme activity. This increase is followed a few hours later by an enhanced membrane expression of AMPA receptor subunits, especially of the GluR1 subunit phosphorylated at the CaMKII site, pGluR1(Ser831) [186]. Recently, CaMKII has been implicated as an *in vivo* downstream effector of Htr1a

[1]Numerous expression systems have shown remarkable consistency in the ability of HTr1a to bind to G proteins of this class with a consensus rank order of $G_{i\alpha3} > G_{i\alpha2} \geq G_{i\alpha1} \geq G_{o\alpha} > G_{z\alpha}$ [rev. in 174, 175]

[94]. In this study, increased levels of phosphorylated αCaMKII were found in the CA1 region of young *Htr1a*^{KO} mice under anxiety-provoking conditions, but not in adult knockout animals, suggesting that postnatal modulation of CaMKII function contributes to the developmental programming of anxiety-related behaviors.

Activation Of GIRK Channels

By means of $G_{\beta\gamma}$ subunits, Htr1a receptors can reduce neuronal excitability by hyperpolarizing the cell membrane by activating GIRK channels, a pathway shared with $GABA_B$, adenosine A1 and Oprm1 receptors [20, 128, 142]. It is thought that native GIRK channels consist of tetramers containing at least two different subunits and four mammalian GIRK channel subunits have been cloned [rev. in 128]. GIRK1–3 (Kir1–3) are expressed in high levels by CA1 and CA3 pyramidal cells as well as by dentate granule cells. Mice lacking the GIRK2 protein [196] (which also show a marked posttranscriptional and probably posttranslational down-regulation of the GIRK1 protein) exhibit spontaneous seizure activity, suggesting impaired inhibition, but otherwise appear normal [196]. As expected, the outward currents evoked by agonists for $GABA_B$, adenosine A1 and Htr1a receptors were essentially absent in mutant mice [128].

In addition to GIRK activation, Htr1a coupled $G_{\beta\gamma}$ subunits can activate phospholipase C (PLC), resulting in the generation of inositol triphosphate (IP3), which regulates intracellular calcium release and diacilglycerol (DAG) which activates protein kinase C (PKC). Htr1a-dependent PLC activation has been extensively demonstrated, but the mechanism seems to be highly cell-type specific [rev. in 174, 175]. Class I phosphoinositide 3-kinases β and γ (PI3Kβ–γ), that are required for axon formation, can be activated by $G_{\beta\gamma}$ and Ras [rev in 144]. Upon activation, PI3Ks produce membrane-bound PI(3,4)P2 and PI(3,4,5)P3. Subsequently, proteins with a pleckstrin homology (PH) domain can bind to these phosphoinositides. Htr1a-mediated signaling through $G_{\beta\gamma}$ has also been linked to transcriptional regulation pathways by activation of Erks and NF-KB [rev. in 174].

1.4 Hippocampal Regulation Of Anxiety-Related Behaviors

The hippocampus has a long-established role in memory formation. However, the hippocampal formation (along with other limbic structures) has also been implicated in the regulation of anxiety, fear and stress. The 'septo-temporal' theory was

the first solid proposal to include the hippocampus in the regulation of emotions, proposing the hippocampus as a core component of the brain behavioral inhibition system. Specifically, it states that the the hippocampal theta rhythm ($\approx 7\,\mathrm{Hz}$) may be have a mediator role in the inhibition of behaviors that lead to punishment or frustrating non-rewards [80, rev. in 9].

Human Studies

In humans, pathological anxiety is characterized by an exaggerated response to a perceived threat or by a bias to interpret ambiguous situations as threatening [8]. It can be classified into six disorders (DSM–IV categories, [8]): generalized anxiety disorder, social phobia, simple phobia, panic disorder, post-traumatic stress disorder (PTSD) and obsessive–compulsive disorder (OCD). Since a common repertoire of pharmacological treatments is shared by the six, it is thought that these disorders underlie similar physiological mechanisms [rev. in 81]. Apart from structures of the frontal cortex, functional MRI (fMRI) studies have consistently involved the amygdala and the hippocampal formation (two limbic structures of the medial temporal lobe) in responses to anxiety-related stimuli. First, conditioning paradigms have shown altered hemodynamic activity in the amygdala and the hippocampus in patients with social anxiety disorder when compared to healthy controls [rev. in 143]. Secondly, comparison studies between twins that developed PTSD after combat experience and their siblings that remained at home. suggested that smaller hippocampal volume increases the susceptibility to the disorder [27, 74]. In addition, other neurochemical studies have associated decreases in benzodiazepine receptors in the hippocampal formation in panic disorders [28].

Lesion Studies

Among all the behavioral effects of hippocampal lesions, the amnestic ones are without doubt the most robust [rev. in 1]. Nevertheless hippocampal lesions also result in behavioral disinhibition and reduced anxiety, a contradiction that specific cytotoxic deletions of hippocampal subregions have tried to clarify. Several studies have provided data supporting a functional subdivision of the hipocampus along its septo-temporal axis: the dorsal region, preferentially involved in spatial learning an memory and the ventral hippocampus, preferentially involved in the regulation of anxiety-related behaviors [rev. in 13]. Indeed, several studies attribute anxiolytic effects to ventral (temporal) hippocampal lesions, e.g.: 1) rats with ventral hippocampal lesions are less fearful on the elevated plus maze but display normal

contextual fear conditioning [105]; 2) ventral lesions cause animals to freeze less to unsignaled foot-shock as well as hyponeophagia (reduced fear of novel foods) [12]; 3) ventral lesions increase social interactions and increase preference for the anxiogenic sections of modified versions of the elevated plus maze [12, rev. in 13]. On the other hand, sham operated controls and animals with dorsal hippocampal lesions display little, if any, increased anxiety-related behaviors [105]. Nevertheless, the reciprocal idea that ventral hippocampus is not involved in spatial learning may be an overstatement. For e.g., rats with only 30% of the ventral hippocampus could learn just as effectively as control rats in the Morris water maze when the reference memory training protocol was changed to one involving fewer trials with longer spacing intervals, suggesting that the temporal hippocampus can indeed support spatial learning as long as the training protocol is adequate [47].

Regional Dissociations Within The Hippocampus

The ventral (temporal) hippocampal subregion differs markedly from the dorsal (septal) in its anatomical connections. It projects to the prefrontal cortex, whereas the dorsal hippocampus does not and is intimately connected with subcortical structures such as the amygdala and areas that contribute to the hypothalamic–pituitary–adrenal (HPA) axis [rev. in 7, 9], a system known to be activated upon stress exposure. Stressors stimulate the secretion of adrenocorticotropic hormone (ACTH) into the bloodstream by the pituitary, which results in corticosterone secretion from the adrenal gland, a process know to help animals adapt to stress [rev. in 82]. In addition, it his thought that the place cells of the ventral hippocampal formation have larger, less well-tuned place fields than the ones found in the septal hippocampus [rev. in 9], supporting further the idea that the ventral hippocampus may have a secondary role in spatial memory. The strong connectivity between ventral hippocampus and both the hypothalamus and the amygdala, could therefore account for some of the effects of hippocampal lesions on emotionality [rev. in 13, 137]. Recently, a pharmacogenetic approach involving Htr1a–$G_{\beta\gamma}$ activation, suggested a pivotal role of the hippocampal formation in the regulation of conditioned anxiety [207]. In this study, selective inhibition of hippocampal dentate gyrus granule cells could suppress the enhanced response to ambiguous conditioned cues seen in *Htr1a*$^{\mathrm{KO}}$, suggesting that the hippocampus is important in the response to ambiguous aversive stimuli [207].

1.5 Hippocampal Anatomy

The hippocampal formation comprises four distinct cytoarchitectonic regions: the dentate gyrus (DG), the hippocampus proper (or *Cornu Ammonis*, divided into three sub-fields: CA3, CA2 and CAl) and the subicular complex (which is also divided into three subdivisions: the *subiculum*, *pre-subiculum* and *parasubiculum*) and the entorhinal cortex (EC). The three-dimensional shape of the rodent hippocampal formation is relatively complex, with an elongated, C-shaped structure with the long (septo-temporal) axis running from the septal nuclei rostrally to the temporal cortex ventrocaudally [7]. A unique feature of the hippocampal formation (already described by Ramón y Cajal in 1901 [172]) is that each of the fields are linked by unidirectional excitatory projections (Figure 1.1). Pyramidal cells are the major component of the pyramidal cell layer of the hippocampus proper. Deep to the pyramidal cell layer is the *stratum oriens*, into which the basal dendrites of the pyramidal cells descend and which contains a number of non-pyramidal neurons. The acellular region superficial to the pyramidal cell layer, where the apical dendrites of the pyramidal cells are located, is divided into a deeper *stratum radiatum* and a more superficial *stratum lacunosum-moleculare*. The CA2 field makes up a small portion of the pyramidal cell layer of the hippocampus sharing many of the connectional characteristics of CA3. It contains four different types of pyramidal neurons with overlapping morphometric characteristics from CA1 and CA3, with the CA2–CA1 transition characterized by an increase in the frequency of monoapical pyramidal neurons [16, 96]. Although, it is thought that CA2 contributes to a functional dissociation between CA3 and CA1, several anatomic studies [e.g., 7] have considered it as the most distal portion of field CA3, a nomenclature that we will adopt for simplication. In CA3, the region just above the pyramidal cell layer contains the mossy fibers from the dentate gyrus and is called the *stratum lucidum*. CA3 pyramidal cells have highly collateralized axons that establish autaptic synapses within the CA3 field and give rise to the major projection to CA1 – the Schaffer collaterals. Unlike the CA3 cells, CA1 pyramidal cells do not give rise to extensive projections within the CA1 but project in a columnar fashion to the *subiculum* and deep layers of the entorhinal cortex [rev. in 7, 9, 96, 217].

Postnatal Ontogenesis Of Hippocampal CA1 Cells

Several morphometric studies have revealed that CA1 pyramidal cells differ significantly from CA3–CA2 pyramidal cells [mainly 96, but also 7, 37, 164, 165]. First

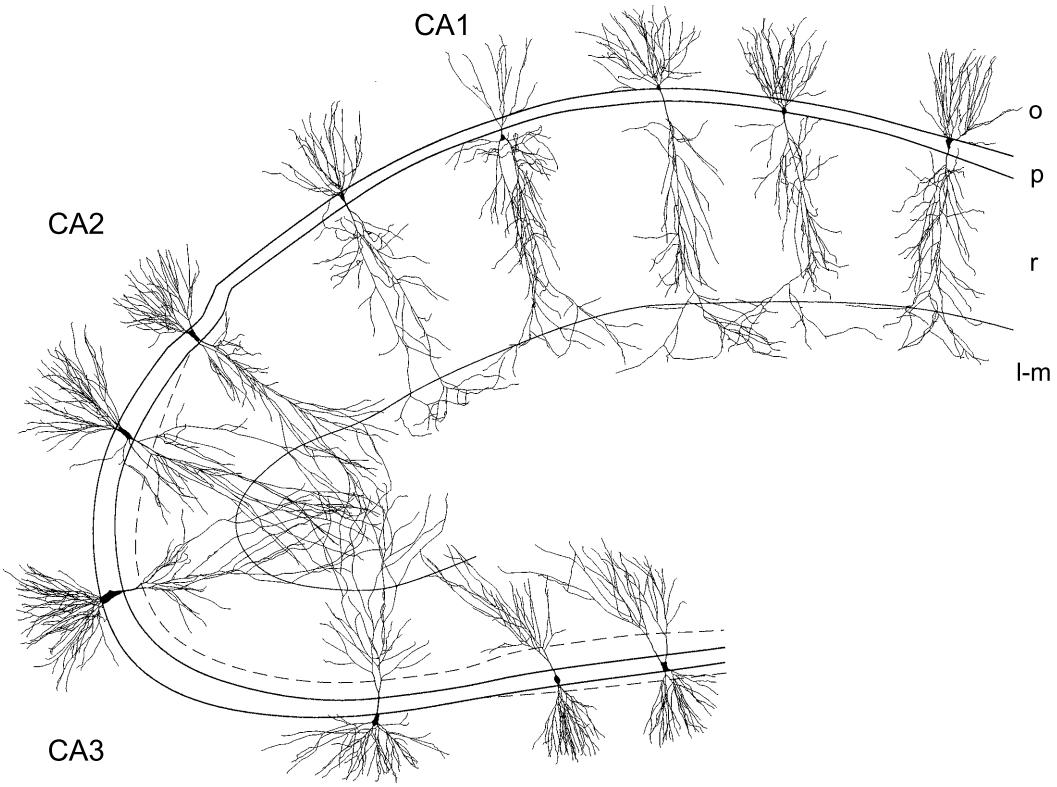

Figure 1.1 Organization of pyramidal cells of the hippocampus proper (*Cornu Ammonis*, CA). **CA3–1** *Cornu Ammonis* areas. CA3–1 sub-regions: **o** *stratum oriens;* **p** *stratum pyramidale;* **r** *stratum radiatum*; **l-m** *stratum lacunosum-moleculare.* Continuous line: boundaries of pyramidal layer. Dashed line: boundaries of infra and supra-pyramidal mossy fibers. Adapted from a computarized composite of Golgi-reconstructed rat cells by Ishizuka et al., 1995 [96].

CA1 cells have a smaller soma and a cross sectional surface two to three times below that of CA3–CA2 cells. Second, CA1 cells have typically one to two primary apical dendrites while CA3–CA2 can display up to seven. Third, CA1 cells display in all *stratum radiatum* short lateral dendritic branches (named *oblique*) that fork from the proximal apical dendrite forming an acute angle. In CA3 and CA2 these oblique dendrites are confined to the bottom of the *stratum radiatum* and branch from primary apical dendrites at wider angles. Third, the distal dendrites of the *stratum lacunosum-moleculare* of CA3–CA2 cells have the same length of those in the *stratum radiatum* while the dendritic plexus of the stratum *lacunosum-moleculare* of CA1 cells is wider, typically running transversely to the hippocampal fissure. Fourth, and probably the most striking, CA1 cells, as a population, share the most homogeneous dendritic arbor among all cells of the hippocampus proper (Figures 1.1 and 1.2, [cf. in 96]). Importantly, CA1 oblique dendrites account for the vast majority of dendritic surface of CA1 neurons and receive the majority

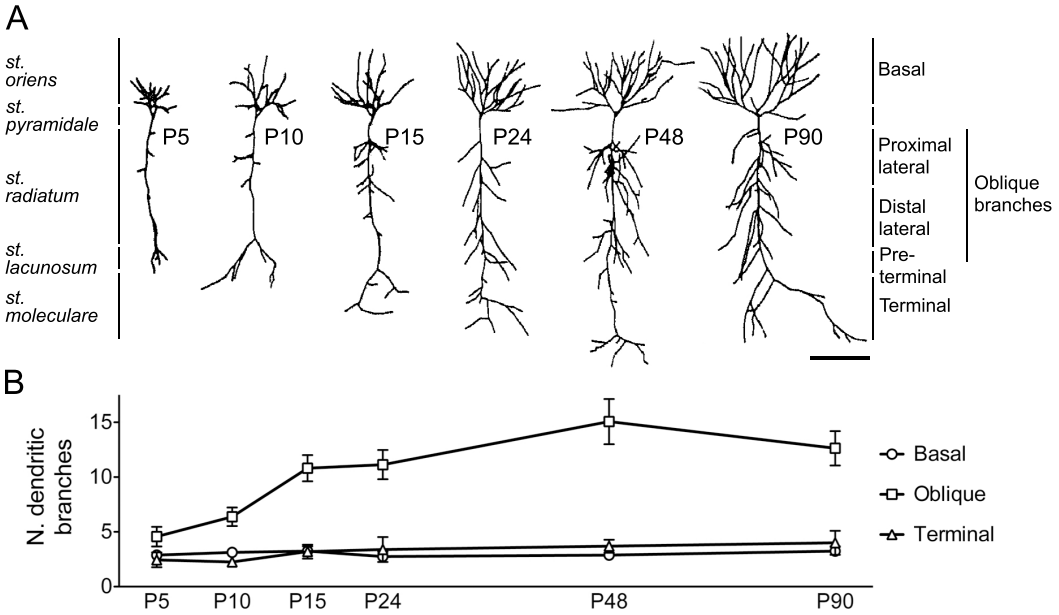

Figure 1.2 Postnatal ontogenesis of CA1 pyramidal neurons as described by Pokorný and Yamamoto, 1981 [164]. **A** Computerized reconstructions of developing hippocampal neurons. Age of animals (rats) is given next to each Golgi-reconstructed cell. CA1 layers are indicated on the left with the classification of dendritic branches within subfields on the right. Oblique dendrites (not considered in this study) contain all proximal branches plus the proximal half of pre-terminal dendrites. In this classification the remaining pre-terminal branches are considered as terminal processes. Scale bar: 100 µm. **B** Oblique dendrites are the only branches of the dendritic arbor to increase complexity during the second to sixth postnatal weeks. Bars represent means ± SEM (N= 8). All data inferred from original publication [164].

(70–100%) of inputs from Schaffer collaterals [15, 139].

While CA1 pyramidal dendrites in *stratum oriens* are nearly complete by the end of the second postnatal week, oblique dendrites in the *stratum radiatum* mature almost entirely during the third through sixth postnatal weeks [164] (Figure 1.2). Indeed, individual parts of the dendritic system of the hippocampal pyramidal neurons develop in a consecutive order. The number of dendrites seems to be established first, followed by elongation and ramification, with the number of segments of higher order branches established before the maximum of total dendritic length has been reached (Figure 1.2–B, [164]). Interestingly, the branches of the main shaft seem to appear mainly during the period when the total length has already been established. As a consequence the length of dendritic segments decreases during development (Figure 1.2–A, [164]).

1.6 Dendritic Growth, Guidance and Branching

The mechanisms of dendritic development have not been examined as extensively as those of axons (or neurites in cases of cultured neurons where axonal/dendritic differentiation is not apparent). Although dendrites and axons differ in important developmental aspects such as growth rate [62], it is reasonable to assume that, given the similarities in the basic cell biology of neuronal processes, axons and dendrites share common cytoskeletal regulators, e.g., at the level of growth cones.

Growth Cones Play A Pivot Role In Neuronal Morphogenesis And Structural Plasticity

Growth cones are the specialized end of developing neuronal processes, composed of finger-like filopodia and veil-like lamellipodia that exhibit amoeboid movement as the growing process explores the neuropil[2]. Although growth cones vary dramatically in shape and size, generally they are composed of a peripheric region (P–domain) containing filopia and/or lammellipodia, a transition domain (T) and a microtubule-enriched central region (C–domain) [rev. in 126].

Growth cone progression is characterized by three morphologically distinct stages [76]: 1) Protrusion, occurs by the rapid extensions of filopodia (primarily composed of F-actin bundles); 2) Engorgement occurs when microtubules invade protrusions bringing membranous vesicles and organelles (mitochondria, ER); and 3) Consolidation, occurs when the majority of F-actin depolymerizes in the neck of the growth cone, allowing the membrane to shrink around the bundle of microtubules, forming a cylindrical axon shaft. These three stages, iterated many times, give rise to the elongated axon. *In vivo* growth cone motility and axon outgrowth also occurs through protrusion, engorgement, and consolidation) [75, 87] but while in culture, growth cones display random outgrowth [5], *in vivo* outgrowth is not random, but directed to specific postsynaptic targets [75, 87, 103]. It is though that the difference between random or induced outgrowth *in vitro* and directed outgrowth *in vivo* is likely to be that gradients of guidance cues in the tissue can bias one side of the growth cone to progress through these stages more rapidly than the other side of the growth cone [rev. in 49].

[2]Remarkably it was Ramón y Cajal, who first described and surmised the function of growth cones, even though he had only imaged fixed tissue [for an extraordinary description see 172]

Growth Cones and Dendritic Branching

Axonal branching can occur through two cellular mechanisms: a) growth cone splitting, in which a growth cone can split at the branching point, generating two sister branches; and b) Interstitial branching, in which a new branch emerges from the middle of an axon trunk [rev. in 126]. In vertebrate as well as *Drosophila* neurons, interstitial branching from dendritic shafts appears to be the mechanism for dendritic branching [e.g., 43, 221]. For instance, *in vivo* imaging of *Xenopus* optic tectal neurons shows rapid addition and retraction of branches along the primary dendrites [221]. Dentritic elaboration occurs by the stabilization of interstitial branches and subsequent branch addition from stabilized branches. Similarly, live imaging of developing pyramidal neurons in hippocampal slices reveals that dendritic shafts constantly extend and retract filopodia. During early development some of these filopodia are stabilized into new dendritic branches, whereas later in development these dynamic filopodial extensions can develop into dendritic spines [43].

Actin Cytoskeleton: A Key Regulator In Growth Cones Motility

The actin cytoskeleton plays a major role in morphological development of neurons and in structural changes of adult neurons such as neurite initiation, growth, guidance and branching and formation, stability and motility of dendritic spines [rev. in 126]. The two principle cytoskeletal components in growth cones are actin filaments and microtubules. Although neurofilaments are an important cytoskeletal component during development of the vertebrate nervous system [120], their function in growth cone motility and axon guidance is unknown, since microfilaments seem to be absent from growth cones of CNS neurons [120] and mice lacking axonal neurofilaments have only few abnormalities in neural connectivity [59].

In neurons as in most eukaryotic cells, actin accounts for 5% of the proteome and exists in a dynamic equilibrium between the monomeric (globular) G-actin and polymeric (filamentous) F-actin. In growth cones, F-actin content is highest in the P and T–regions of the growth cone and diminishes to varying levels in the C–domain [rev. in 49].

Actin Filament Dynamics

Each actin molecule is composed of two lobes clasping an ATPase pocket that can bind to one molecule of ATP, which is hydrolyzed irreversibly after incorporation of the actin monomer into the filament. Actin filaments are double helical polarized polymers of globular subunits in a head-to-tail arrangement, whose ends are

structurally and dynamically distinct. Based on the arrowhead pattern created by decoration with myosin, one end is called the barbed end (the fast-growing end, capped with ATP-actin) and the other the pointed end (slow-growing end, capped with ADP-actin). Since ADP-actin has lower affinity than ATP-actin for the filament, ATP-actin monomers add on to the fast growing end of the filament while ADP-actin monomers are lost from the slow-growing end, in a process known as treadmilling [e.g., rev. in 157].

Neurons contain approximately equal amounts of non-muscle isotypes of actin, β-actin and γ-actin. It is not known if these isotypes of actin have distinctive functions in growth cones (as well as it is not known in which proportions they are present in the actin filaments of growth cones) [rev. in 49] but both their mRNA and protein show differential regulation in neurons [18].

In growth cones, the barbed end of the actin filament generally faces the distal membrane and the pointed end faces the T–region. The bulk of F-actin forms three main types of structures: Actin ribs, intrapodia and meshwork arrays [rev in 126]. Actin ribs, are polarized bundles of F-actin and the core of filopodia that often extends into the T–region. These structures can also be present at the lamellipodial P and T–regions of the growth cone. Meshwork arrays of F-actin form the bulk of the lamellipodia in the P–region of the growth cone. Intrapodia are dynamic 'comet-like' structures that emanate from the T–region and extend into the P–region. The actin structure of intrapodia forms an elongated meshwork array, and thus, intrapodia are a hybrid of the bundled and meshwork arrays that compose the bulk of growth cone F-actin [50, 49, 126, 157, 179]. Other forms of F-actin in the growth cone with distinct kinetics include arc-like structures in the T–region [185] and stable puncta located within the C–domain that are insensitive to G-actin sequestering drugs [50].

1.7 Regulation Of Dendritic Growth By Serotonin

In addition to its actions as a neurotransmitter, serotonin, as others biogenic amines, regulates various aspects of neural development, from cell division and survival to synaptogenesis [rev. in 72]. Thus, several studies have shown that serotonin can alter neurite outgrowth (Table 1.1), regulating both the development of neuronal arborizations and synaptic connectivity [e.g., 45, 54, 66, 136, 166].

In rodents it has been shown that the levels of serotonin in the primary somatosensory cortex during early postnatal life affect the development of the barrel

Table 1.1 Effects of 5–HT treatment on neurite growth. This list does not pretend to be exhaustive, but rather restrictive to most relevant publications focused on neurite/dendritic outgrowth in primary neuronal cultures.

Cell type	Treatment and dosage	Effects	Implicated mechanisms	References
Helisoma bocal neurons	5–HT 1–50 µM	Acute inhibition of growth cone motility	ACh regulated Ca^{2+} influx	[89, 90, 136]
Thalamic neurons	5–HT 25 µM	Promotion of neurite outgrowth[a]	Cell–automonous regulation	[119]
Thalamic neurons	5–HT 0.36–360 nM	Promotion of neurite outgrowth[b]	1B receptor activation	[123]
Purkinje cells	5–HT 2–20 µM	Promotion and inhibition of dendritic branching[c]	1A receptors mediate promotion while 2A mediate inhibition	[111]
Cortical neurons	8-OH–DPAT 20–200 nM	Decreased neurite branching and total neurite length[d]	1A receptor activation	[197]

[a]Concentration specific as no outgrowth differences were observed with 0, 10, 50 or 100 µM, 6 days treatment, dissociated cultures.

[b]The enhancing effects of 5–HT are blocked by the sodium channel blocker tetrodotoxin (TTX), and thus activity-dependent. Outgrowth differences observed with all concentrations, 24 h treatment, dissociated cultures.

[c]4–7 days treatment, organotipic cultures.

[d]Treatment in the presence of media containing a free 5–HT content of 320 nM; 48 h treatment, dissociated cultures.

field by affecting the patterning of thalamocortical axons [rev. in 72]. *In vitro*, it is known that exposing thalamic cells to serotonin enhances their neurite outgrowth in the absence of their cortical targets, an effect reproduced by Htr1b agonist treatment (Table 1.1, [119, 123]). The cortical formation of the cerebellum is also known to be tightly regulated by serotonin. Purkinje cells, that are enervated by serotonergic fibers, express Htr1a in the first postnatal week, but not in adulthood. On the other hand, Htr2a receptors are found in Purkinje cells shortly after birth and its expression is maintained in adulthood [111, 131]. In cultured cerebellum slices it has been showed that dendrite formation of Purkinje cells is stimulated by 5–HT through Htr1a receptors, but inhibited by 5–HT through Htr2a receptors, suggesting that the two receptors may have opposite actions (Table 1.1, [111]). Another demonstration of Htr1a-dependent regulation of neurite growth came from experiments involving primary cultures of cortical neurons (Table 1.1, [197]). First the authors distinguished three neuronal populations based on the density of radioactively-labeled 8-OH–DPAT binding sites: about half of the cells had no detectable binding, 40–

50% had a moderate level of binding, and 2–5% were densely labeled. Then the authors showed that stimulation of these neurons with 8-OH–DPAT decreased the branching of neurites by 70% as well as their total length by more than half. This study was pioneering, because although it studied Htr1a function by means of antagonist/agonist challenge, serotonin was present at all times of treatment, mimicking more accurately the *in vivo* situation in which serotonin signals simultaneously through multiple receptors.

Cytoskeletal Modulation By Htr1a

Studies in which serotonin has been implicated in the regulation of cytoskeletal machinery were typically performed in *in vitro* systems by means of biochemical challenge [e.g., 230], leaving open a series of questions on the physiological occurrence of such regulation. In addition, a possible mechanism by which Htr1a might influence dendritic arborization has not yet been investigated. However, it has been shown that serotonin, by activating Htr1a receptors, can inhibit NMDA receptor-mediated currents in PFC pyramidal neurons, by diminishing the number of surface NMDA receptor 2B subunits (NR2B) on dendrites [228]. The mechanism proposed placed the kinesin motor protein KIF17, which transports NR2B-containing vesicles along microtubule in dendrites downstream of Htr1a activation. Other biochemical evidence also indicated that Htr1a signaling reduced microtubule stability, which was abolished by CaMKII or ERKs inhibitors [228].

One family of proteins that are clearly essential for dendritic remodeling are the RhoGTPases which have a pivotal role in regulating the actin cytoskeleton in all cell types. Small RhoGTPases (i.e., Rho, Cdc42, Rac) have been shown to control the establishment of neuronal polarity, neuronal migration, growth cone guidance and the function of synapses, and it is though that, together, RhoGTPases can regulate every process in a neuron that involves plasticity of the cytoskeleton [rev. in 78, 116, 117, 125, 126]. GTPases function as molecular switches, being inactive when bound to GDP and active when bound to GTP. Inactivation is brought about by the intrinsic GTP hydrolytic capability, which is further increased by GTPase-activating proteins. In contrast, activation, which occurs in response to a variety of stimuli, is mediated by GEFs, molecules which promote the dissociation of bound GDP and subsequent GTP association [rev. in 181].

The regulation of RhoGTPases contributes to the localized polymerisation and depolymerisation of actin filaments. In cultured hippocampal neurons the selective destabilization of actin microfilaments in a single growth cone was shown to predis-

pose the neurite to become an axon [25]. Indeed, application of F-actin destabilizing agents and RhoGTPase inhibitors can prevent the establishment of neuronal polarity, which results in the formation of several axon like neurites [25]. Beside affecting axonal initiation, RhoGTPases also regulate the motility of all neurite terminals, thus affecting both axonal guidance and the shape of dendritic arbors [rev. in 126]. It is thought that Rac and Cdc42 regulate dendritic branch addition, while Rho and Rho kinase inhibit branch elongation [216, 116, 117]. The *in vivo* role of the three GTPases in neurons has been examined in *Drosophila*, *Xenopus* and mice. In *Drosophila*, constitutively active or inactive DRac mutants affected axon initiation and elongation of sensory neurones and intersegmental nerve b (ISNb) motor neurons, without affecting dendrites. In contrast, alterations of *Drosophila* Cdc42 activity affected both axons and dendrites [rev. in 126, 152]. Visualization of optic tectal neurons in *Xenopus* tadpoles expressing active Rac revealed an enhanced rate of dendritic branch outgrowth and retraction, while inactive Rac reduced the formation of new branches. In this system, alterations of Cdc42 caused a similar but much milder phenotype. In contrast, activation of endogenous Rho inhibited overall dendritic outgrowth effect [116]. Rho activity did not affect the dynamics of dendritic branch remodeling and neither Rac nor Cdc42 affected overall dendrite length, demonstrating distinct roles of these three GTPases [116]. In mice, overexpression of an active Rac1 mutant in Purkinje cells resulted in few abnormalities in dendritic branching and severe disruption of dendritic spine morphology, which caused abnormalities in synaptic function and made transgenic mice ataxic [127]. Overall, RhoA, Rac1 and Cdc42 have overlapping and distinct (often opposing) roles in regulating the cytoskeleton of differentiating neurons. In addition, the same signals that activate one, cause the downregulation of another. Currently, the best examples are Rac1 and RhoA and their differential regulation by the ephrins and semaphorins [rev. in 213].

The complexity of pathways that can activate GTPases is further extended by vast subfamilies of GEFs and GAPs [rev. in 181]. Many of the GEFs (e.g., Dbl, Kalirin, Ost, Stef, Tiam1 and Trio) and GAPs (e.g., p190RhoGAP and oligophrenin-1) are highly enriched in the CNS [[79, 92, 129, 130], rev. in[229]]. Of these GEFs, at least one, Dbl, has been shown to be required for proper dendritic maturation *in vivo* [92]. Indeed, cortical neurons of mice lacking Dbl display defective dendritic elongation but no change in axonal morphology or other detectable phenotype, suggesting that Dbl function is critical for dendritic maturation [92].

Chapter 2

Results

Htr1a^{KO} mice [83] display exuberant dendritic arborization in the *stratum radiatum* of CA1 pyramidal cells [42]. This phenotype is restricted to oblique dendrites and is characterized by: 1) increased number of segments; 2) increased number of branch points and 3) increased total dendritic length. Although these morphological changes are already detected at P15, the most striking differences between mutants and control littermates are seen transiently at juvenile ages (P30–P60), with heterozygous mice displaying systematically an intermediate phenotype [42, 106, 146, and J.P. Hornung, personal communication].

2.1 Postnatal Blockade Of Htr1a Phenocopies The Dendritic Phenotype Of Htr1a Knockout Mice

Chronic pharmacological blockade of Htr1a in wild-type mice during the third through fifth postnatal weeks phenocopies the increased anxiety related behavior displayed by knockout animals [94, 207]. We have surmised that the exuberant dendritic arborization seen in *Htr1a*^{KO} mice could contribute to its anxiety phenotype. To test this hypothesis, we assessed the effects of Htr1a antagonist treatment during the same developmental period on the morphology of CA1 cells.

Single-Cell Resolution Labeling In Thy1-GFP-M Transgenic Mice

The mosaic expression green fluorescent protein (GFP) of Thy1-M-GFP transgenic mice [60] allows the imaging of isolated CA1 pyramidal neurons in the septal hippocampus (Figure A.3). We have found the use of this line more effective in obtaining a 'Golgi-like' labeling over other methods, including diOlistic staining (data

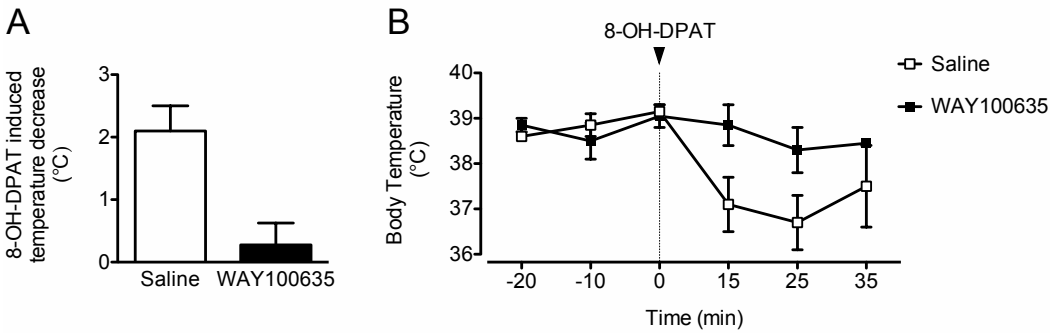

Figure 2.1 Absence of agonist-induced hypothermia in wild-type mice during chronic administration of WAY100635. **A** Maximum temperature decrease at P35 in Thy1-M-EGFP animals treated with either saline or WAY100635 via osmotic minipumps (0.15 mg/kg/h) after acute administration of the Htr1a agonist 8-OH–DPAT (0.3 mg/kg, sc.). **B** Time course of body temperature before and after administration of 8-OH–DPAT. Bars represent means ± SEM; Saline, WAY100635: $N = 2$.

presented on Chapter A). To test whether blockade of Htr1a during development would phenocopy the dendritic phenotype of *Htr1a*^{KO} animals we implanted wild-type (WT) transgenic Thy1-GFP-M mice at postnatal day 14 (P14) subcutaneously with osmotic mini-pumps delivering either saline or the Htr1a-selective antagonist WAY100635 (0.15 mg/kg/day). In order to obtain a better-controlled group we crossed Thy1-GFP-M homozygous males (Section 4.1.3) with WT females from a 129S6/SvEvTac;C57BL/6J;CBA mixed background, as mothers from this strain tend to not reject the pups after surgery [94].

Assessment Of Htr1a Blockage By 8-OH–DPAT-Induced Hypothermia

The efficacy of Htr1a blockade following minipump implantation was confirmed by quantifying hypothermic responses to an acute injection of the Htr1a-selective agonist 8-OH–DPAT (0.3 mg/kg, sc.) at P35 in a subset of animals. Acute treatment with this drug is known to decrease body temperature in rodents, possibly via activation of Htr1a autoreceptors [133]. While a significant drop in body temperature was seen in saline treated mice, WAY100635-treated animals showed a similar resistance to 8-OH–DPAT-induced hypothermia as typically seen in *Htr1a*^{KO} mice [94], suggesting full blockade of the receptor (Figure 2.1).

Increased Dendritic Branching In The *Stratum Radiatum* Of CA1 Neurons In WAY100635-Treated Mice

At P35, mice from both groups were perfused with fixative, processed for immunohistochemical enhancement of GFP signal and CA1 cells of the dorsal (septal half)

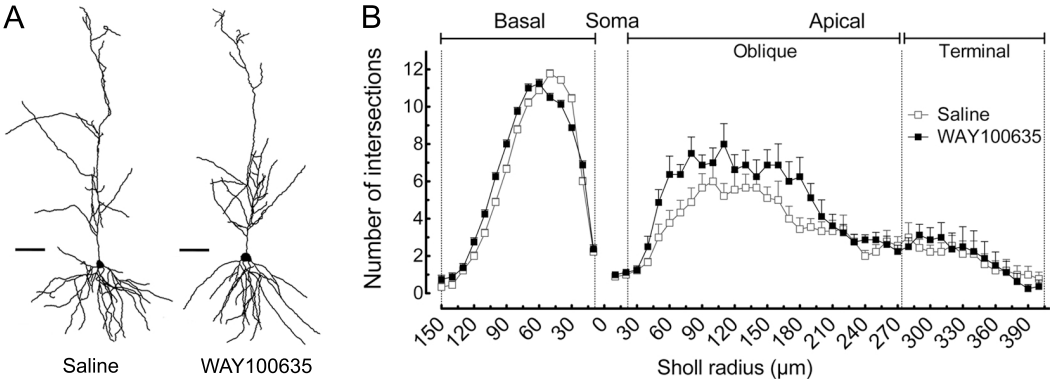

Figure 2.2 Increased dendritic branching in the *stratum radiatum* of CA1 neurons in mice treated during development with WAY100635. **B** Mice treated with the selective Htr1a antagonist WAY100635 from P14–P35 (WAY100635) showed increased branching in the proximal apical arbor when compared to saline-treated littermates (Saline). Basal and distal apical dendrites were unaffected by WAY100635 treatment. **A** Skeletonized reconstruction of representative CA1 cells at P35 (Scale bars: 50 µm). **B** Sholl plot of reconstructed cells showing the number of intersections of basal and apical dendrites as a function of path length from the soma. Bars represent means ± SEM; saline: $N = 8$, WAY100635: $N = 11$.

hippocampus imaged by confocal microscopy (Sections 4.4–4.5). Sholl analysis [194] of digitized 3D-tracings of single cells (Figure 2.2–A, Section 4.6) demonstrated a significant increase in oblique branches in neurons from WAY100635-treated mice compared to saline-treated controls in the proximal apical region of the dendritic arbor (Figure 2.2). No differences were seen in the terminal apical or basal dendritic plexus (Figure 2.2–B). Exuberant arborization of oblique dendrites was associated with an increased number of dendritic segments ($p = 0.042$, unpaired Student's t-test) and increased number of branch points, i.e., dendritic nodes ($p = 0.055$). No significant differences were found in linearized length of oblique dendrites as well as in average segment length, although the measures obtained suggest a trend of WAY100635 treatment to increase total dendritic length (Figure 2.3).

This phenotype matches accurately that seen in *Htr1a*^{KO} mice [42] and demonstrates that Htr1a function during the third through fifth postnatal weeks is necessary to restrict the growth of oblique apical dendrites.

Behavior Of WAY100635-Treated Mice

Since the pharmacological blockade of Htr1a during the third through fifth postnatal weeks phenocopies the anxiety phenotype of Htr1a knockout mice in the open field test [94], we tested WAY100635-treated animals in this paradigm. Previously

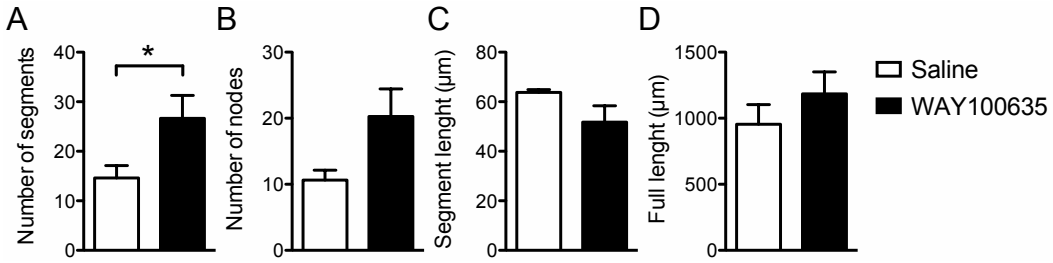

Figure 2.3 Morphometric analysis of oblique dendrites of CA1 neurons in mice treated during development with WAY100635. WAY100635 treatment increased the number of oblique segments (**A**) as well as number of dendritic nodes (**B**). As a consequence of the increased number of branch points, segment length is reduced (**C**). Exuberant branching is also reflected by a trend in increased total length (**D**). Bars represent means ± SEM; saline: N= 8, WAY100635: N= 11; unpaired Student's t-test; *: $p< 0.05$.

[94], a set of WAY100635-treated animals from a 129S6/SvEvTac;C57BL/6J;CBA mixed background had shown significantly reduced time in the center, percentage of path in the center, and total path in the open field when tested in adulthood. However, in our experimental cohort of Thy1-M-GFP animals there were no significant differences between groups in any of the five variables analyzed. Nevertheless, there was a discrete tendency for decreased center activity in WAY100635-treated mice, specially in the initial five minutes of the test (Table 2.1).

Table 2.1 Effects of WAY100635 treatment on the open field test. Reduction in path and time spent in the center, suggest increased thigmotaxis in WAY100635-treated animals, and thus increased innate anxiety-related behavior. N=10 (3 ♂, 7 ♀); WAY100635-treated animals: N=10 (4 ♂, 6 ♀). Values expressed as mean ± SEM.

	Total path length (cm)	Path in the center (%)	Time in the center (%)	Number of center visits	Number of rearings
5 min					
Saline	2136.7 ± 121.21	7.9 ± 1.65	5.1 ± 1.02	8.8 ± 1.63	12.9 ± 2.11
WAY100635	1905.5 ± 218.40	6.4 ± 1.78	4.5 ± 1.38	7.2 ± 1.92	11.7 ± 2.71
20 min					
Saline	6754.9 ± 484.70	12.5 ± 2.12	8.3 ± 1.41	38.0 ± 6.64	56.9 ± 8.68
WAY100635	6486.9 ± 633.47	11.4 ± 2.78	8.1 ± 2.25	37.0 ± 9.14	57.1 ± 12.74

2.2 Motility Of Dendritic Growth Cones Is Relevant For Dendritic Maturation

The exuberant arborization of oblique dendrites following blockade of Htr1a function could be caused either by a indirect modification in hippocampal circuitry or a by cell-autonomous processe. Blockade of Htr1a leads to an increase in neuronal excitability due to $G_{\beta\gamma}$ coupling to inhibitory GIRK channels (Chapter 1, [20, 128]). Increased activity could then alter dendritic maturation via activity-dependent mechanisms [rev. in 38]. On the other hand, Htr1a could modulate mechanisms of autonomous growth, via e.g., cAMP [35, 228] as forskolin, an activator of adenylyl cyclase, can promote stabilization of dendritic branches [112]. To examine a possible role of Htr1a in dendritic growth we studied Htr1a function in postnatal dissociated hippocampal cultures.

Characterization Of Dendritic Growth In Hippocampal Dissociated Cultures

At E15 the generation of hippocampal pyramidal neurons is essentially complete, but the generation of dentate granule cells, which is mainly postnatal, scarcely has begun [187]. Thus, postnatal hippocampal cultures offer the advantage of maintaining all cell types of the original tissue [rev. in 11]. In order to assess *in vitro* viability, we performed a set of descriptive immunostainings. Pyramidal neurons account for 85–90% of the total neuronal population of the hippocampus [187]. Interneurons account for 11% of the hippocampal neuronal population, with the majority of these expressing GABA [217, rev. in 65]. As expected [22], we verified these proportions has well as absence of astro-glia contamination in non serum-free cultures (Figure 2.4, and data not shown).

In order to determine the time course of dendritic maturation we stained cultured neurons with the dendritic marker Map2 [33, 34] at hallmark stages of *in vitro* growth. One and half days after plating, Map2 is uniformly distributed throughout the cell [34] and although processes do not resemble either mature axons or mature dendrites (i.e., neurites), hippocampal cells display already a single long process that later will not stain for Map2 (the axon) and several shorter processes (dendrites). At this stage of *in vitro* development (Banker stage 3) dendritic growth is negligible. Significant dendritic growth begins only after DIV4 (Banker stage 4), being particularly evident at DIV7 (Banker stage 5) [55]. At this stage, in low-density cultures,

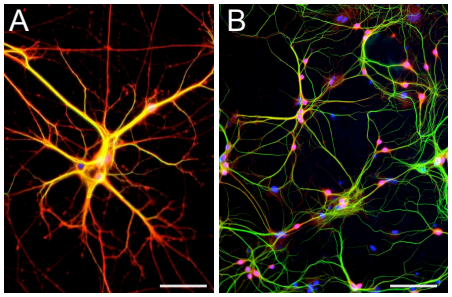

Non-GABAergic neurons	38.0%
GABAergic neurons	6.80%
Astrocytes (serum containing media	55.2%

Figure 2.4 Cell populations in postnatal dissociated hippocampal cultures. **A–B** Proportion of cultured GABAergic neurons determined by anti-GABA (red)/Map2 (green) co-immunostaining. **A** Representative GABAergic interneuron characterized by round somata and extensive colocalization [cf. in 22]. Scale bar: 50 µm. **B** Low magnification image-field depicting non-GABAergic excitatory neurons in which GABA/Map2-colocalization is restricted to somata. Scale bar: 120 µm. Summary of quantification is shown on the right. Count of astrocytes was performed by anti-GFAP/Map2 immunostaining (data not shown). In serum-free conditions glial proliferation is minimum, and consequently the proportion of astrocytes is estimated to be significantly lower [102]. Measurements performed at DIV15 in the presence of DAPI (blue). $N \approx 100$ cells, 2 cultures.

axons (that grow at least 5× faster then dendrites [55]), have already extended to their targets [rev. in 11]. As expected, Map2 immunolabeling confirmed maximal dendritic growth at DIV7 reflected by both total dendritic length and number of branches (total number of branching junctions) with a slight decrease at DIV15 (Figure 2.5–A).

Overall these results indicate that in our hands, cultured neurons recapitulate several canonical landmarks of hippocampal ontogeny.

Forward/Backward Motility Of Dendritic Growth Cones

After DIV3, dendrites and axons begin to make synaptic connections and the number of growth cones substantially diminishes [41 and data not shown]. In order to image growth cones as close as possible to the peak of maximal dendritic branching we performed time-lapse video microscopy at DIV4–5. In this period, growth cones were easily visualized by differential interference contrast timelapse microscopy (Figure 2.7–A). In order to analyze the motility of dendritic growth cones we used a computer-assisted tracking method to classify the movement of DGCs into elongation, lingering, and retraction bouts (Figure 2.7–B). This method is described in detail in Section 4.6 and summarized in Figure 2.6. In short, extremely small interframe dislocations were categorized as 'lingerings' and eliminated from the traced path. In this way, the short-term protean motion of DGCs could be filtered out from the traced path, and forward/backward (elongating/retracting) movements easily

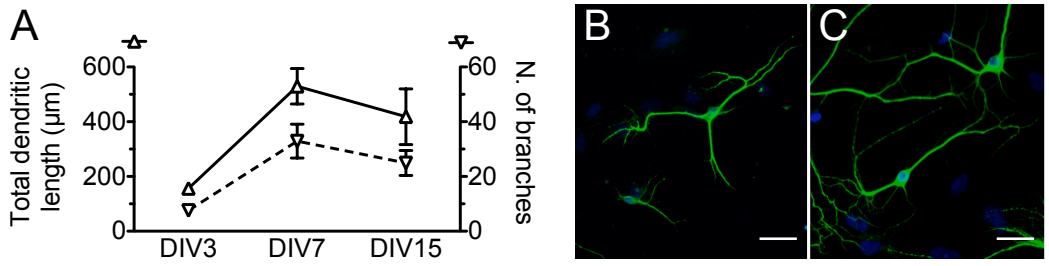

Figure 2.5 Dynamics of dendritic maturation *in vitro*. **A** Quantification of maximal dendritic outgrowth by Map2 immunoreactivity, depicting a growth peak at DIV7, reflected by linearized growth (full line) and number of branching junctions (dashed line). **B–C** Representative illustrations of imaged cells at DIV3 (B) and DIV15 (C). Images were automatically segmented and outgrowth quantified as the linearized length of skeletonized Map2 signal, using dapi-stained nuclei (blue) to individualize somata as outgrowth centers (data not show). Given the inevitable overlap of dendritic processes in mature cultures, it is possible that the values obtained at DIV15 are underestimated (Section 4.6.1). *N*: DIV3: 112 cells, DIV7: 20 cells, DIV15: 37cells. Scale bars: 50 µm.

identified.

The cumulative fraction of bouts that lasted less then the acquisition rate (3 min) corresponded to less of 1/4 of the acquired data (elongations: 14.2%, retractions: 22.9%) suggesting that bout duration was not affected by acquisition frame rate (Figure 2.8–A). Consistent with a correlation between DGC dynamics and gross dendritic maturation in culture, time spent elongating (63%) was greater than the time spent either lingering (25%) or retracting (12%) (Figure 2.8–A, pie chart). Quantification of bout duration showed that median elongation bouts were longer ($\tilde{x}$= 11.3 min) than either median lingering ($\tilde{x}$= 6.0 min) or retraction ($\tilde{x}$= 7.5 min) bouts. Average DGC speed during a bout was significantly greater during retraction than elongation (120 vs. 160 nm/min, respectively, ($F_{48,70} < 4.208, p$= 0.0024; Figure 2.8–B). Also, as expected [26], lingering episodes occurred most frequently flanked by elongation bouts and rarely flanked by retraction bouts (Figure 2.8–C, p= 0.000).

Overall, these results suggest that DGC dynamics in dissociated neuronal cultures accurately reflect several aspects of *in vivo* growth cone extension [43, 87], suggesting that forward/backward motility of DGCs may be relevant to understand the plastic changes underlying dendritic maturation.

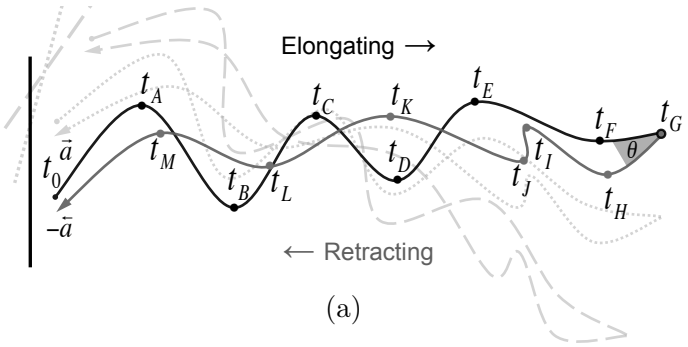

(a)

$j = 0$; for $t_A \leqslant t_i > t_M$:

(1) $\overrightarrow{A_{t_i}A_{t_{i+1}}} < Max_{\,ling} \quad \Rightarrow \quad A(x_{i+1}, y_{i+1}) = A(x_i, y_i)$

(2) $A_{t_{i-1}}\widehat{A_{t_i}}A_{t_{i+1}} > \theta \quad \Rightarrow \quad d = \vec{a};\ BL_j = \sum_{j\,=\,\vec{a}\,j+1}^{-\vec{a}}(\overrightarrow{A_{t_{i-1}}A_{t_i}} + \overrightarrow{A_{t_i}A_{t_{i+1}}});\ BD_j = \sum_{\vec{a}}^{-\vec{a}}(t_{i+1} - t_{i-1})$

(3) $A_{t_{i-1}}\widehat{A_{t_i}}A_{t_{i+1}} \leq \theta \quad \Rightarrow \quad d = -\vec{a};\ BL_j = \sum_{-\vec{a}\,j\,=\,j+1}^{\vec{a}}(\overrightarrow{A_{t_{i-1}}A_{t_i}} + \overrightarrow{A_{t_i}A_{t_{i+1}}});\ BD_j = \sum_{-\vec{a}}^{\vec{a}}(t_{i+1} - t_{i-1})$

(4) $\overrightarrow{A_{t_{i-1}}A_{t_i}} = 0 \wedge \overrightarrow{A_{t_i}A_{t_{i+1}}} = 0 \quad \Rightarrow \quad BD_j = (t_{i+1} - t_{i-1})$
$j = j + 1$

(b)

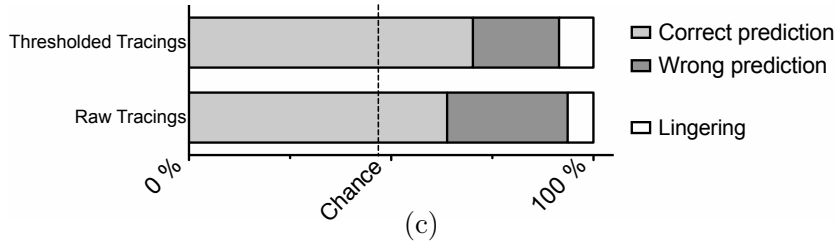

(c)

Figure 2.6 Model for automated analysis of growth cones' motility in terms of forward and backward displacement.

(a) Schematic representation of an imaged DGC. $\boldsymbol{t_A}$–$\boldsymbol{t_M}$ video-tracked points of the growth cone throughout the sampled time (t); $\boldsymbol{t_0}$ initial position of DGC; $\vec{\boldsymbol{a}}$ reference direction (d) at t_0, contra-equivalente of $-\vec{a}$; $\boldsymbol{\theta}$ the putative *turnaround angle* of the grayed vertex $\angle FGH$; **large arrow** DGC's path, divisible into two growth stretches: $[AG]$ (elongation bout) and $[GM]$ (retraction bout); **vertical line** hosting dendrite. Dashed gray lines emphasize that rotations/translations of growing and hosting processes occur frequently over time.

(b) Definition of forward/backward growth based on *turnaround angles* (θ). **(1)** Since very short inter-frame segments can interrupt maintenance of direction (e.g. $\overline{t_I t_J}$), displacement is considered null if below a *lingering threshold* $(Max_{\,ling})$; **(2)** if the angle formed by three consecutive tracked points is wider then θ, maintenance of initial direction $(\vec{a})$ is assumed; **(3)** if acuter, direction is inverted $(-\vec{a})$, and a new growth bout (j) is initiated; **(2–3)** While direction is conserved, magnitudes of consecutive vectors are added – bout length (BL) – as well as their durations – bout duration (BD); **(4)** lingering bouts have no length.

(c) Elimination of short inter-frame segments increases accuracy of automatic detection of forward/backward detection without significant changes in total path length (data not shown). Thresholded tracings ($Max_{\,ling}$= 0.15 µm, empirically determined) can accurately classify 71% of bouts within a DGC path, eliminating 1/3 of the errors verified with raw tracings (N= 50 traced objects; manually classified paths as benchmark).

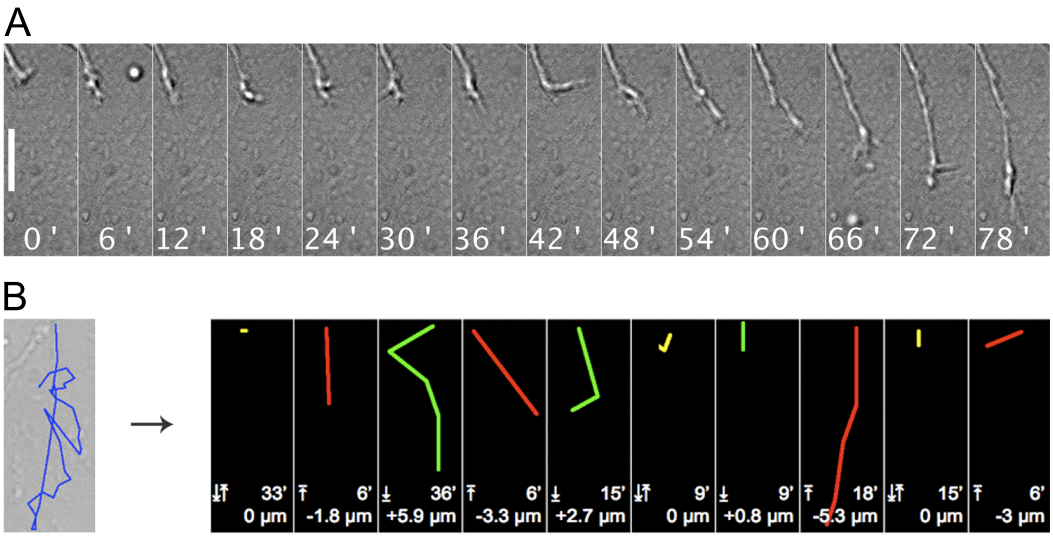

Figure 2.7 Representative examples of *in vitro* growth cone dynamics. **A** Magnified portion of a random image field depicting one DGC extending through the neuropil in a unique elongating bout that lasted 78 min. For simplicity, only every second frame (6 ') were included. Scale bar: 3 µm. **B** Example of a relatively complex path performed by a DGC from an untreated wild type culture. This object was hosted by a secondary dendrite and was video-tracked for 181 min. Its path was divided in 10 bouts of which 3 were classified as elongating (green segments), 4 as retracting (red segments) and 3 as lingering (yellow segments). Total path length was 22.6 µm. Respective bouts duration and length are indicated below each state.

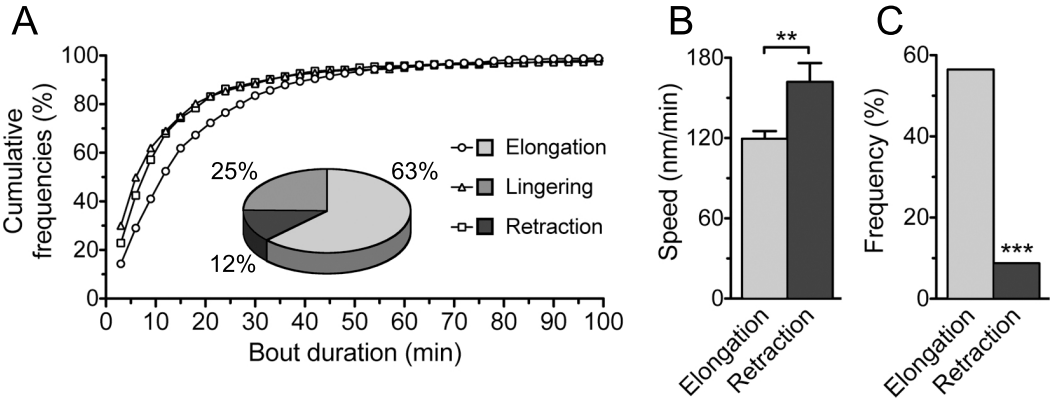

Figure 2.8 Intrinsic properties of DGCs motiliy reveal physiological relevance of forward/backward motility. **A** On average a DGC spent the majority of time elongating and only 12% of time retracting (pie chart). Growth bouts were not affected time resolution as 80–86% of movement bouts lasted longer then the acquisition frame rate (3 min). **B** Elongation bouts were faster then retraction ones ($p = 0.0024$, unpaired Student's t-test). **C** As described for neurite outgrowth [26], the majority of lingering bouts were flanked by elongation rather than retraction bouts (9%) ($p = 0.000$, χ^2 statistics. $N = 2800$ bouts).

2.3 Serotonin Attenuates Growth Cone Motility Via Htr1a

In order to assess if serotonin could regulate DGCs motility, we have imaged growth cones from either wild-type or *Htr1a*^{KO} cells, treated with serotonin (0 or 30 nM). This concentration of serotonin was chosen having the extracellular concentration of serotonin in the adult mouse forebrain (estimated by zero-net flux microdialysis) as a reference [134].

Serotonin Attenuates Motility Of Growth Cones

Cells were cultured for 4–5 days (DIV4–5), treated with serotonin (0 or 30 nM) for 12–16 h and then imaged for 4–6 h at 0.3 frames per minute (fpm) (Section 4.5, Figure 2.7–A). In WT cells, serotonin treatment caused a significant reduction in total distance traveled during elongation and retraction bouts (p= 0.021 and p= 0.024, respectively; Figure 2.9–A, B). This change was accompanied by a reduction in average speed during both elongation and retraction bouts (p= 0.002 and p= 0.027, respectively; Figure 2.9–C,D). The most dramatic effect of 5–HT was seen for total path length traveled, i.e., the total distance of DGCs' taken path regardless of whether elongating or retracting (p= 0.000, Figure 2.9–E). In terms of time spent per motility behavior, 5-HT treatment appeared to decrease time spent lingering, although this effect was not significant (p= 0.163, Figure 2.10–B). Critically, the effect of serotonin on DGCs dynamics was not present in cultures taken from *Htr1a*^{KO} mice, except in the case of retraction speed, where a similar trend was seen in both genotypes (Figure 2.9-D).

All together, these findings suggest an essential role of Htr1a activation for the observed effect of serotonin on growth cone dynamics. In addition, they suggest that serotonin may act directly to modulate cytoskeletal dynamics in DGCs.

2.4 Serotonin Reduces F-Actin In Growth Cones Via Htr1a

Regulation of actin polymerization is critical for motility of growth cones [rev. in 126, and in Chapter 1]. To determine whether serotonin could moderate actin polymerization, we examined levels of F- and G-actin in growing cultures, after a short 3 min 5–HT treatment. Immunoblotting of fractionated protein extracts revealed a

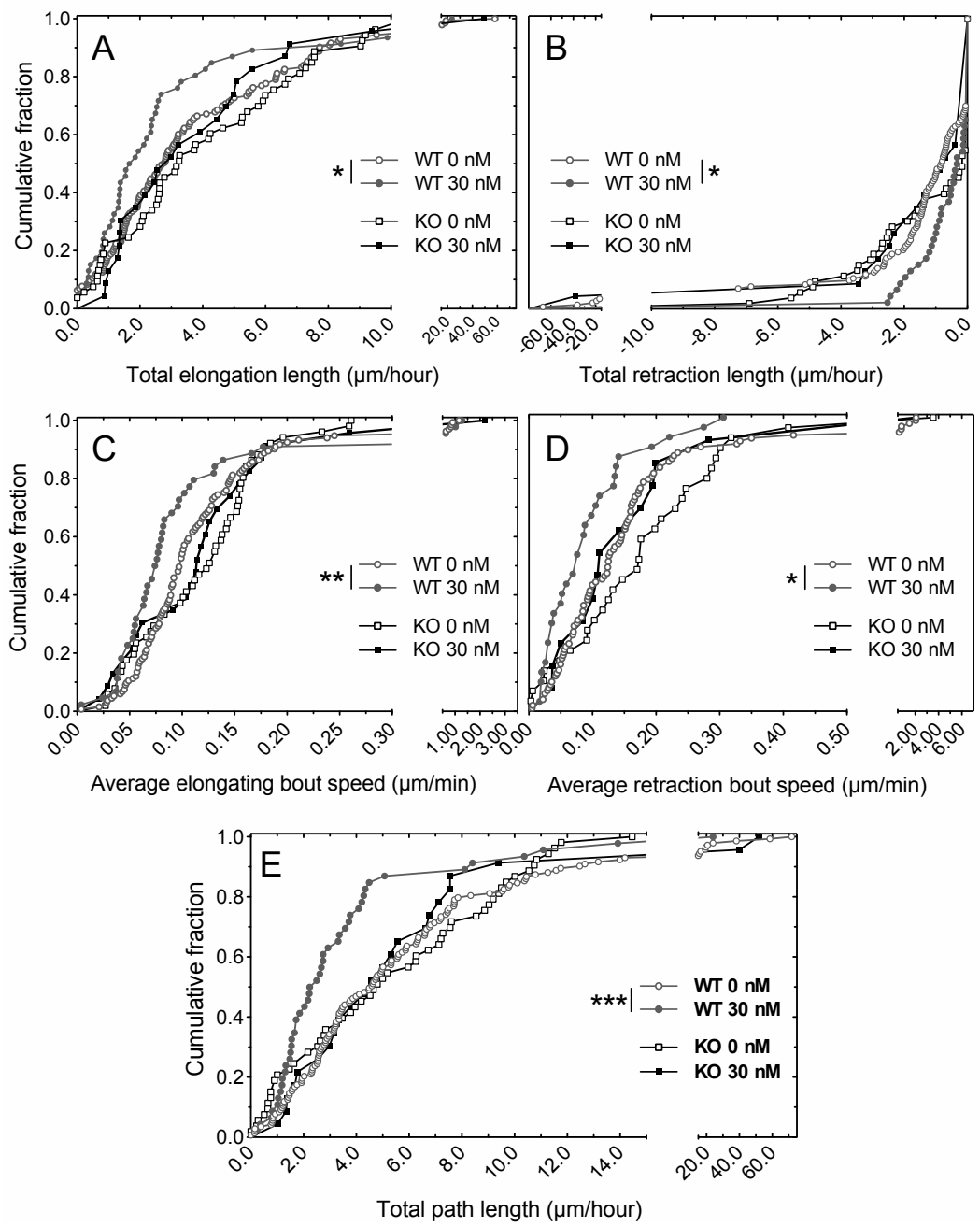

Figure 2.9 Serotonin attenuates dendritic growth cone dynamics via Htr1a. Quantification of dendritic growth cone elongation, lingering, and retraction bouts by time-lapse video microscopy following 12–16 h treatment with serotonin (30 nM) or vehicle (0 nM). 5–HT treatment was associated with a significant (**A**) decrease in total elongating (p= 0.021) and retraction (**B,** p= 0.024) length, (**C**) decrease in elongation (p= 0.002) and retraction (**D**, p= 0.027) bout speed, and (E) reduction in total displacement path length (p= 0.000). No significant effects of serotonin were seen in cultures from *Htr1a*^{KO} mice (KO), although there was trend for decreased retraction speed in KO growth cones. Plots represent cumulative frequencies (WT: N = 143–46; KO: N = 56–49 DGCs from 9 and 6 cultures, respectively; *: $p < 0.05$, **: $p < 0.01$, ***: $p < 0.001$, Kolmogorov-Smirnov test.

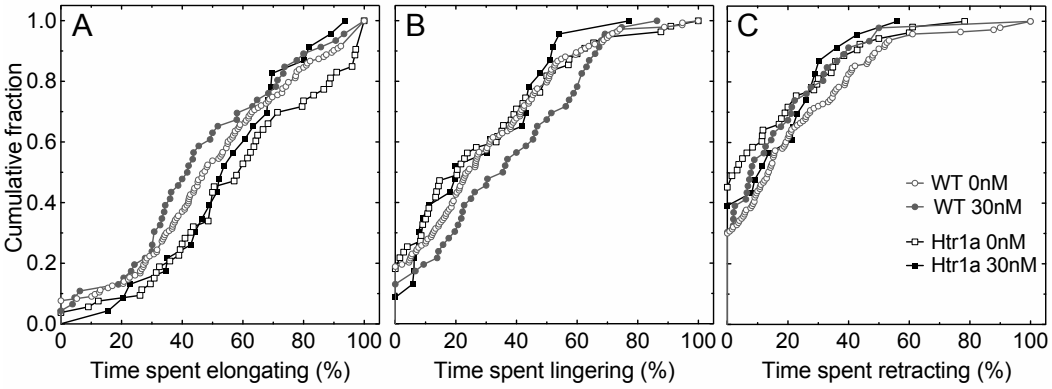

Figure 2.10 Frequencies of elongation, lingering, and retraction time of imaged dendritic growth cones. Quantification of dendritic growth cone elongation, lingering, and retraction bouts by time-lapse video microscopy following 12–16 h treatment with serotonin (30 nM) or vehicle (0 nM). Total time spent elongating (**A**), lingering (**B**), and retracting (**C**) was not significantly different between 5-HT and vehicle treated cultures in both WT and *Htr1a*$^{\mathrm{KO}}$ mice (KO) (WT, WT: N= 143–46; KO: N= 56–49 DGCs from 9 and 6 cultures, respectively).

decrease in the relative amounts of polymerized and unpolymerized in actin fractions from WT hippocampal cultures. On the other hand, serotonin treatment did not affect the F/G actin ratio in *Htr1a*$^{\mathrm{KO}}$ cultures (Figure 2.11).

Since this approach cannot measure direct effects of serotonin on actin polymerization at the level of the DGC, we labeled the cells with fluorescent-conjugated phalloidin, a phallotoxin that binds specifically at the interface between F-actin subunits, locking adjacent subunits together. Given the high contents of F-actin in the growth cone when compared to dendritic shafts, phalloidin can be used as a specific growth cone marker [e.g., 98, 223 and data not shown]. After a 1 min treatment, 5–HT caused a reduction in F-actin at the level of DGCs and quantification of phalloidin binding revealed a significant reduction of DGCs' F-actin in wild-type (p= 0.000, Figure 2.12–A), but not in *Htr1a*$^{\mathrm{KO}}$ neurons (p= 0.4870, Figure 2.12–B), corroborating previous analysis. In addition, morphometric analysis of DGCs (Section 4.6 and Table 4.4) revealed changes in growth cone shape that paralleled changes in phalloidin mean intensities. We have analyzed three shape descriptors: circularity, compactness and shape factor. Circularity (also known as 'form factor') and compactness are related and describe relationships between area and perimeter, both varying from 0 (infinitely elongated polygon) to 1 (perfect circle) (Table 4.4) . Essentially, they differ in the fact that circularity considers the complexity of the perimeter of the object, so e.g., a round cell covered in microvilli will maintain a high compactness value, but a low value of circularity). Shape factor is the relationship

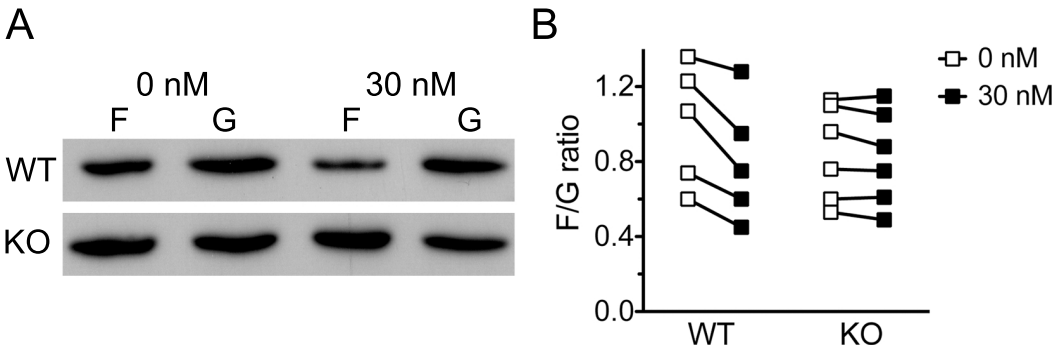

Figure 2.11 Serotonin promotes actin depolymerization in cultured cells via Htr1a. **A** Representative Western-blot of F/G-actin fractions from WT and *Htr1a*^{KO} (KO) in cultures stimulated for 3 minutes with serotonin. **B** Quantification of F/G-actin ratios from six independent protein extractions depicting the 5–HT-induced decrease of F/G-actin ratio in WT but not in KO cultures ($p = 0.0625$, Wilcoxon signed rank test). On the plot, each connected point represents a matched replicate (N: WT= 2, KO= 3).

between perimeter and area and has the minimum value of $2\sqrt{\pi}$ (perfect circle). In cultures from wild-type, but not knockout mice serotonin treatment (30 nM vs. 0 nM) caused a significant decrease in DGCs' circularity ($p < 0.0001$), shape factor ($p < 0.0001$), perimeter ($p < 0.0001$), maximum caliper length ($p = 0.0021$), and perimeter ($p < 0.0001$, Table 2.2). None of these measurements were altered by 5-HT in KO growth cones. On the other hand, compactness that was not altered in WT DGCs, was slightly increased in KO treated cells ($p < 0.005$, Table 2.2). In addtion, no change was seen in total DGC area in any of the groups ($p = 0.1694$, Table 2.2)

Together, these results suggest that serotonin acts via Htr1a to reduce polymerized actin in the growth cone changing its shape. In addition it is possible that the local effects of serotonin on DGCs' anatomy may be related to its motility behavior, and thus its physiology.

2.5 Behavioral Analysis Of Dbl;Htr1a Double Knockout Mice

Cortical neurons of *Dbl*^{KO} mice RhoGEF Dbl [92] display defective dendritic elongation. Given that this is one of the few described mutations interfering specifically with dendritic maturation (Chapter 1) we have decided to study the role of Dbl in dendritogenesis in the context of the dendritic phenotype of *Htr1a*^{KO} mice.

Preliminary data obtained from a group of single *Dbl*^{KO} animals and WT litter-

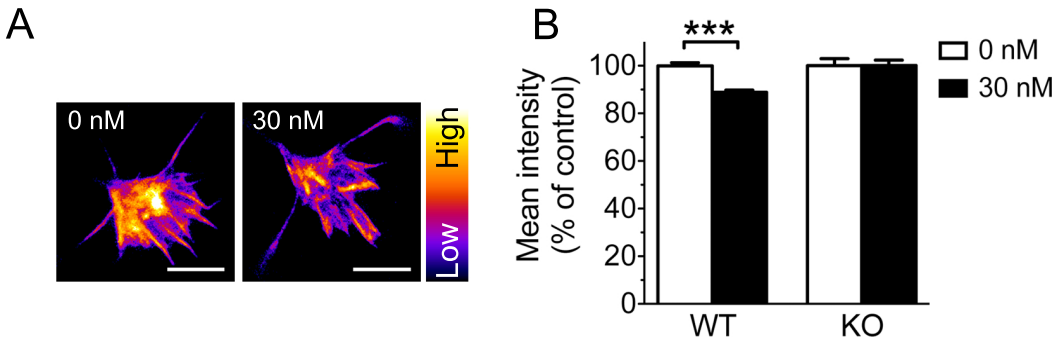

Figure 2.12 Serotonin promotes actin depolymerization in dendritic growth cones via Htr1a. **A** Representative phalloidin staining of dendritic growth cones from WT cultures treated with serotonin (30 nM) or vehicle (0 nM). Images are pseudo-colored with a warmer hue indicating higher signal intensity. Scale bar: 5 µm **D** Quantification of phalloidin staining revealing a significant decrease ($p < 0.0001$, Kruskal-Wallis test) in filamentous actin in serotonin vs. vehicle treated samples from WT, but not KO cultures. (WT, $N = 223$–265; KO, $N = 130$–170; 2 independent cultures per genotype) On the plot, each connected point represents a matched replicate (N: WT$= 2$, KO$= 3$).

Table 2.2 Morphometric parameters of phalloidin-stained DGCs. Growth cones from *Htr1a*^{KO} cells are resistant to morphological changes induced by acute serotonin treatment. Shape descriptors are described in detail on Table 4.4. Values are expressed as mean ± SEM. (Kruskal-Wallis test: *: $p < 0.05$, ***: $p < 0.0001$; WT, $N = 223$–265; KO, $N = 130$–170; 2 independent cultures per genotype).

	WT			KO		
	0 nM	30 nM		0 nM	30 nM	
Area (µm^2)	30.78 ± 1.01	33.58 ± 1.21	n.s.	30.05 ± 1.31	32.83 ± 0.98	n.s
Circularity	0.4395 ± 0.01	0.3577 ± 0.01	***	0.3700 ± 0.01	0.3572 ± 0.01	n.s.
Compactness	0.6622 ± 0.01	0.6631 ± 0.01	n.s.	0.6166 ± 0.01	0.6504 ± 0.08	*
Feret ⌀ (µm)	11.26 ± 0.39	9.742 ± 0.19	***	9.945 ± 0.24	9.805 ± 0.23	n.s.
Perimeter (µm)	31.18 ± 0.90	36.66 ± 1.04	***	33.30 ± 1.04	35.22 ± 1.15	n.s.
Shape factor	5.714 ± 0.09	6.429 ± 0.11	***	6.226 ± 0.12	6.502 ± 0.13	n.s.

mates suggested that alone, this mutation causes an overall increase in exploratory activity in the open field and elevated plus maze tests without affecting anxiety-related behavior (data not shown). Importantly, *Htr1a*^{KO} mice shows decreases in exploratory behavior in these tests. In order to strengthen our hypothesis that changes in dendritic arborization can modulate anxiety-related behaviors and are necessary for the behavioral phenotype of *Htr1a*^{KO} mice, we have analyzed the behavior of Dbl;Htr1a double knockout mice with the expectation that the behavioral phenotype of *Htr1a*^{KO} animals could be, at least, partially reversed by the *Dbl*^{null} mutation.

In order to assess whether the anxiety-related phenotype of *Htr1a*^{KO} mice could be modulated by the lack of Dbl, we performed open field and elevated plus maze tests in adult wild-type and *Htr1a*^{KO} mice in the presence or not of the *Dbl*^{KO} mutation (Tables 2.3 and 4.2). Strikingly, the significant decrease in time in center of the open field associated with the *Htr1a*^{KO} mutation in a wild-type background (2.13A–C; ANOVA[Htr1a×Dbl], $p = 0.0484$) was absent in *Htr1a*^{KO}*;Dbl*^{KO} littermates. In the elevated plus maze a more complex interaction was found between the two mutations (2.13D–F; Table 2.3). Decreased time spent in the central platform observed in *Htr1a*^{KO} animals was rescued by the introduction of the *Dbl*^{KO} mutation (2.13F; ANOVA[Htr1a×Dbl], $p = 0.0261$). On the other hand, double mutant animals spent the double amount of time in the open arms comparatively to single *Htr1a*^{KO} and single Dbl^{KO} (2.13D; ANOVA[Htr1a], $p = 0.0033$; ANOVA[Htr1a×Dbl], $p = 0.0051$). No differences were found between genotypes in the home cage locomotion test (2.13G), confirming that the decreased locomotion in the open field seen in *Htr1a*^{KO} mice reflected altered response to novelty.

Overall these results highlight a significant behavioral interaction between *Dbl*^{KO} and *Htr1a*^{KO}, with the behavioral phenotype of *Htr1a*^{KO} being absent in a *Dbl*^{KO} background.

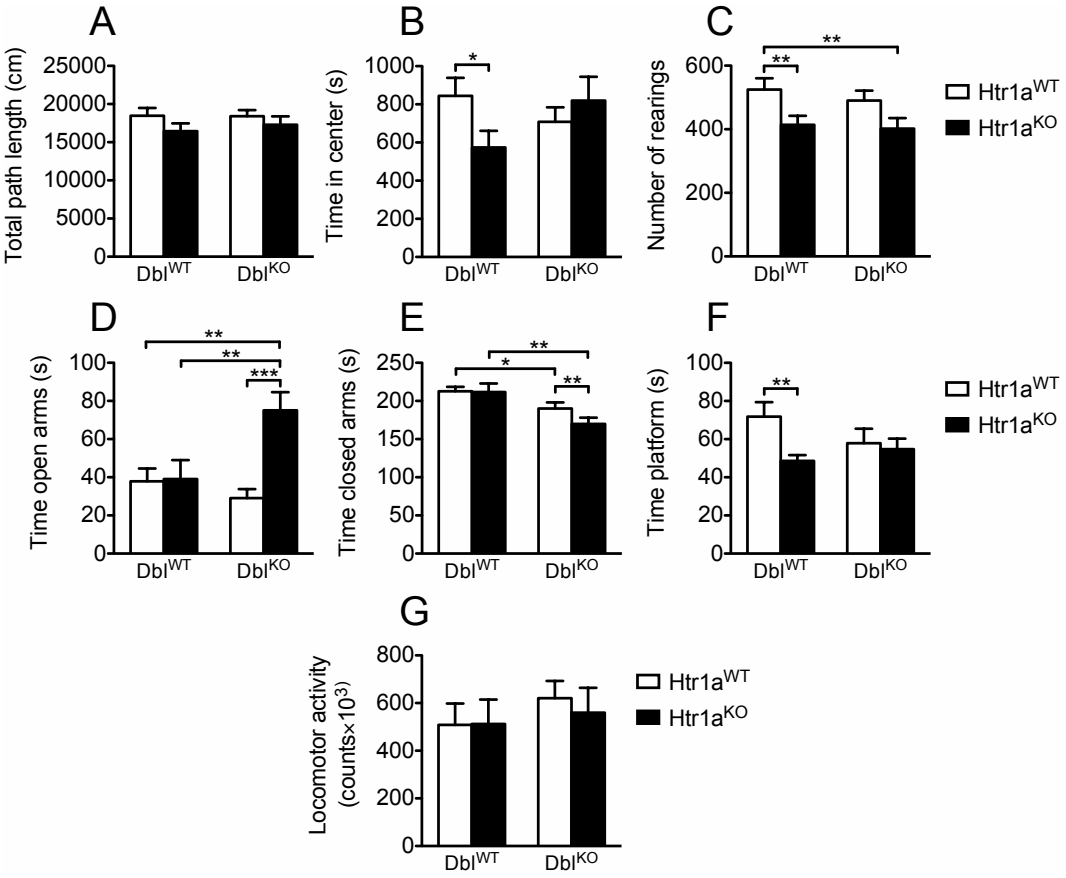

Figure 2.13 Behavioral characterization of *Dbl*;$^{\mathrm{KO}}$;*Htr1a*$^{\mathrm{KO}}$ mice. **A**–**C** Open field test: decreased center activity of *Htr1a*$^{\mathrm{KO}}$ animals is rescued by the *Dbl*$^{\mathrm{KO}}$ mutation (B). Vertical activity in maze was not reverted in double mutants (C). **D**–**F** Elevated plus maze: Avoidance of center platform is reversed in a *Dbl*$^{\mathrm{KO}}$ background (F) Open arms are the second most preferred region of the maze for double mutants (E). **G** Home cage activity: No differences between genotypes were found in locomotor activity (summed counts from 72 h of continuous sampling) (N= 5/6 animals per group). For simplicity only males have been included in this analysis. Description of the full cohort of animals is detailed in Table 4.2. Bars represent means ± SEM. Fisher's post hoc test *: $p < 0.05$, **: $p < 0.01$, ***: $p < 0.001$.

Table 2.3 Behavioral characterization of *Dbl*;^{KO};*Htr1a*^{KO} *mice.* Detailed results of the open field and elevated plus maze for the entire cohort of animals (described in Table 4.2). Values are expressed as mean ± SD. (ANOVA: ns: $p > 0.05$, t: $p = 0.05$, *: $p < 0.05$, **: $p < 0.001$).

	Htr1a$^{+/+}$;Dbl$^{+/+}$	Htr1a$^{-/-}$;Dbl$^{+/+}$	Htr1a$^{+/+}$;Dbl$^{-/-}$	Htr1a$^{-/-}$;Dbl$^{-/-}$	ANOVA		
					Htr1a	Dbl	Htr1a×Dbl
Open field (first 5 min)							
Total path length (cm)	2106.9 ± 590.0	1639.6 ± 357.7	2048.3 ± 437.2	1623.9 ± 427.4	**	ns	ns
Distance center (cm)	393.3 ± 185.4	226.4 ± 191.1	374.3 ± 169.2	243.2 ± 127.9	**	ns	ns
Distance border (cm)	1713.6 ± 463.9	1413.3 ± 263.2	1674.0 ± 388.5	1380.7 ± 398.8	*	ns	ns
% Path center	18.2 ± 6.3	12.9 ± 9.0	18.2 ± 7.2	15.1 ± 7.5	ns	ns	ns
Time center (s)	38.1 ± 21.3	29.7 ± 31.5	37.8 ± 21.2	26.4 ± 13.3	ns	ns	ns
Visits center	19.8 ± 8.5	13.2 ± 9.9	18.4 ± 7.5	12.3 ± 7.1	*	ns	ns
Total n. rearings	30.5 ± 10.9	26.4 ± 7.1	30.4 ± 12.7	20.6 ± 7.8	*	ns	ns
N. rearings center	1.2 ± 1.9	0.5 ± 1.0	1.5 ± 1.9	0.6 ± 0.7	ns	ns	ns
N. rearings border	29.3 ± 10.1	25.9 ± 6.7	28.8 ± 12.2	20.0 ± 8.0	*	ns	ns
Latency to enter center (s)	25.7 ± 27.7	50.3 ± 61.0	35.4 ± 29.0	62.0 ± 69.9	ns	ns	ns
Open field (1 hour)							
Total path length (cm)	18473.6 ± 3636.0	16456.0 ± 3521.3	18412.6 ± 3255.8	17294.2 ± 3274.0	ns	ns	ns
Distance center (cm)	4869.8 ± 2270.7	3688.7 ± 2056.4	4712.3 ± 1742.1	5027.8 ± 2239.9	ns	ns	ns
Distance border (cm)	13603.8 ± 2012.8	12767.3 ± 2143.6	13700.3 ± 2578.4	12266.4 ± 1714.3	ns	ns	ns
% Path center	25.5 ± 7.8	21.1 ± 9.8	25.3 ± 7.4	28.0 ± 9.5	ns	ns	ns
Time center (s)	844.5 ± 339.7	574.1 ± 301.4	708.7 ± 312.8	819.3 ± 37.6	ns	ns	*
Visits center	207.9 ± 83.4	165.8 ± 83.0	207.7 ± 65.7	204.6 ± 78.9	ns	ns	ns
N. rearings (total)	524.2 ± 129.0	414.1 ± 98.4	489.9 ± 128.9	401.9 ± 99.9	**	ns	ns
N. rearings (center)	122.5 ± 75.3	71.6 ± 42.8	102.6 ± 58.2	92.3 ± 52.8	ns	ns	ns
N. rearings (border)	401.8 ± 80.3	342.5 ± 68.6	387.3 ± 103.3	309.6 ± 77.9	**	ns	ns
Elevated plus maze							
Total path length	1063.5 ± 157.7	1075.3 ± 273.0	1018.8 ± 288.8	904.5 ± 352.4	ns	ns	ns
% entries in open arms	17.5 ± 5.4	16.0 ± 7.4	15.8 ± 6.2	24.2 ± 6.5	ns	ns	*
Distance in open arms	158.4 ± 91.5	139.0 ± 126.5	116.9 ± 78.4	228.3 ± 93.6	ns	ns	ns
% Distance in open arms	14.8 ± 8.1	13.3 ± 12.1	11.5 ± 7.4	26.3 ± 9.3	*	*	**
Distance in closed arms	863.4 ± 36.6	832.3 ± 42.6	846.9 ± 40.9	693.0 ± 39.3	**	ns	t
% Distance closed arms	82.6 ± 16.1	82.4 ± 25.1	87.2 ± 23.2	87.1 ± 35.0	ns	ns	ns
Time in closed arms	190.1 ± 28.9	211.7 ± 38.9	212.7 ± 23.5	169.8 ± 24.9	ns	ns	**
Time open arms	37.9 ± 24.4	39.1 ± 34.2	29.1 ± 19.0	75.1 ± 28.5	**	*	*
% Time open arms	12.6 ± 12.6	13.1 ± 11.4	9.7 ± 6.3	25.1 ± 9.5	**	*	*
Time center	71.8 ± 27.2	48.6 ± 10.6	57.9 ± 19.7	54.8 ± 16.6	*	ns	ns
Latency open arms	2.9 ± 4.5	30.7 ± 53.3	4.4 ± 6.2	5.3 ± 8.4	ns	ns	ns
Total entries	44.2 ± 9.9	37.5 ± 9.1	36.2 ± 10.8	37.4 ± 12.3	ns	ns	ns

Chapter 3

Discussion

Two major conclusions can be drawn from these findings. First, Htr1a is essential during the late postnatal period for the correct maturation of proximal apical dendrites of CA1 pyramidal neurons. Second, Htr1a is necessary for serotonin to reduce dendritic growth cone dynamics in vitro.

Htr1a Is Essential For Postnatal Ontogenesis Of CA1 Pyramidal Neurons

Pharmacological blockade of Htr1a function during the third through fifth postnatal week causes increased arborization of oblique dendrites of CA1 principal cells (Figures 2.2 and 2.3). The ability of systemic WAY100635 treatment during the third through fifth postnatal weeks to reproduce the dendritic phenotype of *Htr1a*$^{\mathrm{KO}}$ mice [42] is consistent with earlier studies showing that the same postnatal treatment is able to reproduce the behavioral phenotype of *Htr1a*$^{\mathrm{KO}}$ mice [207, 94].

At least three phenomena could justify the sensitive period for Htr1a function in the dendritic maturation of CA1 cells. First, activation of Htr1a receptors by endogenous serotonin is particularly high during this period. Second, in this period, Htr1a is selectively coupled to critical signaling pathways. Third, Maturation of dendrites is particularly sensitive to Htr1a activation during this period. The time-window in which we have blocked Htr1a, overlaps with the period of greatest maturation of the oblique plexus of CA1 pyramidal neurons as described in the rat (Figure 1.2, [164]). Thus, a plausible justification for the specificity of antagonist treatment is the fact that all other parts of the dendritic arbor have already matured at the time of Htr1a blockade. On the other hand, an absence of functional coupling of the receptor during the first and second postnatal weeks could spare the

basal and distal apical dendrites from Htr1a-dependent remodeling. Indeed, electrophysiological recordings show that functional coupling of Htr1a is inefficient in cortical slices taken from animals younger than P14 [20], despite robust expression of the receptor in these neurons at earlier times [83, 197]. Although hippocampal concentrations of serotonin increase over the first two weeks of life, and show a peak at P14 [145], *in vivo* electrophysiology studies suggest that tonic activity of Htr1a is absent in the adult hippocampus [86], which could justify the closure of the sensitive period for Htr1a function at the fifth postnatal week [94, 207].

In our hands, WAY100635-treated animals did not display increase anxiety-related behaviors in the open field test (Table 2.1) even though 8-OH–DPAT-induced hypothermic responses confirmed Htr1a blockade (Figure 2.1). Several reasons can argue for this result. First, it is possible that increased anxiety levels in WAY100635-treated may only appear in adulthood [94]. Second, since open field performance is vulnerable to genetic background modulation [e.g., 36, 51], the genetic background (Section 4.1.2) and the biased sex ratio of the tested animals could be modulating thigmotaxis levels in WAY100635-treated animals. Nevertheless, the fact that WAY100635-treated animals already display a dendritic phenotype at P35 but not yet a behavioral phenotype may be an indication that critical period of Htr1a function is sufficient to alter CA1 dendritic maturation but may not be sufficient to regulate behavior.

Compartmentalized Specificity Of WAY100635 Treatment

The morphological differences in CA1 pyramidal neurons after WAY100635 treatment are restricted to the *stratum radiatum*, the area that receives input from the Schaffer collateral terminals. However one cannot exclude an effect of WAY100635 treatment in other cells types, e.g., granular cells of the dentate gyrus that express high levels of Htr1a [177, 83]. In rats, it is know that neonatal (P3) serotonin depletion results in a significant decrease in the density of dendritic spines of dentate granule cells with how affecting dendritic branching [225, 224]. Following 5–HT depletion with parachloroamphetamine (PCA), pups treated with daily injections of NAN-190, another Htr1a antagonist, display comparable loss of dendtric spines in granular cells to that obtained after neonatal PCA. Interestingly, this loss is permanent providing further evidence that the first two postnatal weeks may represent a critical period for the action of 5–HT on the developing hippocampus [224]. Thus,

it is possible that WAY100635 treatment could also alter spine density in granular cells.

Serotonin Acts Through Htr1a To Reduce Dendritic Growth Cone Dynamics

In the absence of Htr1a, serotonin is not able to induce actin depolymerization (Figures 2.12 and 2.11) and reduce DGC motility (Figures 2.9 and 2.10). Together these findings suggest that Htr1a functions to restrict DGC dynamics and dendritic arborization by directly promoting depolymerization of actin in the growth cone. In this sense, these studies support a cell autonomous role for Htr1a in moderating actin polymerization and dendritic growth. Although we cannot completely rule out indirect effects of serotonin mediated by Htr1a located on other cell types, the rapid changes in filamentous actin we observe in DGCs in culture (Figures 2.12) argue for a cell autonomous effect. On the other hand, it is not know whether Htr1a is expressed at DGCs or if all hippocampal cells express the same levels of Htr1a. In cultured cortical neurons, e.g., it is know that a low number of cells present significantly higher levels of Htr1a binding sites that the majority of cultured cells [197], a finding that is not obvious from *in vivo* autoradiograms [83]. Nevertheless, the intercellular variation of Htr1a expression is randomized in our experiments, and should be unrelated to our findings.

An appealing hypothesis arises from the finding that serotonin significantly suppresses DGC extension and retraction: that both dendritic growth and dendritic pruning could be affected in *Htr1a*$^{\mathrm{KO}}$ animals. During ontogenic development, neurons elaborate exuberant dendritic arbors that later, will require elimination of non-specific connections (see Chapter B), a process that seems to occur (as described in axons [e.g., rev. in 126]) either by removal of terminal branches or by pruning of collateral branches (Wallerian degeneration). Pruning occurs in the reorganization of the nervous system of insects during metamorphosis [e.g., 101] and in mature neurons of the mammalian CNS. An illustrative example was given by repeated imaging of single identifiable neurons revealing that dendritic branching patterns are significantly changed over the course of a few months in adult mice [169]. These alterations may reflect changes of neural circuits in response to learning and experience, and they must involve both destructive and constructive mechanisms. In this speculative scenario the observed *in vitro* retraction could be associated to Wallerian degeneration of dendrites, and thus *Htr1a*$^{\mathrm{KO}}$ animals could lack the ability to

prune unspecific processes. Recent molecular studies of dendritic branching seem to be consistent with this working model. The Rho family of small GTPases, which are important regulators of actin polymerization, are important for controlling different aspects of dendritic development [e.g., rev. in 125]. *Xenopus* tectal neurons expressing constitutively active Rac experience an increase in both sprouting and retraction rates [116], which results in a high turnover rate of dendritic branches. In addition, dominant negative Rac has the opposite effect in branching turnover rate, at least in retinal ganglion cells [216]. This hypothesis could be tested by a detailed *in vivo* morphometric analysis of *Htr1a*$^{\mathrm{KO}}$ animals through the first five weeks of postnatal development.

Regulation of Cdc42 and Rac1 by Htr1a activation

One aspect that is not addressed in this thesis is the molecular cascade that starting from Htr1a activation reaches the polymeraztion machinery of the actin cytoskeleton. Htr1a is a $G_{i/o}$–linked GPCR that exhibits coupling to several signaling pathways, including membrane hypopolarization by activation of GIRK channels and reduction of cAMP levels by inhibition of adenylyl cyclase. Recently, it has been shown that *Htr1a*$^{\mathrm{KO}}$ mice as well as wild-type mice treated during postnatal development with WAY100635 show increased auto-phosphorylation of αCaMKII in the CA1 region of the hippocampus. These findings are consistent with a increase of adenylyl cyclase activity in the absence of Htr1a [35]. Both cAMP and CaMKII signaling are important regulators of actin dynamics in neurons [67, 193, 221, 223], suggesting that this signaling pathway may also be critical for the dendritic phenotype of *Htr1a*$^{\mathrm{KO}}$ mice.

Both *in vivo* and *in vitro* genetic studies have shown that activation of Rac and Cdc42, known cytoskeletal regulators [17, 31, 78, 99, 181, 205, 229], promotes dendritic growth, whereas activation of RhoA either inhibits growth or promotes retraction [rev. in 116, 117]. Given the facts that *in vitro*, Dbl is known to activate mainly Rho and Cdc42 and that dendritic elongation is impaired in *Dbl*$^{\mathrm{KO}}$ mice, it is possible that Dbl acts via Cdc42 to modulate dendritic growth. Since cAMP has been shown to stimulate Cdc42 [61] we had hypothesized that Htr1a could also modulate Cdc42. To test this, we have performed 'pull-down' experiments on hippocampal lysates of *Htr1a*$^{\mathrm{KO}}$ and *Dbl*$^{\mathrm{KO}}$ mice (at P21), using a GST-tagged PAK-PBD domain that has affinity for both active forms of Cdc42 and Rac1. Unfortunately, we were not able to obtain consistent and reproducible baseline levels of both Cdc42-GTP and Rac1-GTP among *Htr1a*$^{\mathrm{KO}}$, *Dbl*$^{\mathrm{KO}}$ and *Htr1a*$^{\mathrm{KO}}$*;Dbl*$^{\mathrm{KO}}$

double mutants (data not shown). Such variability has already been described in immunoprecipitations performed in brain extracts from Dbl^{KO} [E. Hirsch, personal communication], which suggests that *in vivo* detection of activated RhoGTPases is problematic. Since activation of small GTPases is not expected to be synchronous *in vivo*, we have repeated the same experiments *in vitro*, upon 5–HT stimulation. However, similar results were obtained in cultured neurons challenged with serotonin (similar treatment as the one used for actin fractionation, Section 4.3.2; data not shown). Given the non reproducibility of these immunoprecipitations, we were not able to state any conclusion on the regulation of Cdc42 and Rac1 by serotonin-dependent signaling. Furthermore, it is also possible that other members of the vast family of small Rho GTPases [rev. in 181] could be implicated in Htr1a signaling.

Since several mechanisms could explain the epistatic relationship between $Htr1a^{null}$ and Dbl^{null} mutations, it is not clear how to interpret the behavioral interaction between Htr1a and Dbl. First, it is not known if exuberant arborization of CA1 cells is absent in double mutants. Second, and assuming that Dbl and Htr1a could interact biochemically, it is not know if the behavioral interaction of Dbl and Htr1a is due to cell-autonomous expression of both molecules, or a cause of Dbl generalized expression [226]. Morphometric analysis of $Htr1a^{KO}$ animals overexpressing Dbl specifically in CA1 principal cells, could be used to address this question.

Growth Cone Dynamics May Reflect Remodeling Of Hippocampal Circuitry

The results obtained *in vitro* suggest that a relatively modest decrease (≈10%) in actin polymerization in the growth cone (Figures 2.12) is associated with decreased motility of DGCs. It is known that inhibiting actin polymerization and myosin motors prevents axon retraction [2, 199], which suggests that retraction of growth cones is an active process that requires complex actin dynamics. Our *in vivo* data, in turn, suggest that a suppression of DGC motility can significantly influence the elaboration of dendritic arbors. All together, our results support a direct link between DGC dynamics and the wiring of neural circuitry, suggesting that a modest suppression of DGC motility can produce a highly selective change in dendritic architecture if it occurs during a restricted time in development. If changing dendritic growth cone dynamics alone is able to drive permanent changes in the architecture of the dendritic plexus, then powerful cell-autonomous programs that determine dendritic growth must exist in the developing brain. Thus, it seems legitimate to

predict that the study of fundamental processes of cell motility in the context of the developing CNS will certainly allow a better better understanding of how neuronal networks are formed.

Chapter 4

Material And Methods

4.1 Mice

Animal experiments were performed according to European Molecular Biology Laboratory and Italian guidelines for ethical animal treatment following authorized protocols.

4.1.1 Husbandry

Unless stated all animals were maintained in a congenic C57BL/6J background (*Htr1a*^{KO} mice were back-crossed to the 6th generation from a 129S6/SvEvTac;C57-BL/6J;CBA mixed background [83]). Animals were weaned at 3–4 weeks (P 21). housed in same-sex groups of 3–5 per cage with pellet food and water *ad libidum*, in a room with controlled temperature and humidity ($21 \pm 0.5\,^{\circ}$C, 55–75%), on a 12 h light/dark cycle (lights off at 19 h:00 m). Tail biopsy and ear-tagging were performed at weaning age.

4.1.2 Breedings

Behavioral Experiments

Breedings were performed in heterozygocity. Fathers were removed one week before parturition and mothers and offspring were left undisturbed for the first week.

Tissue Culture

Pups used for dissociated hippocampal cultures were provided through homozygous breedings, in trios of two females and one male kept present at birth.

In Vivo Pharmacology

To avoid pup rejections after mini-pump implantation mothers of a 129S6/SvEv-Tac;C57BL/6;CBA mixed background [83, 94] were used. Single-housed females were crossed to Thy-1-M-EGFP homozygous males (Section 4.1.3). Males were removed after a positive plug check and mothers were left undisturbed in the first week after parturition.

4.1.3 Genotyping

Genotyping By PCR

Tail fragments (stored at -20 °C) were thawed at RT, digested in 200 µL of digest buffer (50 mM Tris−HCl, pH 8.0; 1 mM EDTA, pH 8.0; 20 mM NaCl; 1% SDS; 1 mg/mL proteinase K) and incubated at 55 °C until tails were thoroughly disintegrated. Digests were removed from heat and tail DNA was extracted by addition of 200 µL of equilibrated phenol/chloroform (1:1) solution. Tubes were vortexed and centrifuged for 10 min at 10,000 rpm at 4 °C. 80 µL of the upper phase were transferred into a flat-bottom 96-well plate and DNA was precipitated by addition of 160 µL of cold 100% ethanol. The plate was left for 5 min at RT without agitation and then was rapidly inverted onto paper to remove ethanol and let air dry for 10–15 min. Precipitated DNA was re-suspended in 20 µL of double-distilled sterile H_2O. 1.5 µL were added to 24 µL of PCR reaction buffer (0.2 mM dNTPs; 10 mM Tris−HCl, pH 9.0; 50 mM KHCl; 1.5 mM $MgCl_2$; 0.1 mg/mL BSA; 1 µM of each genotyping primer; 0.04 U/µL Taq Polymerase). PCR products were resolved by electrophoresis on 2% agarose gels [in TAE (Tris–Acetate–EDTA) buffer with 0.5 µg/mL ethidium bromide, ran at 80–150 V , constant current]. Table 4.1 describes primer sequences and respective PCR thermo-cycles.

Genotyping By Flow Cytometry

In order to identify homozygous Thy1-M-GFP animals, blood (100–150 µL) from the progeny of heterozygous transgenic animals was collected from the vein tail in a 1.5 mL tube containing 10 µL 0.5 M EDTA. Erythrocytes were lysed in 14 mL of 'Gay solution' [(in mM): 155 NH_4Cl, 10 $KHCO_3$] for 10–15 min at RT and cells spun down for 5 min at 1200 rpm. Pellet was re-suspended in 3 mL of ice cold PBS–1% FBS and subjected to flow cytometry analysis on a FACSCanto™ I system (Becton Dickinson, San Jose, CA, USA). After acquiring 1.5–2$\times 10^4$ cells, three fluorescence profiles concerning the proportion of GFP^+ cells were routinely distinguishable:

Table 4.1 Oligonucleotide sequences and PCR cycles used for tail genotyping.

Locus	Sequence (5'→3')	Description	Temperature cycles
Dbl	a) aat acc acc caa gaa gca gc	With c) amplifies ≈350 bp of the WT allele	(1) 94 °C for 90 s
	b) ctg ctc ttt act gaa ggc tc	With c) amplifies ≈500 bp of the KO allele	94 °C for 90 s (2) Ta^*= 65 °C for 90 s [2×] 70 °C for 90 s
	c) atg act acc tcc tcc act tc	Common primer	(3) *(2)* with $Ta = 61$ °C [2×]
Htr1a	d) ggg cgt cct ctt gtt cac gta g	With f) amplifies ≈750 bp of the WT allele	(4) *(2)* with $Ta = 58$ °C [10×]
	e) aag ggc aaa agt gag tat ggt g	With f) amplifies ≈340 bp of the KO allele	(5) *(2)* with $Ta = 54$ °C [20×]
	f) cag tct cta gat ccc ctc cct t	Common primer	(6) 94 °C for 10 min
Thy1-M-GFP	g) aag ttc atc tgc acc acc g h) tcc ttg aag aag atg gtg cg	Together amplify ≈170 bp of the transgene	(1) 94 °C for 90 s 94 °C for 90 s (2) $Ta = 65$ °C for 90 s [35×] 70 °C for 90 s
	i) cta ggc cac aga att gaa aga tct j) gta ggt gga aat tct agc atc atc c	Together amplify ≈350 bp of the Il2 locus (control reaction)	(3) 94 °C for 10 min

animals having less then 0.03% of GFP^+ cells (WT mice), animals with 2–6% (heterozygous mice) and animals with 8–10% positive cells[2] (later confirmed as homozygous transgenic mice by WT back-crossings).

4.1.4 Osmotic Mini Pump Implantation

Osmotic minipumps (0.20 mg/h, Model 1002, Alzet, Cupertino, CA, USA) were implanted subcutaneously to deliver WAY100635 (Sigma-Aldrich, St Louis, MO, USA) or saline (0.9% NaCl) continuously for twenty one days. Pumps were filled with 7.1 mg/mL (1.5 mg/h) WAY100635 as estimated to achieve a constant dose of 0.3 mg/kg of body weight. Drug dosage was adjusted to the average weight of animals at P 21. Pumps were soaked overnight in sterile saline solution at 37 °C to assure steady-state pumping following implantation. Before surgery, all pups were removed from the dam, placed in a tray containing home cage bedding and kept on a heating pad. Mice were anesthetized by halothane inhalation (Merial Animal Health, Harlow, UK); a short (≈ 0.5 cm) transversal cut was performed onto the skin in the dorsal thoracic area, and pumps were subcutaneously implanted and wounds were closed with a 9 mm stainless steel clip (Stoelting, Wheat Lane, IL, USA).

[2]Further immunostaining analyzes revealed that, in homozygous mice, 13.5% of all GFP^+ live cells were $CD3^+$. Of these, 70% were $CD8^+$ (12.5% $CD8^+$ $CD4^+$ double positive) while 90% of $CD8^-$ were also CD4 negative (data not shown).

4.1.5 8-OH–DPAT Induced Hypothermia

Test was performed immediately after the open field test (page 45), with single housed animals. 8-OH–DPAT (Sigma-Aldrich), was dissolved in saline (0.9% NaCl) and administered subcutaneously at a concentration of 0.3 mL/kg of body weight.

Temperature was was recorded in 10 min intervals with a digital rectal thermometer (Bioseb, Bordeaux, France), and after two baseline recordings, 8-OH–DPAT solution was injected (5 mL/kg of body weight) into the scruff of the neck of the animal using 1 mL syringe with a 27-gauge needle (Becton Dickinson, Franklin Lakes, NJ, USA).

4.1.6 Behavioral Procedures

Testing colonies were transferred to behavioral facilities one week in advance under similar husbandry conditions. Behavioral tests were sparsed by one-week intervals to reduce inter-test interactions and performed in the order listed below. Prior to testing, mice (8–10 weeks old) were habituated to the testing room (illuminance: 15 lx) at least for a period equivalent to the duration of the test. After testing, mice were weighted, identified and held in a holding cage until all home littermates had been tested.

Open Field

Mice were placed into a 50×50 cm gray plastic arena with 45 cm high walls for 60 min. Locomotion data were collected by a video-tracking system (TSE, Bad Homburg, Germany), and rearing activity assessed by an infrared detection system. Center region was defined as the central 26×26 cm area.

Elevated-Plus Maze

Mice were placed into the central platform (5×5 cm) of a gray plastic maze facing toward an open arm (open arm: 30×5 cm, surrounded by a 0.25 cm-high border; closed arms: 30×5 cm, surrounded by 15 cm high walls). The entire apparatus was elevated 45 cm above the floor. Locomotion data were collected for 5 min by a video-tracking system (TSE).

Home Cage Locomotion

Mice were place individually into novel cages with fresh bedding with food and water provided *ad libitum*. Gross locomotor activity was binned every 10 min over

Table 4.2 Description of *Dbl*;^{KO};*Htr1a*^{KO} behavioral group. *Dbl*^{KO} mice [92] and *Htr1a*^{KO} mice [83] were maintained in a C57BL/6J genetic background. Breedings and behavioral tests were performed as described in Section 4.1.6. A: age (days) immediately after the open field test (mean ± SD).

				Dbl		
		$^{+}/_{Y}$	$^{-}/_{Y}$	$^{+}/_{+}$	$^{+}/_{-}$	$^{-}/_{-}$
♂	$^{+}/_{+}$	A: 72.5 ± 11.1 *N*= 13	A: 70.1 ± 11.4 *N*= 17			
	$^{+}/_{-}$	A: 69.8 ± 9.9 *N*= 37	A: 72.6 ± 10.1 *N*= 24			
	$^{-}/_{-}$	A: 71.4 ± 10.3 *N*= 12	A: 70.0 ± 12.0 *N*= 9			
Htr1a						
	$^{+}/_{+}$			A: 65.5 ± 15.1 *N*= 2	A: 70.3 ± 12.3 *N*= 9	A: 70.1 ± 10.1 *N*= 19
♀	$^{+}/_{-}$			A: 72.5 ± 14.1 *N*= 6	A: 69.8 ± 10.2 *N*= 21	A: 70.0 ± 10.9 *N*= 19
	$^{-}/_{-}$			A: 72.5 ± 9.5 *N*= 2	A: 70.0 ± 9.8 *N*= 10	A: 71.1 ± 12.9 *N*= 2

a period of 72 h using an infrared detection system (TSE).

4.2 Dissociated Postnatal Hippocampal Cultures

Protocol was performed as described by others [11, 102, 227]. Glass coverslips (12 mm diameter) were pre-washed overnight in 1 N HCl followed by several 100% ethanol washes. After a flame sterilization, coverslips were placed in 24-well plates and coated with 40 µL of 1:25 Matrigel™ (Becton Dickinson, San Jose, CA, USA) diluted in Neurobasal™ medium without phenol red and placed for 1–6 h at 37 °C. For time-lapse experiments 35 mm cell dishes with a glass-bottomed surface were used (MatTek, Ashland, MA, USA). In this case, Petri dishes were HCl treated for 15 min inside a laminar flow hood, washed thourougly with PBS, rinsed with deionized water, air-dried, and coated as above described.

Hippocampi from a litter (typically 4–6 pups) were dissected from P2–P2.5 pups under a stereoscope on a laminar flow cabinet and placed in a ice-cold HBSS-based dissecting solution [(in mM): 161 NaCl, 5.0 KCl, 2.9 $CaCl_2$, 5.0 HEPES, 5.5 glucose, 0.53 $MgSO_4$ and 0.0056 phenol red, pH 7.4] with 100 µg/mL gentamicin. Tissue was further cleaned from cortex and *corpus callosum*, fragmented in smaller pieces (4–5 each) and incubated with papain (Worthington Biochemical, Lakewood, NJ, USA) [20 U/mL in 10 mL of dissecting solution supplemented with (in mM, purchased from Sigma-Aldrich): 1.7 L-cysteine·HCl, 1 $CaCl_2$, and 0.5 EDTA] for 20–30 min at 37 °C. Digestion was interrupted by replacing the solution with 10 mL of a

'stop' solution [MEM with Earle's salts (without L-glutamine) supplemented with: 20 mM D-glucose, 5% FBS, 2.5 mg/mL BSA (Sigma-Aldrich) and 2.5 mg/mL soybean trypsin inhibitor (Sigma-Aldrich)]. The tissue was again centrifuged (2 min at 1,000 rpm), eluted in 4 mL of stop solution and triturated with a fire-polished Pasteur pipette. Cells were then collected at 5,000 rpm (5 min) and re-suspended in culture medium[227] [Neurobasal medium without phenol red, 2× B-27 serum-free supplement and 2 mM Glutamax-I™]. After determining cell concentration with a hemocytometer, final volume was adjusted so that 100,000 cells could be plated in 1 mL per coverslip/1.5 mL per glass-bottomed dish.

Cells were grown on a humidified tissue culture incubator at 37 °C, 5% CO_2 and half of media was replaced the day after plating (DIV 1), at DIV 3 and concomitantly every three days. At DIV 3, FUDR–uridine (Sigma-Aldrich) was added to the replacement media to inhibit glial proliferation to a final concentration of 90 ng/mL–1.8 µM, respectively. Unless stated, all reagents were purchase from Invitrogen, Carlsbad, CA, USA.

4.2.1 5–HT Treament

Serotonin (5–HT·HCl, Sigma-Aldrich) was prepared fresh in Neurobasal (vehicle) from frozen stock solutions and applied in a volume of 100 µL/mL of culture volume. Duration of treatments was as follows: phalloidin stainings: 1 min; F-/-G ratio measurements: 3 min; timelapse experiments: 12–16 h before acquisition.

4.3 Biochemistry[3]

4.3.1 Western Bloting

Protein extracts were compounded with 5× loading buffer (Laemmli dye), heat denatured (5 min, 95 °C), spun down, resolved by SDS-PAGE (100–130 V, 1–1.5 h) and electrophoretically transferred onto a pre-equilibrated polyvinylidone difluoride (PVDF) membrane (Immobilon™, Millipore, Bedford, MA, USA) using a Mini Trans-Blot® transfer cell (Biorad, Hercules, CA, USA) at 4 °C. Membranes were then washed in TBS/0.05% Tween 20 (TBST), incubated in TBST/5% BSA (blocking solution) for 30 min, incubated with primary antibody (diluted in blocking solution) for 1 h, washed with TBST (3×5 min) and incubated with a horseradish peroxidase-conjugated secondary antibody (diluted in TBST). All incubations were

[3]Antibodies and affinity molecules used in these procedures are listed in detail on Table 4.3.

performed at room temperature. Unbound antibodies were washed with TBST (3–5×10 min), and chemiluminescence (ECL™, Amersham Biosciences, Uppsala, Sweden) detected in autoradiographic films (Hyperfilm™, Amersham Biosciences). Signals from scanned films were quantified using ImageJ [173].

4.3.2 F-/G-actin Separation

Protocol was adapted from McRobbie and Newell, 1983 [138]. On DIV 4–5 hippocampal cells were treated with serotonin for 3 min (Section 4.2), washed with PBS and placed on ice. Immediately after, 200 µL of ice-cold PHEM buffer [in mM: 60 PIPES, 25 HEPES, 10 EGTA, 2 $MgCl_2$, pH 6.9] with 0.5% TX-100 and plate was gently swirled for 1 min. Volume (containing G-actin) was collected in a 1.5 mL tube, and 200 µL of cell lysis buffer [in mM: 300 NaCl, 10 $MgCl_2$, 50 Tris pH 7.5; 2% IGEPAL] were added to the well. After thorough scraping with a sharp tool, volume (containing F-actin) was transferred into a new tube. Extracts were stored at -80°C until being processed side-by-side by Western blotting. Reproducibility of extractions was assessed by silver staining of gels reload with the same samples.

4.3.3 Immunoprecipitation

The activation of Cdc42 /Rac1 was determined by using an assay kits (BK034, Cytoskeleton, Denver, CO, USA). Cultured neurons were growth on 6 cm dishes, previously treated with HCl, in order to increase the efficiency of diluted Matrigel™ coating, and thus the attachment of neurons. One single dish was used for each determination. Protein extracts were reacted with GST-tagged p21 binding domain (PDB) of the Cdc42/Rac1 effector protein, p21 activated kinase 1 (PAK) in cell lysis buffer followed by the addition of 50% glutathione beads. Pelleted beads were collected after centrifugation at 7000 rpm for 3 min at 4 °C. The pellet was boiled in loading buffer and separated by 15% SDS-PAGE.

4.4 Histology[3]

4.4.1 Immunohistochemistry

Heterozygous Thy1-GFP-M mice were anesthetized with 2.5% avertin and transcardially perfused with 4% paraformaldehyde (PFA, Sigma-Aldrich) in 0.1 M phosphate buffer. Brains were removed from the skull and post-fixed overnight at 4 °C. Coronal

[3]Antibodies and affinity molecules used in these procedures are listed in detail on Table 4.3.

sections (200–250 µm) were cut on a vibratome (VT1000S, Leica Microsystems, Wetzlar, Germany), washed in PBST (1% Triton-X, 100 mM glycine in PBS), blocked with blocking buffer (2% BSA in PBST) for 1 h at room temperature, and incubated with an anti-GFP antibody (Table 4.3) diluted in blocking buffer for 4 h. Sections were then rinsed several times with PBS, incubated overnight a FITC-conjugated secondary antibody (Table 4.3), stained with DAPI for 20 min and mounted in gelvatol.

4.4.2 Immunocytochemistry

Cells were fixed in 4% PFA/PBS for 30 min and permeabilized for 10 min in PBS-0.2% TX-100. Cells were washed in 50 mM glycine (Sigma-Aldrich) in PBT (PBS-0.05% Tween 20), and incubated in blocking buffer (PBT-4% BSA) for 30 min. Primary antibodies were diluted in blocking buffer and incubated for one hour. After washing with PBS, fluorescent-conjugated secondary antibodies diluted in blocking buffer were incubated in the dark for 30 min. Nuclei were stained by including a dilution of DAPI in PBS in one of the final washing steps. After briefly dipped in water cover slips were mounted on glass slides in gelvatol.

4.4.3 Cytoskeletal Staining

Cells were fixed in 0.5% glutaraldehyde (Sigma-Aldrich) for 2 min followed by a secondary fixation in 0.1% glutaraldehyde for 20 min, pearmeabilized with 0.5% TX-100 (5 min) and washed twice (5 min each) [211]. PHEM buffer was used in all these steps. After sodium borohydride (Sigma-Aldrich) treatment (3× 10 min, 0.5% in PBS) to reduce background fluorescence from glutaraldehyde, cells were washed in PBS (3× 10 min), and incubated with phalloidin (Table 4.3) for 30 min. Cells were again washed three times with PBS and coverslips mounted as above described.

4.5 Image Acquisition

4.5.1 Time-Lapse Microscopy

Time-lapse videos were aquired on an inverted microscope (Axiovert 100 TV, Zeiss, Oberkochen, Germany) equipped with a ORCA-ER CCD camera (Hamamatsu Photonics, Hamamatsu, Japan) and a z-motorized stage (Nikon, Tokyo, Japan). Mi-

Table 4.3 Antibodies and dyes used for immunofluorescence and Western blotting.

Antibodies

Antigen [conjugate][a] (species)	Basic reactivity	Clone / Catalog N.	Supplier[b]	Dilution[c]
Actin (mouse)	Actin	C-4	CHMC	1 : 2000 (WB)
Cdc42 (donkey)	Cdc42 (not: Rac2, Rac3, RhoA, RhoB, RhoC, H-Ras)	ACD03	CTSK	1 : 800 (WB)
Dbl (rabbit)	C-terminus of Dbl (mouse and rat)	M-138	SCBT	1 : 200 (IC)
GABA (rabbit)	GABA	A2052	SGAL	1 : 100 (IC)
GFAP (rabbit)	Mammalian GFAP	AB5804	CHMC	1 : 200 (IC)
GFP (chicken)	WT and engineered GFP	GFP-1020	AVSL	1 : 500 (IH)
Map2 (mouse)	MAP2a and MAP2b	AP-20	SGAL	1 : 1000 (IC)
Rac1 (rabbit)	Rac1 (not: Rac2, Rac3)	ARC03	CTSK	1 : 800 (WB)
Synapsin I (mouse)	Mouse synapsin I	106 011	SYSY	1 : 1000 (IH)
Chicken IgY [FITC] (goat)	Chicken IgY	F-1005	AVSL	1 : 500 (IH)
Mouse IgG [A488/555/594] (goat)	Mouse IgG	A11008/ A21428	MP/I	1 : 100/200 (IC)
Mouse IgG [HRP] (sheep)	Mouse IgG	NA931	AMBS	1 : 2,000 (WB)
Rabbit IgG [Cy™3] (goat)	Rabbit IgG	711165152	JIMR	1 : 100/200(IC)
Rabbit IgG [HRP] (goat)	Rabbit IgG	NA9340	AMBS	1 : 10,000 (WB)
Sheep IgG [HRP] (donkey)	Sheep IgG	SG01	CTSK	1 : 25,000 (WB)

Dyes and high-affinity molecules

	Affinity	Catalog N.	Supplier[b]	Dilution [Stock][c]
Streptavidin [A488/594]	Biotin	S32355/6	MP/I	1 : 200 [2 mg/mL] (IH)
Phalloidin [A488]	Filamentous actin	A12379	MP/I	1 : 200 [300 U] (IC)
DAPI	DNA	D1306	MP/I	1 : 30.000 [5 mg/mL] (IC, IH)

[a] A: Alexa Fluor®; FITC: fluorescein isothiocyanate; HRP: horseradish peroxidase; Ig: immunoglobulin

[b] AVSL: Aves Labs (Tigard, OR, USA); AMBS: Amersham Biosciences (Uppsala, Sweden); CHMC: Chemicon (Temecula, CA, USA); CTSK: Cytoskeleton (Denver, CO, USA); JIMR: Jackson ImmunoResearch Laboratories (West Grove, PA, USA); MP/I: Molecular Probes/Invitrogen (Carlsbad, CA, USA); SGAL: Sigma-Aldrich (St Louis, MO, USA); SCBT: Santa Cruz Biotechnology (Santa Cruz, CA, USA); SYSY: Synaptic Systems, Göttingen, Germany

[c] (IC): Imunocytochemistry; (IH): Imunohistochemistry; (WB): Western blotting. Unless otherwise specified, probes were applied in PBS (IC and IH) and TBS (WB). Stock solutions prepared according to supplier's instructions

croscope was assembled on a custom-made humidified incubator with temperature and CO_2 control reproducing tissue culture incubator conditions (EMBL Workshop, Heildelberg, Germany). Z-stacks (3–5 slices, step-size: 1 µm) of random image fields (typically containing 1–2 somas) were acquired every 3 min for at least 6 h with a 40×, 1.3 NA oil lens using DIC illumination. Setup was controlled by MetaMorph® 6.2 software (Universal Imaging, Downingtown, PA, USA). On average, 3 video time-lapses were acquired per culture. Imaged plates were not re-imaged.

4.5.2 Confocal And Wide-Field Microscopy

Confocal images (assembled image tiles were used in some cases) were acquired on a TCS SP5 AOBS microscope (Leica Microsysystems). For Thy-1-M-GFP reconstructions images were acquired with a 20×, 0.7 NA lens (1.3×–2× digital zoom, 1–1.5 µm z-step. Wide-field images (phalloidin staining and immunocytochemistry experiments) were acquired in a DMRXA microscope (Leica Microsystems). For phalloidin imaging a 100× 1.4 NA lens was used.

4.6 Image Analysis

Unless stated all digital image processing was perfomed with ImageJ software[173] (v. 1.39–1.41), loaded with: `Action Bar`[4], `IJ Robot`[5], `Image5D`[6], `LOCI-bioformats`[7], `MtrackJ`[8], `NeuronJ`[140], `Sync Windows`[9] and other custom additions (Appendix D).

4.6.1 Map2 Immunostainings

Background was subtracted from acquired images, and total dendritic length was quantified using MetaMorph® software (v6.2, Universal Imaging, Downingtown, PA, USA). Total dendritic growth was defined as skeletonized outgrowth (corrected for diagonal lengths) associated with individual DAPI-stained nuclei. At DIV15, the high complexity of arbors difficult individual segmentation due to frequent overlapping of centrifugal processes. In these cases, processes were considered to be shared

[4] J. Mutterer, http://rsb.info.nih.gov/ij/plugins/action-bar.html
[5] G. Landini, http://www.dentistry.bham.ac.uk/landinig/software/software.html
[6] J. Walter, http://rsb.info.nih.gov/ij/plugins/image5d.html
[7] Open Microscopy Environment – Laboratory for Optical and Computational Instrumentation, University of Wisconsin, USA), http://www.loci.wisc.edu/ome/formats.html
[8] E. Meijering, http://www.imagescience.org/meijering/software/mtrackj/index.html
[9] J. Walter, http://rsb.info.nih.gov/ij/plugins/sync-windows.html

by neighboring cells, and linearized lengths averaged. At all time points only cells completely contained on the image field were considered.

4.6.2 DGCs Motility Analysis

Tracing And Bouts Extraction

Z-dimension of 4-D images was eliminated by automatic frame-by-frame choice of a best-of-focus plane. Images were assigned a unique number and filenames randomized. DGCs were then manually videotracked at a 200% magnification using `MTrackJ`. Paths were labeled by their forward/backward directionality and frames labeled with one of three tags (*elongating*, *retracting*, *lingering*) using keystrokes. Tracking was based on subjective criteria based on three general principles:

1. All DGCs on the image field were traced if visible (not growing above/under established processes) for at least three consecutive frames

2. Traces were terminated if untraceable for three consecutive frames. Most frequent causes of untraceability were due to: (1) fasciculation of growing processes; (2) extensions beyond image field boundaries; (3) obstruction by cell bodies and other cellular material and (4) failure of automatic camera focus

3. Multifid DGCs were considered as one structure unless clear divergent migration between lobes occurred

Tracking paths were divided into bouts defined as a continuous time stretch in which the DGC showed uninterrupted forward/backward directionality. Consecutive frames sharing the same motility tag were clustered according to the following criteria:

1. Inter-frame DGC displacement less than 0.15 µm (empirically determined in preliminary studies) was reset to 0 µm

2. Inter-frame DGC displacements sharing the same motility tag were summed, forming a *growth bout*: elongation bouts were arbitrarily assigned a positive displacement and retraction bouts a negative one

3. Single lingering frames interrupting two consecutive bouts sharing the same motility tag were assumed to reflect brief slowing of movement and flanking bouts were fused

The implementation of Bout extraction is summarized on Figure 2.6 and was performed using an *ad hoc* VBA script for Excel 11.5.2 (Microsoft, Redmont, WA, USA). This script – *Bouts extractor* – is highly specific to this analysis as it is limited to `MTrackJ` output files and the motility tagging above described. Unfortunately, it was written in a restricted obsolete proprietary language and a conversion to any other format (e.g., OOo Basic) would require a complete redesign of its modules. As a consequence, it is unlikely that this macro would be useful in any other context. For these reasons this script is not included in Appendix D.

4.6.3 DGS Morphometric Analysis

Background and dark current subtracted images were smoothed with a median filter (2 pixel radius) and thresholded. DGCs were then analyzed using ImageJ's particles analyzer controlled via a customized macro toolset (Appendix D – Section D.1). Morphological parameters are described in Table 4.4.

Table 4.4 Shape descriptors used in morphometric analysis of DGCs.

$\text{Circularity} = \frac{4\pi Area}{Perimeter^2}$	$\text{Compactness} = \frac{\sqrt{\frac{3}{4}\pi Area}}{Feret's\,diameter^a}$	$\text{Shape factor} = \frac{Perimeter}{\sqrt{Area}}$

[a] Caliper length: the largest distance between the first two parallel lines that enclose the particle without intersecting it (i.e. the longest distance between any two points along the ROI boundary).

4.6.4 Neuronal Reconstruction

After volume integration of tilling stacks with VIAS 2.2[180] cells were reconstructed using Neurolucida® (MicroBrightField, Williston, VT, USA). Sholl analysis [194], branch-point number, and segment length were determined using NeuroExplorer® (MicroBrightField). Oblique dendrites were defined as all processes branching from the apical trunk at a distance not greater then 2/3 of the apical trunk length. Similar results were obtained using a more subjective assessment of oblique dendrites defined as all diverging dendrites not part of the apical terminal tuft.

4.7 Statistical Analysis

Behavioral was analyzed by Analysis of Variance (ANOVA) followed by post-hoc comparisons using the Fisher's test in case of significance. For morphometric and biochemical experiments, normally distributed data (assessed by D'Agostino-Pearson and Shapiro-Wilk test) were analyzed for statistical significance using two-tailed Student's t-test. For data whose distribution did not appear to be normal Kolmogorov-Smirnov test (DGCs motility data), Wilcoxon rank-sum test (Western-blot experiments) or Mann Whitney test (phalloidin-staining experiments) were used. $p < 0.05$ was considered statistically significant (*: $p < 0.05$, **: $p < 0.01$, ***: $p < 0.001$). Analyzes were carried out using StatView® 5.0 (SAS Institute, Cary, NC, USA) GraphPad Prism® 5.0 (GraphPad, CA) and SPSS® 16.0 (SPSS, Chicago, IL).

Appendices

Appendices Foreword

The following chapters included in this part were not included in the main matter of this thesis for two main reasons. First, they either describe experiments that are not directly related with the ones earlier described. Second, they either refer to preliminary incomplete experiments or they describe too many technicalities that would overload the fluent reading of the previous Chapters. Nevertheless, they should not be interpreted as mere additional matter, but as complimentary material. This section is divided as follows:

Chapter A Describes the diOlistic methodology we have tried to implement to perform full 3–D reconstruction of CA1 pyramidal cells.

Chapter B Describes the behavioral characterization of animals that lack functional T cell receptors, as the starting point for a wider study of the role of MHC-I function on anxiety-related behaviors.

Chapter C Describes a expression of a transgenic mouse model that hopefully will provide insights on the cellular substrates required for hippocampal regulation of anxiety-related behaviors.

Chapter D Lists simple automated routines for digital imaging processing. They were created as a need for the imaging analysis described before and are presented as a tool to the community.

Appendix A

DiOlistic Staining Of Hippocampal Cells

> "The Golgi method (despite its unjustly exaggerated capriciousness) remains essentially the only approach to clarify the morphological types of neurons, along with their intercellular connections."
>
> Ramón y Cajal, 1910 [172]

Stainings providing single-cell resolution are critical for the study of neuronal function and circuitry, and have been historically challenging. Currently, there are several staining methodologies (reviewed in Table A.1) that provide single-cell resolution, in a 'Golgi-like' pattern from improved Golgi stainings [77, 171] to viral transduction or complex genetic systems in which Cre/loxP recombination is used to create a stochastic expression of multiple fluorescent proteins [122]. This chapter describes our attempts to establish a diolistic approach for 3–D reconstructions of CA1 pyramidal cells in pre-fixed hippocampal slices.

In the last decade two 'revised approaches' have been made available to label different subsets of neurons: diOlistics and transgenic mice expressing GFP (or its spectral variants). DiOlistics (ballistic delivery of lipophilic carbocyanine dyes) uses a 'gene gun' to propel dye-coated particles into neuronal preparations. Using particles coated with different combinations of dyes, this technique allows the simultaneous labeling of many cells within a neuronal network. This approach is most effective in living material but it can be applied to fixed samples. Transgenic mice expressing selectively red, green, yellow, or cyan fluorescent proteins (together termed XFP) in a unique pattern have been generated [60] becoming a valuable tool for the study of neuronal structure, function, and development. Among these, the Thy1-GFP-M line features intense labeling of small neuronal subsets in the forebrain

as in a 'Golgi-like vital stain'. Importantly, long-term expression and continuous live imaging of XFPs has no side effects on these animals [60].

Table A.1 Most frequent neuronal labeling techniques used for whole-cell reconstructions in mouse brain slices. Several other transfection techniques are not listed as they are typically restricted to dissociated cultures.

	Features	Limitations	References
Histologic Methods			
Golgi/ Golgi–Cox	Well established Technically simpler High number of labeled cells	Partially inefficient[a] Limited to wide-field imaging Single color labeling[b] Compromises immunostainings	[14, 77, 159, 164, 194, 206]
Anterograde/ retrograde labeling	Tracing of neuronal pathways	Requires long diffusion times Complete fillings are rare Efficiency[a] is affected by density of extracellular matrix	[64, 92, 149, 200, 204]
DiOlistics[c]	High number of labeled cells (through iterations) Rapid *in vivo* and multi-color labeling[b]	Partially inefficient[a] Lacks reproducibility *In vivo* labeling is associated with high cytotoxicity[d]	[70, 84, 104, 147, 153, 220]
Intracellular/ iontophoretic injections	Highly efficient[a] Can be used to correlate electrophysiological data with morphometry	Very low yield Technically more elaborated	[37, 52, 88, 121, 167, 224]
Genetic Methods			
XFP mice[e]	High number of labeled cells (dependent of transgene insertion site)	May require tedious breedings Multispectral labeling requires several generations Crossings with XFP lines may disrupt congenic backgrounds	[60, 122]
Biolistics	Technically simpler	Optimized protocols are required to minimize cytotoxicity	[95, 100, 215]
Viral transfections	Highly efficient transfection	Establishment of viral lines is demanding and cumbersome Patch expression is frequent after intracranial microinjection	[57, 163, 192]

[a] Efficiency as a measure of completely filled cells

[b] Multi-spectral differential labeling increases yield and can be use to discriminate cellular interactions

[c] DiOlistics methods are not restricted to lypophilic dyes and can also be applied to the delivery of water-soluble molecules [84, 104]

[d] This effect can be minimized, e.g., by using a modified gene gun barrel [153]

[e] Transgenic mice selectively expressing red, green, yellow, or cyan fluorescent proteins [60] or mosaic mice expressing stochastically multiple transgenes [122]

A.1 Material And Methods

If not stated, all materials and reagents used in this section are specific to the Helios® Gene Gun System (Biorad, Hercules, CA, USA).

A.1.1 Tissue Preparation

Animals were anesthetized and transcardially perfused as previously described (Section 4.4.1) with the exception that the post-fixation period was shortened to 1 h. For labeling of hippocampal dissociated cultures, cells were fixed as described in Section 4.4.2 without any permeabilization step.

A.1.2 Microcarriers Preparation

Tefzel tubing (≈ 75 cm) was mounted on the Tubing Prep Station, dried completely by purging N_2 for 45–60 min and coated with PVP (20 mg/mL) [220]. 30 mg of gold beads (1.6 µm ⌀, Figure A.1) were evenly spread on a glass slide (2×2 cm^2) using a razor blade. To achieve better homogeneity some drops of CH_2Cl_2 (# 66740, Fluka; Sigma-Aldrich, St Louis, MO, USA) were added in such a way that a monolayer of slurry could be obtained. 10 mg of dye (DiO or DiI, Molecular Probes/Invitrogen, Carlsbad, CA, USA) were dissolved in 150 µL of CH_2Cl_2 and added to the beads. Particles were rapidly spread across the surface of the glass slide to form a thin film. Once dried, several minutes later, the resulting fine powder was gently scraped from the slide with a clean razor blade into weighing paper and then poured into a 15 mL tube. 3 mL of deionized water were added, the suspension vortexed, and sonicated at 30 min at low power/frequency to avoid overheating.

A.1.3 Cartridges Preparation

Sonicated slurry was gently vortexed for 4–5 seconds and immediately pulled into the Tefzel tubing using a 5–10 mL syringe fitted snugly by means of a (≈ 1 cm) silicone tube. The dye-coated particles were allowed to precipitate and settle onto the tube wall for 15–30 min and water pulled up using the same syringe at a constant rate (≈ 75 cm/min). Finally, the tube was dried through a constant low flow of N_2 (0.2–0.4 lpm) for 2 h with permanent rotation. Cartridges were then obtained by 13 mm spaced cuts of the dried tubing and kept in a dark exsiccated environment until shooting.

A

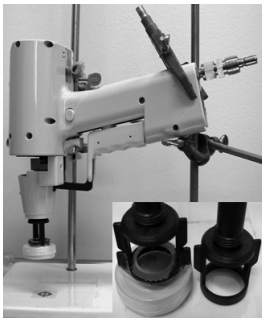

B

	Fixed vibratome slices	Fixed dissociated cultures
Microcarriers	Au; 1.6 µm ⌀	Au; 1.6 µm ⌀ W; 1.1 µm ⌀
Beads : diX ratio (mg)	30 : 10	30 : 10
Delivery pressure (psi)	300	150–200
N. Diffusion screens	1	1
N. filters (3 µm pore)	1	1–2
Diffusion	overnight, 4 °C	6 h, 4 °C / RT

Figure A.1 Modified diOlistic setup and microcarriers description. **A** The customized stand stabilizes the gun from vibrations and maintains a constant delivery distance minimizing the variability inherent to hand-held shooting[84, 220]. Inset: Comparison of the modified gun muzzle (left) with the original one (right). The earlier allows the placement of membrane filters that retain clustered beads. **B** Tungsten is less dense then gold and does not penetrate as deep. As a consequence it is not suitable for thick specimens. Brain tissue requires higher propelling power and longer diffusion times. diX: diI or diO.

A.1.4 Delivery

Shooting was performed within 24 h of cartridges preparation by means of a custom-fabricated gun head. Since hand-held versions are prone to human error, an adjustable stand was used to minimize shooting variability. This modified diOlistic system is described in Figure A.1–A and as others have described [84, 220], has the main advantage to fix the flight distance of the particles between the gun and the targeted tissue (3–4 cm). Additionally it facilitates targeting by pinpointing the center of the landing field. In order to filter out clusters of beads and to attenuate shock wave damage, a 22 mm PET filter with a 3 µm pore size (Falcon; BD Biosciences Discovery Labware, Bedford, MA, USA) was placed between the gun and the tissue in addition to the manufacturer's diffusion screen (*spacer*). In order to avoid filter damage after air blast, a custom gun header was maid by fitting a fully perforated Petri dish (14 mm) into the original header in such a way that the dish hoops could stretch the membrane filter, behaving as embroidery rings (Figure A.1–A, inset). The particles were accelerated at 150–300 psi using helium gas (Figure A.1–B).

A.1.5 Image Acquisition

Brain slices were kept in PBS and imaged on a confocal microscope (Leica Microsystems, Section 4.5.2) with a 40× HCX APOL 0.80 water lens. In cases in which labeling yield could be enhanced slices were re-shot (from both cut surfaces)

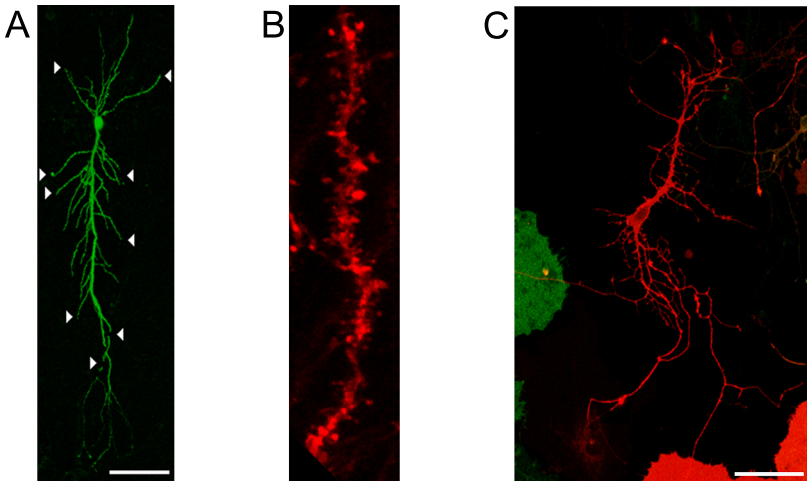

Figure A.2 Labeling of hippocampal neurons with lipophilic dye–coated particles. **A** Labeled CA1 cell depicting several unfilled, truncated processes (arrowheads) in which the tapering of the dye (diO) is absent. **B** Segment of a CA1 secondary oblique dendrite (*st. radiatum*) with completely labeled spines (diI). **C** Dissociated hippocampal neuron at DIV 14 after a multicolor diI–diO shooting. Scale bars: 100 µm.

after imaging completion. Dissociated hippocampal cells were mounted and imaged as earlier described in Section 4.4.2.

A.2 Results

Ballistic techniques have been used successfully to label neurons in both live and fixed tissues ranging from cultured isolated neurons to brain slices and whole brain (Figure A.2, [70, 100, 129, 215, 219]). Nevertheless, the use of *in vivo* diOlistics in whole-cell reconstruction studies is not frequent as the conditions to obtain an ideal 'Golgi-like' staining are quite demanding. First, the beads should be dispersed at very low density and only a single particle should contact the soma of the cell to be labeled. Second, the diffusion of the dye has to proficient. Lastly, enough number of cells of the same anatomical region must be obtained. Given the appealing properties of this method (Table A.1), we have predicted that the diOlistic staining would be suitable for efficient whole-cell reconstructions of CA1 cells (Figure 2.2). As others have reported [84, 220], we found that good-quality labeling is difficult to obtain and that tissue fixation and microcarriers preparation/delivery are critical steps of this methodology.

Tissue Fixation

Inefficient perfusion and over-fixation (Section A.1.1) can disrupt the integrity of membranes in the tissue and cause dye to spread between cells or nearby processes. In this aspect, unspecific diffusion of dye appears to be more frequent in older animals, probably due increased extracellular density (data not shown).

Microcarriers Preparation And Delivery

In order to determine the best bullet particle density we tested multiple conditions (microcarrier type, filter pore density, propelling pressure, and shooting distance) by mock shootings into agar (data not show). These small optimizations are summarized in Figure A.1 and include the use of a fixed stand and the placement of membrane filters in the shooting path to block clustered beads (Section A.1.4, [84, 220]). In our hands, the depth of penetration for the Biorad Helios® Gene Gun System lied typically between 10–50 µm. Therefore, most of the labeled cells were located near the surface, and presented truncated processes. However in some few cases of deeper penetration and/or efficient retrograde transfer of dyes deeper cells were labeled. Furthermore, as others have also reported[220], we have noticed a maximal labeling efficiency when the coated particle contacts the soma and not a branch of the dendritic/axonal arbor (even if majority of times, a single bead contained enough dye to label one cell through retrograde and anterograde diffusion).

Efficient Labeling Of Multiple Cells

We found the labeling efficiency to be highly variable even between shootings (data not shown). Furthermore in our hands even after thorough effort to optimize the critical steps of the protocol the number of complete filled cells was scarce and below our expectations. Figure A.2–A shows a CA1 pyramidal neuron labeled in a fixed mouse brain slice and was one of the few cells we obtained with a satisfactory labeling of its dendritic arbor. On the other hand, we obtained several other complete filled cells in different cortical structures. Concerning the labeling of neurons in dissociated hippocampal cultures, in which cells are obviously more accessible, staining was most of the times satisfactory, with many cells labeled per culture. Furthermore, by delivering a mixture of particles coated with different combinations of dyes, more cells and can be distinguished from each other even at higher density of beads (Figure A.2–C). We have also found that tungsten beads, that have restricted penetration depth on vibratome slices but are significantly cheaper then gold ones, can be used on these cultures without noticeable drawbacks (Figure A.1–B).

A.3 Discussion

The ballistic method allows rapid delivery of fluorescent probes into multiple cell types in both fixed and live tissue. In comparison to other techniques (Table A.1) this approach target multiple cells simultaneously, achieves labeling within minutes and is independent of gene transcription and protein synthesis unlikely GFP transfections. It can be used in fixed and live tissue or in living animals studies where micropipette injection of dyes can cause substantial tissue damage due to cardiorespiratory movements. In addition, it can perform multicolor labeling and deliver water-soluble indicators [104]. Nevertheless, diOlistics methods do restrict immunostaining analyses that typically require extraction of lipids with detergents to facilitate exposure of antigens. On the other side, lipophilic labeling cannot be performed in frozen tissue as it requires intact cell membranes. As a consequence only antibodies that do not require tissue permeabilization can be used in combination with lipophilic dye labeling. One alternative however, would be to first label neuronal structures with lipophilic dyes, photoconvert the labeled structures in the presence of diaminobenzidine [69, 220], and subsequently perform immunohistochemistry. Another option would be to label cells with 'fixable' lipophilic dyes such as CM-DiI or water soluble molecules such as CMTMR. Indeed this approach has been successfully combined with *in situ* hybridizations and immnohistochemistry to characterize migrating neurons in the developing central nervous system [6]. Accordingly, photoconversion would allow ultrastructural analyses of dendritic spines of diOlistically labeled neurons [69].

The implementation of this method for *in vivo* whole-cell reconstructions has also severe drawbacks: first, we found this approach to be highly variable: dye precipitation into the beads, microcarriers density inside the cartridge and tissue penetration are extremely difficult to control. Second, it is not possible to target a particular cell or region, and multiple iterations are required until the desired cell type is targeted. Third, multiple iterations of shootings cause ectopic patches of dye diffusion, compromising cell resolution. As a consequence, and frustrating our initial expectations, the diOlistic staining did not provide, in our hands, enough cells with the dendritic arbor completely labeled. On the other side, the yield and quality of Thy1-M-GFP labeled cells (specially after anti-GFP immunostaining, as described in Section 4.4.1) overcomes by large extent the advantage of rapid labeling offered by diOlistic shooting (Figure A.3). Thy1-M-GFP mice were described in 2000 [60] and since then have been used successfully in several circuit-mapping studies [rev. in 118]. Although the mosaic GFP expression is not homogeneous throughout the forebrain,

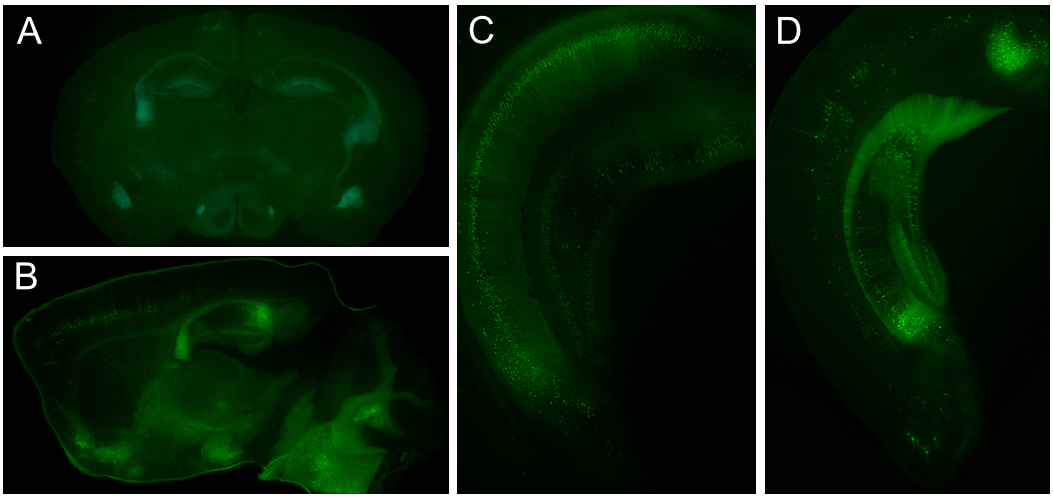

Figure A.3 Mosaic expression of GFP in Thy1-M-GFP transgenic mice. **A–B** Paracoronal (A) and sagital (B) vibratome sections (250 µm) from a heterozygous transgenic animal depicting the sparse 'Golgi-like' staining in the forebrain. **C** Detail of a ventral (temporal or anterior) coronal section in which the sparse labeling is lost in the CA1 region of hippocampus due to a very high number of cells expressing GFP. However, on the dorsal (septal or posterior) extreme only few cells express GFP (D). Interestingly, the dorsal–ventral (posterior–anterior) gradient of expression in the CA1 area is reversed in the granular cells of the dentate gyrus with the highest number of GFP-expressing cells situated dorsally (C and D). Images acquired on at 1.25–2× magnification (endogenous GFP fluorescence).

the GFP-expression pattern in the CA1 region of the dorsal hippocampus offers a sparse 'Golgi-like' labeling (Figure A.3–D).

Although others have used diOlistic shooting in fixed brain sections to successfully reconstruct dentate granule cells [219], the absence of literature reporting the use of this technique for full reconstructions of CA1 cells suggests that indeed, this method is disadvantageous for tracing complex cellular morphologies. It remains however, a valid and efficient approach to study embryonic development of cortical structures [71], spine morphology [147, 210], dendritic and spine maturation in organotypic [73, 79, 100, 176, 178, 208, 215, 231] and dissociated cultures [108, Figure A.2] and for morphometric analyses in mammalian species in which other alternatives are not available [84]. Additionally, combining ballistic techniques with XFP expressing mice may further extend the value of these mouse lines.

Appendix B

Behavioral Analysis Of CD3ζ Knockout Mice

Many proteins expressed in the immune system shown to have critical functions in cell-cell signaling are also expressed in neurons, where their function is poorly understood. An interesting hypothesis is that cell–cell signaling between neurons parallels similar mechanisms in the immune system, suggesting that imune molecules have a functional role in synaptic plasticity [rev. in 23].

Class I MHC (MHC-I) molecules are expressed on most somatic cells and are responsible for presentation of antigens on cell surface, an essential feature for elimination of infected cells in the immune system [rev. in 212]. The complete MHC-I molecule has four domains, three formed from the MHC-encoded α-chain, and one smaller chain contributed by B2-microglobulin (B2-m). There are four regions on the H-2 complex on chromosome 17 in mice that code for the alpha chain (*K*, *D*, *Qa* and *Tla*), a polymorphic transmembrane glycoprotein. On the other hand, B2-m is a relatively non-polymorphic protein encoded on chromosome 2.

Known receptors for MHC-I in the immune system include T-cell antigen receptors (TCRs), NKG2/CD94 receptors and mouse Ly49 proteins. Signaling pathways in immune cells include SYK/ZAP70, MAPK and SAP-1 and the activation of transcription factors such as NF-KB and NFAT [rev. in 53]. Mice with altered MHC-I function or that lack functional TCR (CD3ζ null mice [124]) have altered retinal innervation's of the lateral geniculate nucleus (LGN) and show defects in hippocampal synaptic plasticity. In particular, they show enhanced LTP and absence of LTD, whereas mice overexpressing MHC-I in neurons are resistant to LTP induction [93].

MHC-I mRNA and protein have been detected in diverse neuronal populations in rodents (e.g. CA1, CA3, dentate gyrus, visual cortex, LGN) , including developing

and adult hippocampal pyramidal cells and its expression is activity-dependent [40] suggesting that this molecule mediates structural changes at synapses [rev. in 24]. To date, no complete MHC-I-binding receptors have been detected in neurons, although transcripts for members of the TCR complex (e.g. CD3ζ and TCRζ have been detected in neurons [93, 203]. Moreover, CD3ζ has proven to affect neuronal development [93] and recently, to restrict dendritic arborization in hippocampal neurons [19].

Interestingly, behavioral differences have been reported in MHC-congenic mice in exploration, fear and learning [29, 201] raising the question whether the lack of MHC-I is associated with behavioral deficits. Since the absence of B2-m and CD3ζ protein in hippocampal-dependent behaviors have not yet been studied (when raised in a germ-free facility, both knockout mice are outwardly normal) we proposed to characterize anxiety-related behaviors of CD3ζ knockout mice [124].

B.1 Material And Methods

CD3ζ^{KO} mice [124] were purchased from the Jackson Laboratory (Bar Harbor, ME, USA) in a C57BL/6J genetic background. Behavioral group (described in detail on Table B.1) was tested in the open field, elevated-plus maze, free exploration and social transmission of food preference tests with one week intervals as described in Section 4.1.6. The home cage locomotion test was performed on a subset of animals at the end of the battery of tests.

B.1.1 Free Exploration Test

Animals were placed in a 20 cm×30 cm×10 cm free exploration box[51], divided into six compartments (10 cm×10 cm each) each connected by a small aperture

Table B.1 Description of *CD3*ζ^{KO} behavioral group. The population was obtained by heterozygous breedings as described in Section 4.1.2. When required, heterozygous mice were randomly excluded at weaning so that no more than 6 animals would be housed per cage. Measurements were performed immediately after the open field test and are expressed as mean ± SD.

	WT		Het		KO	
	♂	♀	♂	♀	♂	♀
Age (days)	72.5 ± 3.96	69.7 ± 8.23	70.0 ± 7.59	69.8 ± 8.66	70.0 ± 8.07	65.9 ± 9.71
Weight (g)	28.5 ± 2.39	19.9 ± 1.59	20.2 ± 1.58	19.9 ± 1.58	26.8 ± 2.60	20.69 ± 1.84
N	15	16	19	17	15	18

(5 cm×5 cm). A removable insert blocked the three central apertures dividing the apparatus into two separate partitions (10 cm×30 cm each). Animals were habituated overnight to one side of the box (*familiar* side) that contained bedding, two food pellets, and a water bottle. The wall was manually removed and the animals gained access to the *unfamiliar* side that lacked bedding and food. Animals were video-tracked during 10 min. Latency to enter the unfamiliar side was scored as the first time the animal placed all four paws in that side.

B.1.2 Social Transmission Of Food Preference

The protocol was performed was previously described [110]. Two days before training all food pellets were removed from the cage, and a glass jar with a perforated metal grid (Dyets, Bethlehem, PA, USA) with ground chow (powderized pellets) was placed at one end of the cage on top of the bedding. This food jar remained in place until the day before the experiment.

Demonstrator Training

Ground chow was scented with either cinnamon (1% w/w) or cocoa (2% w/w). For each cage an animal was chosen as *demonstrator*, removed from its home cage, single-housed in duplex cages, food-deprived overnight and allowed to eat from a food cup containing a scented food for 1 h. Jars were weighed before and after to determine the total amount of food consumption with mice eating less then 0.2 g being discarded. Scent foods and demonstrators genotype were counterbalance to control for food/genotype bias.

Induction Of Food Preference

Immediately following scented food consumption, the *demonstrator* was placed back into their home cage and allowed to associate freely with observers for 30 min, after which the *demonstrator* was removed from the cage.

Observers Testing

Observers were food-deprived overnight and tested 24 h later. During the test, mice were isolated in duplex cages containing two weighed jars with flavoured-food, placed at the ends of the cage, so that each duplex contained both cinnamon and cocoa scent food. Observers were allowed to eat freely for 1 h, after which jars were re-weighed to determine the total amount of each food eaten.

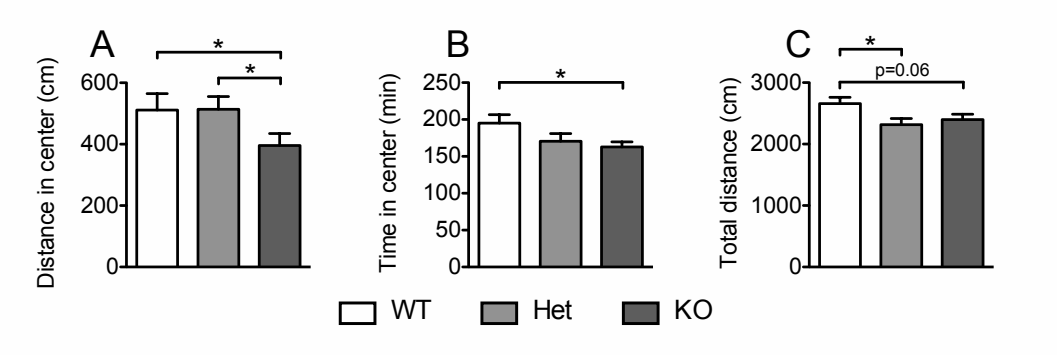

Figure B.1 Decreased exploratory activity of *CD3*ζ^{KO} mice in the open field test. **A–B** Decreased center activity in *CD3*ζ^{KO} animals as well as decrease total traveled distance (**C**). Number of animals are indicated in Table B.1. Bars represent means ± SEM; Fisher's post hoc test *: $p < 0.05$, **: $p < 0.01$, ***: $p < 0.001$.

B.2 Results

Assessment of anxiety-related behavior in CD3ζ^{KO} mice was performed in the open field, elevated-plus maze and free exploration tests when mice reached adulthood (9–11 weeks).

Decreased Lomotion In Response To Novelty

In the open field., *CD3*ζ^{KO} mice traveled less than wild type mice in the center of the open arena (Figure B.1–A; ANOVA, $F_{2,94} = 3.796, p = 0.026$), spending also less time in center (Figure B.1–B; ANOVA, $F_{2,94} = 2.971, p = 0.056$). In addition, knockout mice showed an overall decrease in locomotion (Figure B.1–C; ANOVA, $F_{2,94} = 3.339, p = 0.040$) while conserving the same rearing activity of WT controls (data not shown). This decreased in locomotion may reflect an altered response to novelty, as locomotion in the home cage was unaltered (Figure B.2–B; ANOVA, total: $F_{2,94} = 0.827, p = 0.448$, day: $F_{2,32} = 1.223, p = 0.301$, night: $F_{2,29} = 0.798, p = 0.460$) in mutant mice. Similarly, no significant effect of the mutation was found in the free exploration test in global locomotion or exploratory activity of either compartment (Figure B.2–A).

Increased Anxiety-Related Behavior In The Elevated Plus Maze

In the elevated-plus maze knockout mice showed less global locomotor activity (Figure B.3–C; ANOVA, $F_{2,98} = 5.178, p = 0.007$) and made fewer entries into the open arms (Figure B.3–D; ANOVA, $F_{2,98} = 4.540, p = 0.013$) where they walked less

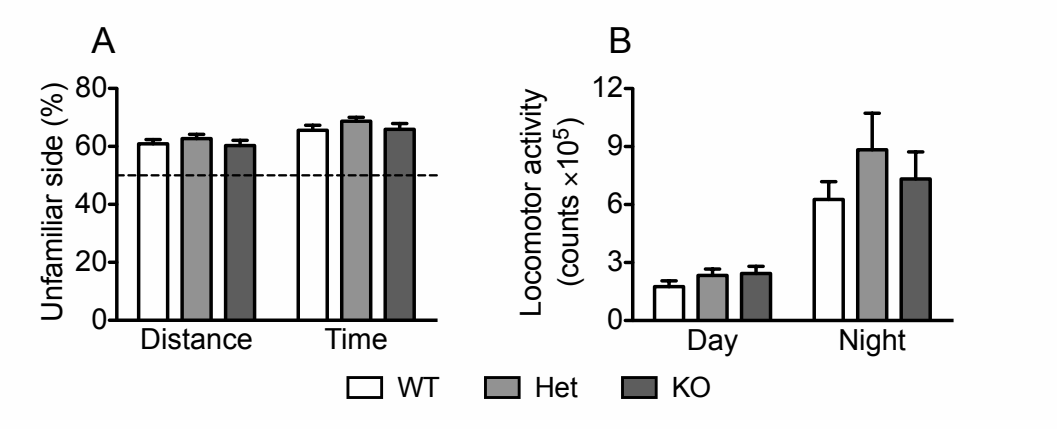

Figure B.2 Normal *CD3*ζ^{KO} mice behavior in the free exploration and home cage locomotion tests. **A** Free exploration test: Proportions of time spent and distance traveled on the unfamiliar compartment (WT, N= 30; Het, N= 32; KO, N= 28). **B** Home cage activity: Locomotor activity (summed counts from 72 h of continuous sampling) split in day/night activity (WT, N= 11; Het, N= 10; KO, N= 11). Bars represent means ± SEM. No differences between genotypes were found in either tests.

(Figure B.3–A; ANOVA, $F_{2,98} = 3.161, p = 0.047$). Locomotion in the closed arms was not altered (Figure B.3–B; ANOVA, $F_{2,98} = 2.803, p = 0.066$). Confirming avoidance of the open arms *CD3*ζ^{KO} mice stayed most of test in the closed arms avoiding also maze's central platform (Figure B.3–E and B.3–F; ANOVA, $F_{2,98} < 6.800, p = 0.0017$).

Long Term Memory In Socially Transmitted Food Preference Task

To further extend the behavioral characterization *CD3*ζ^{KO} mice, we tested these mutants in the social transmission of food preferences test, an hippocampal dependent task used to evaluate both short-term and long-term memory [32, 214]. In this paradigm, originally described in rats [68], information about a novel food odor is acquired by an *observer* animal smelling the breath of a *demonstrator* littermate mouse that has previously eaten that food. In this way, the safety of the cued food is learned from a social interaction rather than through actual consumption. This task was chosen to test whether *CD3*ζ^{KO} mice have long-term memory deficits in a hippocampus-dependent test that involves neither aversive stimuli nor spatial learning, exploiting an ethological meaningful rodent behavior [68]. The social transmission of food preferences test takes place in three phases. First, demonstrators were given a distinctively scented food (ground mouse chow with cinnamon or cocoa). Second, observers were allowed to interact with demonstrators in a single session. In the third phase, 24 h later, food deprived observer mice were given a

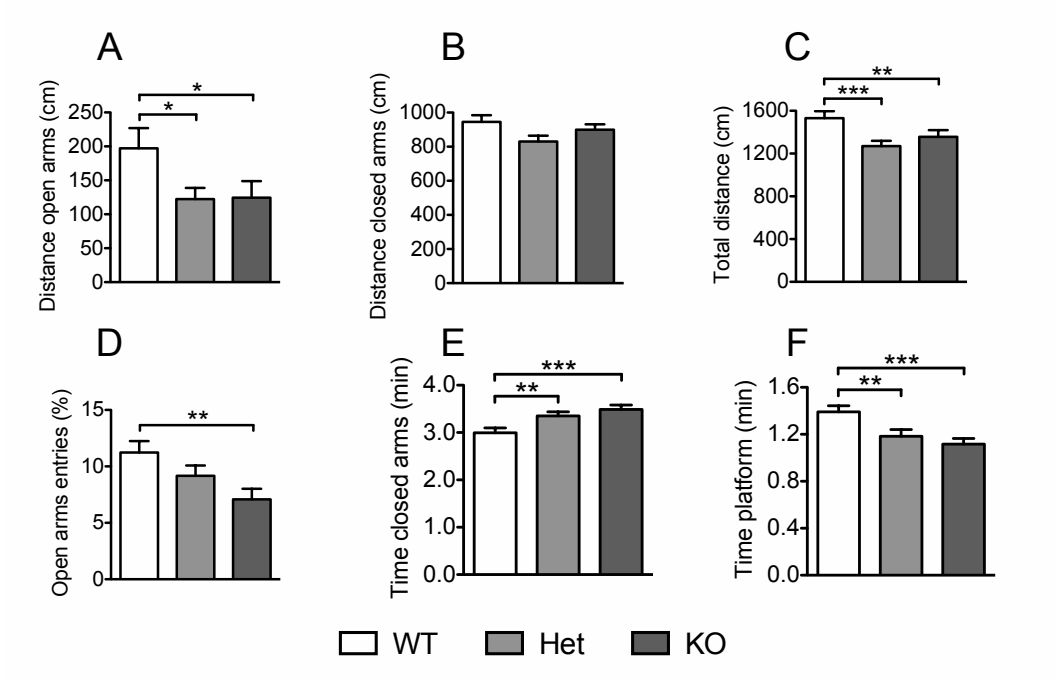

Figure B.3 *CD3*ζ^{KO} mice display increased anxiety-related behavior in the elevated-plus maze. **A–C** *CD3*$\zeta^{+/-}$ and CD3$\zeta^{-/-}$ mutants traveled significantly less in the open arms (A) while traveling the same distance as WT controls in the closed arms (B). As a consequence, total traveled distance in the maze was also decreased (C). **D** Reduction in open arms entries in *CD3*ζ^{KO} mice corroborates avoidance of this part of the maze. **E–F** Time spent in the closed arms was increased in *CD3*$\zeta^{-/-}$ mice (E) followed by decreased time in the central platform (F). Number of animals are indicated in Table B.1; Fisher's post hoc test *: $p < 0.05$, **: $p < 0.01$, ***: $p < 0.001$.

choice between two scented foods: either the same scented food that the demonstrator had eaten (cued) or another distinctively scented food (non-cued or novel). The day after social interaction with demonstrators, wild type control observers showed a strong preference for the cued food compared to the novel food (Figure B.4–A). *CD3*ζ^{KO} mutants, however, ate comparable amounts of both foods. To assess if olfaction or taste perceptions could be on the basis of these differences, we checked observers preference for the two used scented foods (Figure B.4–B). Indeed, food preference was lost in animals cued with cocoa food (approximately half of the experimental group). Interestingly observers probed with this food ate 83% less of both cued and novel chow. It is important to note that scent modality had also affected demonstrators' consumptions (Table B.2). Since cued food preference was disrupted in observers probed with cocoa food (Figure B.4–B) it is reasonable to think that animals developed a sensorial bias to this cue. Nevertheless, this scent has previously been used in a similar paradigm to successfully confirm abnormal

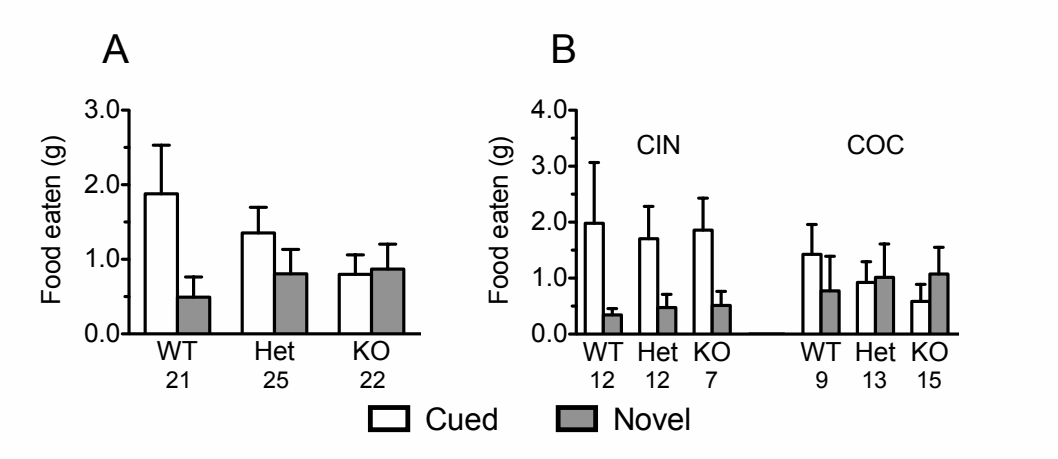

Figure B.4 Behavior of *CD3*ζ^{KO} mice in the social transmission of food preferences paradigm. **A** Selective preference for the cued food trends to be absent in knockout animals, although no significant genotype effect was found. **B** Modality of cue affected observers' food preference in all genotypes (ANOVA: $p = 0.03$). In the case of cocoa (COC) flavoured chow, total amount of eaten food was decreased in both *CD3*$\zeta^{+/-}$ and *CD3*$\zeta^{-/-}$ mice relatively to WT littermates (ANOVA: $p = 0.04$). There was no genotype effect in observers' total consumption in the case of cinnamon (CIN) cued food. Bars represent means ± SEM. Number of animals are indicated below each bar.

long-term memory in CREB$^{\alpha\delta}$ knockout mice [110].

B.3 Discussion

The idea that immune molecules may have novel neuronal functions in the brain gained strong support from studies with mutant mice deficient for cell surface class I MHC (B2-M) or lacking a critical class I MHC receptor component (CD3ζ). A set of key experiments have undoubtedly confirmed a role for 'immune molecules' in neuronal development and plasticity: 1) MHC class I genes and CD3ζ are expressed

Table B.2 Scent bias in *demonstrator* mice. Demonstrators which were trained with cinnamon scented food (CIN) ate twice as much powdered chow then those trained with cocoa cued food (COC). There was no sex effect in this bias (ANOVA, $p = 0.59$), although females always ate more then males (ANOVA, demonstrators: $p = 0.07$, observers: $p = 0.17$). Observers consumption can be inferred from Figure B.4–B. Measurements are expressed as mean ± SEM.

	WT		Het		KO	
	CIN	COC	CIN	COC	CIN	COC
Consumption (g)	5.6 ± 3.81	10.7 ± 6.18	0.8 ± 0.248	5.68 ± 2.22	5.62 ± 2.29	11.75 ± 7.94
N (♂ : ♀)	3 (2 : 1)	4 (2 : 2)	4 (3 : 1)	5 (2 : 3)	6 (3 : 3)	4 (2 : 2)

in neurons and are regulated by neuronal activity [39, 93]; 2) CD3ζ^{KO} mice lack refined connections between the dorsal LGN and 3) display enhanced hippocampal LTP and no detectable long-term depression (LTD) [93]; 4) the expression of the T cell antigen receptor β (TCRβ) locus is dynamically regulated over development in neurons of the central nervous system [203]; 5) axotomized motoneurons from B2-M knockout mice show stronger synaptic elimination when compared to WT animals [156]; 6) ligands for major histocompatibility complex (MHC) class I molecules function as sensory stimuli for sensory neurons of the vomeronasal epithelium [113]. Finally, and importantly, CD3ζ localizes selectively at dendritic growth cones and cultured CD3ζ^{KO} neurons show increase dendritic arborization, with activation of endogenous CD3ζ inhibiting dendritic branching [19]. Here we present supporting data for a role of CD3ζ in the regulation of anxiety-related behaviors.

Increased Innate Anxiety Related Behavior In CD3ζ Mutant Mice

In the open field, the initial level of locomotor activity in the first 5 min did not differ between *CD3*ζ^{KO} mice and control mice (data not shown); however, mutant mice exhibited an overall decrease in locomotor activity relative to controls after 1 h of testing as well as significant avoidance of the center part of the arena, known to be aversive to mice (Figure B.4). In order to assess if this hypo-locomotion phenotype was reflecting altered responses to novelty or altered basal levels of locomotor activity, we tested CD3ζ mutants on the elevated plus maze. On this test, reduction in overall activity was also detected (Figure B.3–C) as well as a notable increase in open arms avoidance (reflected by less locomotion and decreased entries, Figure B.3–A and D as well as closed arms preference, Figure B.3–E), clear measures of increased anxiety-related behavior in rodents. Furthermore heterozygous mice showed an intermediate phenotype in several measured of the elevated plus maze (open arms entries, time closed arms and time in central the platform, Figure B.3–D, E and F) , suggesting that the regulation of anxiety responses by CD3ζ is dosage dependent. Thus, it is possible that the sustained decrease in locomotor activity on the open field could represent increased stress responsiveness in CD3ζ mutants. This hypothesis is further corroborated by the results of the home cage locomotion test that showed not differences on the between knockout and control animals (Figure B.2–B). In order to better understand the decreased locomotion of CD3ζ mutants, we have tested knockout mice on the free exploration test that differs from the open field in that animals are given a permanent choice to explore a familiar or an unfamiliar environment, which may mimic more accurately an etho-

logical context [51]. As for the home cage locomotion test, we didn't find any effect of the mutation in this task, in either locomotion of side preference (Figure B.2–A). We have interpreted this result to be a consequence of the mild stressor this test represents, since, in opposition to the open field, the animal is not handled by the experimenter prior to testing. Altogether these results reflect increased behavioral inhibition and avoidance responses in *CD3*ζ^{null} mice.

Long-Term Memory In CD3ζ Mutant Mice

In order to assess if CD3ζ may also play a role in hippocampal function we tested knockout mice in the social transmission of food preferences test, a hippocampal-dependent paradigm [rev. in 9]. This task takes advantage of the ethological fact that rodents develop a natural preference for foods that they have recently smelled on the breath of other conspecifics [68], and thus does not involve either spatial learning, aversive stimuli nor a strong locomotion component. In addition, given the actual data on differential functions of the dorsal and ventral hippocampus (Section 1.4), it is possible that social transmission of food preferences is specially sensitive to ventral hippocampal lesions [rev. in 9]. Frustrating our expectations, we found an effect of the modality of scented food in both demonstrators and observer mice with no significant food preference for cocoa scented chow (Figure B.4, Table B.2). This effect complicates the interpretation of this experiment and may be caused by several modifications to the original protocol [110], including: 1) *CD3*ζ^{KO} mice were established on a pure C57BL/6J background and not the F2 progeny derived from a cross between C57BL/6 and 129SV mice; 2) Testing of both demonstrators and observers lasted for one and not two hours and 3) demonstrator-observer interaction lasted 30 min and not 5. However given that cued cinnamon food did condition food preference in all genotypes (FigureB.4–B), it may be reasonable to hypothesize that *CD3*ζ mutant mice do not display long-term memory deficits in this task. Nevertheless, given the reduced number of animals tested with this probed food this interpretation may be an overstatement.

Behavioral Role For MHC I

In summary, these results suggest a novel role of CD3ζ in anxiety-related behavior. Whether this phenotype is due to the loss of CD3ζ expression in the brain, the result of the absence of the CD3ζ gene in the immune system, or some combination of both effects remains to be determined. Moreover, implicating a neurobiological action of MHC-I in behavior would provide new insights into important processes of

brain formation. MHC-I are highly polymorphic molecules functioning as individuality signals in mate recognition tasks [113], suggesting that indeed, MHC genotypic diversity can influence social behavior. Having a role in CNS formation would suggest that MHC class I molecules may be related with the incidence of psychological dysfunctions in humans. All these aspects could be clarified with tissue specific $CD3\zeta^{\text{null}}$ and $B2m^{\text{null}}$ conditional mutants.

Appendix C

Transgenic Channel Expression And Assembly In Camk2a–GluCl Mice

Tissue-specific delivery of benzodiazepines in rodents have implicated several forebrain regions (periaqueductal grey, lateral septum, hippocampus, and basolateral amygdala) in the regulation of anxiety-related behaviors [141]. Benzodiazepines (but also other anxiolytic drugs such as barbiturates, and neurosteroids) agonize $GABA_A$ receptors leading to membrane hyperpolarization and reduced neural excitability [rev. in 182]. $GABA_A$ receptors are expressed on both principal excitatory cells and inhibitory interneurons [150] and wich of these cell types is responsible for the effects of these anxiolytic drugs remains unknown.

To address this question transgenic mice expressing an ivermectin-sensitive chloride channel from *C. elegans* [115, 198] in principal forebrain neurons – Camk2a–GluCl – were generated with the intention to pharmacologically inhibit principal forebrain neurons (Audero et al., in preparation). To interpret elecrophysiological and behavioral data of Camk2a-GluCl mice it was critical to characterize the expression and assembly of the transgenic avermectin-gated chloride channels. The experiments described in this chapter describe the preliminary studies performed in this direction.

The *C. elegans* glutamate and ivermectin-gated chloride channel (GluCl) system allows tissue and cell-type specific inhibition of neural activity in behaving mice and was developed to allow rapid and reversible suppression of neuronal activity in mammalian cells [198] and has been shown to mediate ivermectin-dependent

neuronal inhibition and alterations in amphetamine-induced locomotion behavior following viral delivery into the mouse striatum[115]. These channels are constituted by two subunits (α and β) fluorescently tagged by EYFP and ECFP, respectively, into the third intracellular loop. In addition the β subunit carries a Y182F point mutation, shown to reduce the affinity of the channel for glutamate while retaining sensitivity to ivermectin [198].

Camk2a-GluCl mice were generated by pronuclear injection of a mixture of cDNAs for the GluClα-EYFP or GluClβY182F–ECFP subunits both cloned downstream of a 8.5 kbp fragment from αCaMKII promoter, a gene expressed only in forebrain principal neurons [21, 135]. Three founder lines showing germline transmission were obtained, each containing one or more copies of both constructs, as detected by PCR and Southern blot (Audero, et al., in preparation). The founder with highest transgenic expression ('Tg 81') was selected by western blotting of hippocampal extracts for the analyses detailed in here.

C.1 Material and Methods

Perfusion and antibodies staining was performed as earlier described (Chapter 4.4.1). For FRET experiments, coronal vibratome sections (50 µm) were DAPI stained for 10 min and washed twice with 100 mM glycine in PBS and mounted in gelvatol. ECFP was sampled between 470–500 nm and EYFP between 525–600 nm (pinhole: 2.0 airy). EYFP was bleached at ¾ laser power after 20 iterations. For each bleached area a similar ROI placed outside the puncta (sham ROI) was also bleached and monitored for changes in FRET signal. The ECFP image was acquired before and after bleaching of EYFP. Images were background corrected, smoothed with a median filter (radius = 2 pixel) and a threshold was applied. Apparent FRET efficiencies were calculated as described before [218] using ImageJ [173]. All measurements were performed in CA3 pyramidal layer.

C.2 Results

Confocal microscopy was used to confirm expression of channel subunits. Fluorescence of transgenic GluClα-EYFP and GluClβ^{Y182F}-ECFP fusion proteins could be detected in hippocampal pyramidal cells with the channel subunits expressed in a homogeneous somatodendritic pattern (Figure C.1 A–D). In addition, colocalization of the channel subunits was observed in a perisomatic punctate pattern. Anti-GFP immunofluorescence confirmed channel expression in pyramidal cells of

hippocampus and cortex (Figure C.1 I–J, M–N). No channel expression was seen outside the pyramidal cell layer in hippocampus, in cerebellum (data not shown), or in wild-type littermates (Figure C.1 E–H, K–L, O–P). Double immunofluorescence for the channel subunits and the synaptic protein synapsin I indicated that the channel puncta were not enriched at synaptic sites (Figure C.1 Q–T).

These experiments show that GluCl channels are localized to the somatodendritic compartment of principal neurons of hippocampus and cortex but they cannot confirm their location in the cell membrane, which would be a strong indication of functional assembly. Since FRET can occur between CFP and YFP when physically closed (2–6 nm) [rev. in 97], we hypothesized that FRET changes between GluClα-EYFP and GluClβ^{Y182F}-ECFP could be used to infer GluCl subunits assembly. Indeed, Förster resonance energy transfer (FRET) measurements in combination with TIRF microscopy has been routinely used to assess assembly, subunit stoichiometry and surface micro-localization of acetylcholine receptors (AChRs) [56, 148]. Accordingly, we performed *in vivo* acceptor photobleaching experiments in the CA3 pyramidal layer of transgenic mice, finding high levels of apparent FRET efficiencies in perisomatic puncta of the CA3 field (Figure C.2).

C.3 Discussion

The expression of Camk2a-GluCl transgenic channels is extremely low even when assessed by Western-blotting of whole forebrain extracts (data not shown), and thus visualization of fluorescent subunits is challenging. Inhibitory interneurons of the hippocampus synapse to pyramidal cells almost exclusively in their perisomatic region [e.g., rev. in 65]. The fact that channels do not co-localize with synapsin I (Figure C.1 Q–T) suggests that the observed puncta are not the result of a synaptic enrichment of the channels. This finding may be relevant, given the possibility that high levels of endogenous glutamate found at excitatory synapses might activate GluCl channels since the β^{Y182F} mutation does not reduce the affinity for this neurotransmitter completely [198]. In addition, the fact that subunits are expressed in non synaptic aggregations raises the suspicion that transgenic proteins could be mis-processed and accumulated inside expressing neurons.

Although we were not able to confirm that these puncta were located on the cell surface and thus potentially functional, inter-subunit Förster resonance energy transfer measurements suggest that transgenic channels may be functionally assem-

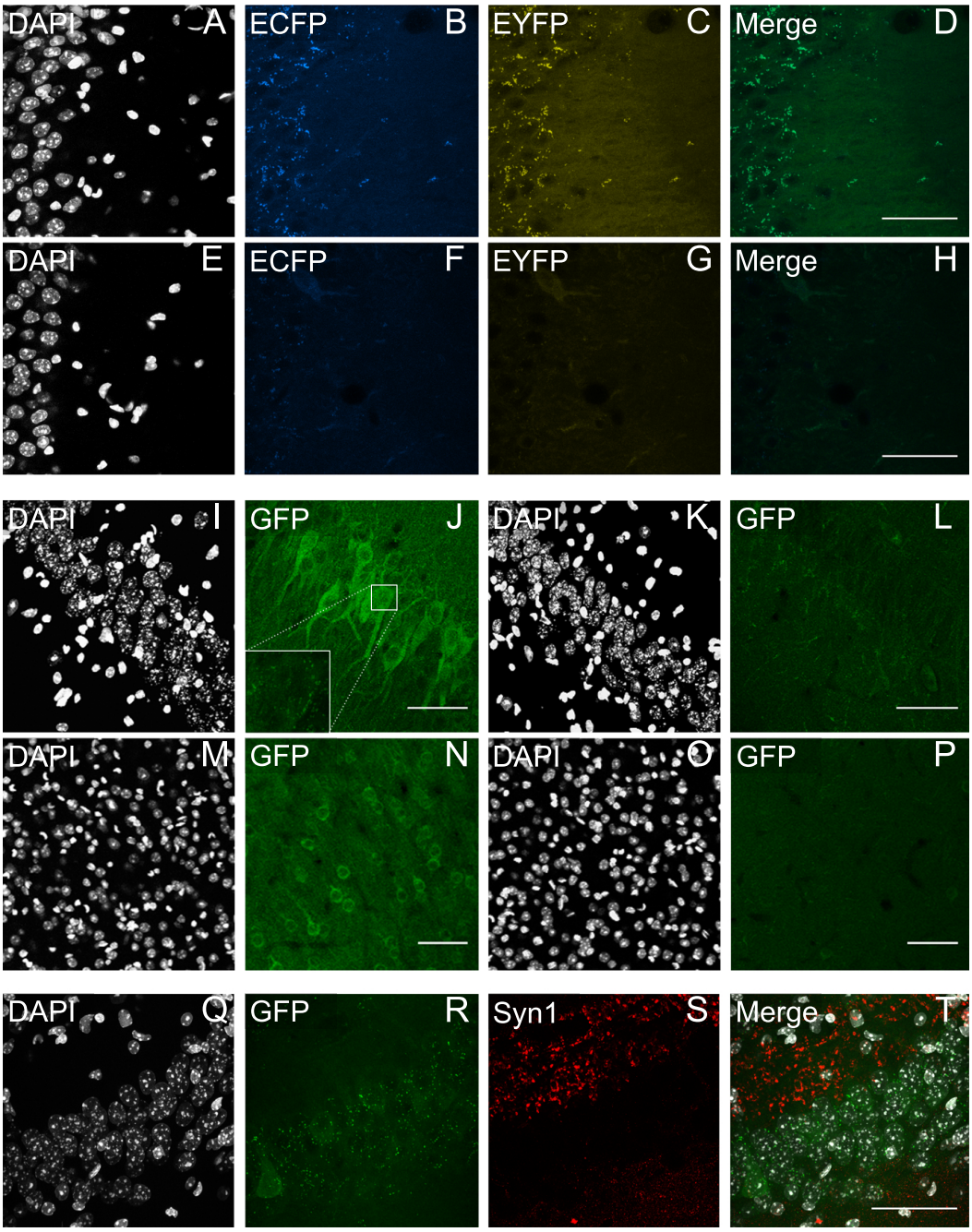

Figure C.1 Localization of GluCl channels in hippocampus and cortex. Fluorescence imaging depicting somatodendritic expression of GluClα-EYFP and GluClβ^{Y182F}-ECFP proteins in the hippocampal CA3 pyramidal cell layer from transgenic (**A**–**D**), but not wild type (**E**–**H**) mice. (**I**–**P**) Anti-GFP immunohistochemistry confirmed channel expression in pyramidal neurons of hippocampus (**I**–**J**) and cortex (**M**–**N**) in transgenic mice (insert: high magnification of somatic staining showing channel puncta). No signal was seen in wild type controls (**K**–**L**, **O**–**P**). (**Q**–**T**) Double immunofluorescence for GFP and synapsin I, a presynaptic marker, demonstrated that channel puncta were not synaptically localized (black/white images: DAPI; scale bars: 50 µm).

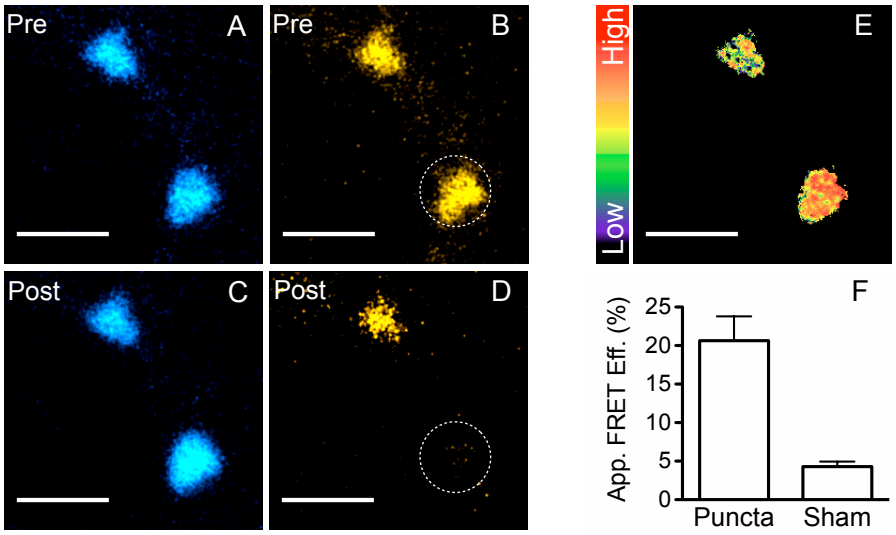

Figure C.2 FRET in perisomatic channel puncta. (**A**–**D**) Representative acceptor bleaching experiment in perisomatic puncta in the hippocampal CA3 pyramidal layer of Camk2a-GluCl transgenic animals. (**A**–**B**) Increased GluClβ^{Y182F}-ECFP fluorescence after bleaching of GluClα-EYFP (**C**–**D**). (**E**) FRET image in which a warmer hue indicates higher efficiency (color scale below). (**F**) Apparent FRET efficiencies in bleached puncta (dashed circle) and a bleached control ROI (sham). Images refer to a single z-plane. Scale bars: 2 µm. Error bars: SEM of 21 experiments (N= 2 animals).

bled (or at least, closely associated). Nevertheless, these experiments are not able to determine cell surface localization and the observed punctated expression could still reflect intracellular aggregation of channels. This question could nevertheless be addressed by other approaches. involving TIRF imaging of cultured neurons from transgenic animals [56, 148].

Appendix D

Digital image processing

Scientific digital image processing is critical for the quantitative examination of microscopic images and required for unbiased and reproducible image analysis. Typically dealing with large data sets, imaging experiments demand automated routines and specialized software packages such as ImageJ, a public domain, Java-based image processing program developed at the US National Institutes of Health by Wayne Rasband. ImageJ (IJ) was released in 1997 as a successor of a similar software by the same author – NIH Image – developed for Macintosh computers running pre-OS X operating systems[1]. IJ has an open architecture, is highly extensible via plugins and (recordable) macros, featuring a well-documented and powerful built-in macro language and a knowledgeable worldwide user community with c. 2000 advanced users and developers[2]. Recently, it became the core of other open source initiatives that further extend its potentialities[3]. Thus, it is not surprising that among the most frequently used imaging software in the life sciences[4].

This appendix lists four scripts for ImageJ (v.141 or higher) – `DGCs analyzer`, `Session logger`, `Rename and Save ROI Sets` and `Toolset Creator` – as the corollary of the image processing learned during this thesis preparation. These scripts are presented here with the hope of usefulness to others and as an acknowledgment to the ImageJ community for all the technical help it provided me during the last four years.

[1] http://en.wikipedia.org/wiki/imagej
[2] http://rsbweb.nih.gov/ij/features.html
[3] Fiji, http://pacific.mpi-cbg.de/
[4] A Google Scholar™ query restricted to the Life Sciences performed on October 06, 2008 retrieved 14.400 hits for *ImageJ*, 7.860 for *Metamorph Universal Imaging* (MetaMorph®, Universal Imaging Corp., Downingtown, PA, USA) and 1.260 for *Imaris* (Imaris®, Bitplane AG, Zürich, Switzerland).

D.1. *DGCs analyzer*

Allows interactive changes in ImageJ's *'Particle Analyzer...'* settings and automatic identification of saturated pixels. It is listed on the following page.

D.2. *Session logger*

Registers processing steps in a semi-educated way. Its goal is to obtain a text file that is both a "laboratory book" registry and a macro template that can be used to reproduce key routines between users and work sessions. Jerome Mutterer has adapted it to run on a separated toolbar[5]. It is listed on page 85.

D.3. *Rename and Save ROI Sets*

Helper toolset for analyses that require manual contouring of multiple ROIs (e.g., quantification of brain autoradiograms). Features: 1) bilateral mirrors and edge adjustments of selections via keystrokes; 2) fast renaming of drawn selections and 3) association of ROI-sets to an image. It has been added to the repertory of ImageJ's macros[6]. It is listed on page 87.

D.4. *Toolset Creator*

Creates toolbar menus for running plugins, macros and scripts. It was though for logical clustering of ImageJ commands (e.g., by uniting all image filters related to confocal microscopy on a unique toolbar). An edited version by Wayne Rasband was included in the v1.41 distribution of ImageJ[7]. It is listed on page 94.

Detailed information on these macro files can be found on the ImageJ web site[8] or on the links provided on the respective file headers.

[5] http://rsb.info.nih.gov/ij/plugins/action-bar.html
[6] http://rsb.info.nih.gov/ij/macros/toolsets/
[7] http://rsbweb.nih.gov/ij/download.html
[8] http://rsb.info.nih.gov/ij/search.html

D.1 *DGCs Analyzer*

```
/* Macro thought for semi-automatic measurements of cell morphologies of
 * fluorescent stained cell using IJ's 'Analyze particles'
 */
var minsize= 0.09;
var subtractValue= 3;
var medianrad= 2;.
var thresmin= 2;
var favLut= "HighContrast";
var extensions= newArray("tif","tiff","TIF","TIFF","jpg","jpeg","JPG","JPEG","stk","STK");
var separator= "\n --- --- --- --- --- ---\n";

macro "Arrange windows Action Tool - C444R01fdR2397" {
    os= getInfo("os.name");
    cr= fromCharCode(13);
    mngrWidth= 285;
    trshldWidth= 280;
    wrnngsHeight= 145;
    ijHeight= 95;
    sideborder= 5;
 setBatchMode(true);
 if(os=="Mac OS X"){
    a= String.paste;
 String.resetBuffer;
 String.append('tell application "System Events"' +cr);
 String.append(' set dockProps to property list file "~/Library/Preferences/com.apple.dock.plist"'+cr);
 String.append(' set docVisible to not the value of the property list item "autohide" of dockProps'+cr);
 String.append('end tell'+cr);
 String.append('if docVisible then'+cr);
 String.append(' tell application "System Events" to keystroke "d" using {command down, option down}'+cr);
 String.append('end if'+cr);
 String.append('tell application "ImageJ" to activate'+cr);
 String.append('tell application "System Events" to tell process "ImageJ" to keystroke "h" using {command
            down, option down, shift} & (keystroke return)');
 exec("osascript", "-e", String.buffer);
 String.resetBuffer;
 String.copy(a);
}
 if(isOpen("Log")) {selectWindow("Log"); setLocation(sideborder, ijHeight);}
 if(isOpen("Warnings")) {selectWindow("Warnings");setLocation(sideborder, screenHeight-wrnngsHeight);}
 if(isOpen("ROI Manager")) {selectWindow("ROI Manager");setLocation(screenWidth-mngerWidth,0);}
 if(isOpen("Threshold")) {selectWindow("Threshold");setLocation(screenWidth-mngrWidth-trshldWidth,0);}
 if(isOpen("Results")) {selectWindow("Results");setLocation(screenWidth/2.2, screenHeight/1.6);}
 setBatchMode(false);
 if(nImages>0) selectWindow(getTitle);

}

macro "Open Image list.(shift to list current directory) Action Tool - C444L00a0L03f3L06a6L09c9L0cfcL0fbf" {
 if(nImages!=0 && isKeyDown("shift")) imagesDir=getDirectory("image");
 else
    imagesDir= getDirectory("Choose a Directory to list");
 PrintListFiles(imagesDir);
}

macro "Settings Action Tool - C444D3eD4eD5eD6bD6cD6dD7aD89D98Da7Db6Dc6Dd6De4De5D2aD5dDa2Dd5D59D68D69D77D78
D86D87D96D1aD1bD1cD29D2bD39D49D4bD4cD4dD58D67D76D85D92D93D94Da1Db1Db2Db4Dc1Dc4Dd4De3D5aD6aD79D88D95D97Da5Da6
D19D91D4aD5bDa4Db5D3aD5cDa3Dc5" {
    extensions2= extensions[0];
 for (i=1; i<extensions.length; i++) extensions2 = extensions2 +", "+ extensions[i];
 Dialog.create('Settings');
 Dialog.addMessage("Background subtraction");
 Dialog.addNumber('       ', subtractValue);
 Dialog.addMessage('Median radius');
 Dialog.addNumber('', medianrad);
 Dialog.addMessage('Minimum DGC size');
 Dialog.addNumber('', minsize);
 Dialog.addMessage('Minimum Treshold');
```

```
 Dialog.addNumber('', thresmin);
 Dialog.addMessage('Lut to be used (without extension)');
 Dialog.addString("",favLut);
 Dialog.addMessage("Extensions beeing filtered by [Open image list...]");
 Dialog.addString("",extensions2,35);
 Dialog.show();
     subtractValue= Dialog.getNumber();
     medianrad= Dialog.getNumber();
     minsize= Dialog.getNumber();
     thresmin= Dialog.getNumber();
     favLut= Dialog.getString;
     extensionsUser= Dialog.getString;
}

macro "Prepare Image Action Tool - C444F113fC888F413fCaaaF713fCbbbFa13fCcccFd13f"{
     ijdir=getDirectory("startup"); lutdir=ijdir+"luts"+File.separator;
     lutpresent=File.exists(lutdir+favLut+".lut");
 if(bitDepth==24) {run("8-bit");showStatus("RGB Image converted to 8-bit");}
 if(lutpresent)run(favLut);
 else
 run("Fire");
 roiManager("reset");
 run("Set Scale...", "distance=1 known=1 pixel=1 unit=[]");
 run("Set Measurements...", "area mean standard modal min centroid center perimeter fit circularity
     feret's integrated median display redirect=None decimal=3");
 if(selectionType()!=-1) {s=selectionType(); getSelectionCoordinates(xsel,ysel);
     xselArray= xsel; yselArray= ysel; }
 else {s='line'; xselArray= newArray(0,0); yselArray =newArray(0,0);}
 exposureWarning("Warnings",separator);
 run("Select None");
 run("Subtract...", "stack value="+subtractValue);
 run("Median...", "radius="+medianrad);
 makeSelection(s, xselArray, yselArray);
 setTool(3);
 showStatus("DGC smallest length: "+minsize);
}

macro "Measure Action Tool - C444D2cD2dD2eD2fD3aD3bD3cD3dD3eD3fD48D49D4aD4bD4cD4dD4eD4fD56D57D58D59D5aD5bD
5cD5dD5eD5fD64D65D66D67D68D69D6aD6bD6cD6dD6eD6fD72D73D74D75D76D77D78D79D7aD7bD7cD7dD7eD7fD82D83D84D85D86D87D
88D89D8aD8bD8cD8dD8eD8fD92D93D94D95D96D97D98D99D9aD9bD9cD9dD9eD9fDa2Da3Da4Da5Da6Da7Da8Da9DaaDabDacDadDaeDafD
b4Db5Db6Db7Db8Db9DbaDbbDbcDbdDbeDbfDc6Dc7Dc8Dc9DcaDcbDccDcdDceDcfDd8Dd9DdaDdbDdcDddDdeDdfDeaDebDecDedDeeDefD
fcDfdDfeDff"{
     searchValue=pow(2, bitDepth)-2;
 setThreshold(thresmin, searchValue);
 if(!isOpen("Threshold")) run("Threshold...");
 setTool(3);
 showStatus("DGC smallest length: "+minsize);
 waitForUser("Adjust the optimal treshold\nDraw a ROI over every DGC");
 run("Analyze Particles...",
 "size="+minsize+"-Infinity circularity=0.00-1.00 show=Nothing display include add");
}

macro "Define DGC size Tool - C444L15f5L1219Lf2f9L8882L5753Lb7b3" {
 if(selectionType()!=-1) {
     s=selectionType(); getSelectionCoordinates(xsel,ysel); xselArray= xsel; yselArray= ysel; }
 else {s='line'; xselArray= newArray(0,0); yselArray =newArray(0,0);}
 getCursorLoc(x, y, z, flags); xstart= x; ystart= y; x2= x; y2= y;
 while (true) {
   getCursorLoc(x, y, z, flags);
   if(flags&16==0) {
   printandset("Warnings");
   makeSelection(s, xselArray, yselArray);
   exit;
  }
 if(x!=x2 || y!=y2) makeLine(xstart, ystart, x, y);
     a=(x-xstart)*(x-xstart);b=(y-ystart)*(y-ystart);
     minsize=sqrt(a+b);
     x2=x; y2=y;
 wait(10);
 }
}
```

```
macro "Define DGC size Tool Options" {minsize=0;printandset("Warnings");}

function PrintListFiles(dir) {
      list = getFileList(dir);
      count=1;
 print("\n*** Tifs and Jpegs on " + dir +":\n");
 for (i=0; i<list.length; i++) {
    for (j=0; j<extensions.length; j++)
       if(endsWith(list[i],extensions[j])) {count++; print(count + ": " + dir + list[i]);}
    if(endsWith(list[i], "/")) PrintListFiles(""+dir+list[i]);
    }
}

function exposureWarning(title1,separator) {
      searchValue=pow(2, bitDepth)-1;
      countValue=0;
      title2 = "["+title1+"]";
 for( i = 1; i <= nSlices; i++ ) {
           setSlice(i);
           for( x = 0; x < getWidth(); x++ ) {
        for( y = 0; y < getHeight(); y++ )
              if( getPixel(x,y) == searchValue ) countValue += 1;
           }
 if(countValue>1) {
    setThreshold(searchValue, searchValue);
    run("Create Selection");
    roiManager("Add");
    roiManager("Select", 0);
    roiManager("Rename", "saturated pixels");
    resetThreshold();
    setOption("Show All",true); }

 if(isOpen(title1)) print(title2, separator);
 else
     run("Text Window. . .", "name="+title2+" width=50 height=6");
     print(title2,        "("+bitDepth+"-bit) "+getTitle+"\n");
     print(title2, countValue + " saturated pixels");
     print(title2, separator);
}

function printandset(title1){
      title2 = "["+title1+"]";
 if(isOpen(title1)) print(title2, "DGC smallest length: "+minsize+"\n");
 else {
    run("Text Window. . .", "name="+title2+" width=50 height=6");
    print(title2,        "("+bitDepth+"-bit) "+getTitle+"\n");
    print(title2, minsize+"\n");
  }
}
// For convenience 'Dynamic Stats and Histogram Tools' are appended here:
// http://rsb.info.nih.gov/ij/macros/toolsets/Dynamic_Stats_and_Histo.txt


// End of file
```

D.2 *Session Logger*

```
// Action Bar description file: Session_Log
//
// Defines a set of logging commands available as a 'logger toolbar' for the Action_Bar plugin:
// http://rsb.info.nih.gov/ij/plugins/action-bar.html
//
// Installation:
// Install Action_Bar and save this file as 'Session_Log.txt' in the ActionBar folder
// TF, JM 2007

run("Action Bar","/plugins/ActionBar/Session_Log.txt");
exit();

<line>
<button> Start Recorder
         label= Recorder
         icon= noicon
         action= run_macro_string
         arg= if(!isOpen("Recorder")) run("Record..."); exit();

<button> Set Session Log window name
         label= Set Log
         icon= noicon
         action= run_macro_string
         arg= <macrocode>
         wn= call("ij.Prefs.get", "sessionlog.name","");
         wn= getString("Session Log Name",wn);
         if(!endsWith(wn,".txt")) wn=wn+".txt";
         call("ij.Prefs.set", "sessionlog.name",wn);
         if(!isOpen(wn)) {
                  run("New... ", "name=["+wn+"] type=Table");
                  getDateAndTime(year, month, week, day, hour, min, sec, msec);
                  print("["+wn+"]", "// *** "+year+"."+pad(month)+"."+day+" "+
                  hour+":"+pad(min)+":"+pad(sec)+" ***");
                  }
         if(nImages>0) selectWindow(getTitle));
    function pad(n) {n=toString(n); if(lengthOf(n)==1) n="0"+n; return n;}
</macrocode>

<button> Clear last line
         label= Clear Last
         icon= noicon
         action= run_macro_string
         arg= <macrocode>
         wn= call("ij.Prefs.get", "sessionlog.name","");
         if((wn=="")||(!isOpen(wn))) exit("Please set a session log window first");
         print("["+wn+"]", "\\Update: ");
         if(nImages>0) selectWindow(getTitle));
</macrocode>

<button> Clear all
         label= Clear All
         icon= noicon
         action= run_macro_string
         arg= <macrocode>
         wn=call("ij.Prefs.get", "sessionlog.name","");
         if ((wn=="")||(!isOpen(wn))) exit("Please set a session log window first");
         showMessageWithCancel("Are you sure ?");
         print("["+wn+"]", "\\Clear");
         if(nImages>0) selectWindow(getTitle));
</macrocode>
</line>

<line>
<button> Log opened image
         label= Image
         icon= noicon
         action= run_macro_string
```

```
        arg=<macrocode>
        wn=call("ij.Prefs.get", "sessionlog.name","");
        if((wn=="")||(!isOpen(wn))) exit("Please set a session log window first");
        if(nImages==0) showStatus('No images are open.');
        else {print("["+wn+"]", "// Opened: "+getDirectory("image")+getTitle());}
        if(nImages>0) selectWindow(getTitle));
</macrocode>

<button> Log comment
        label= Comment
        icon= noicon
        action= run_macro_string
        arg= <macrocode>
        wn= call("ij.Prefs.get", "sessionlog.name","");
        if((wn=="")||(!isOpen(wn))) exit("Please set a session log window first");
        Dialog.create('Comment');
        Dialog.addString('', String.paste, 55);
        Dialog.addCheckbox("Precede with        '//'", true);
        Dialog.show();
        note=split(Dialog.getString(), "\n");
        conv=Dialog.getCheckbox();
        for (i=0; i<note.length; i++) {
                if(conv) print("["+wn+"]", "// "+note[i]);
                else
                print("["+wn+"]",note[i]);}
        if(nImages>0) selectWindow(getTitle));
</macrocode>

<button> Log clipboard
        label= Clipboard
        icon= noicon
        action= run_macro_string
        arg= <macrocode>
        wn= call("ij.Prefs.get", "sessionlog.name","");
        if((wn=="")||(!isOpen(wn))) exit("Please set a session log window first");
        print("["+wn+"]", String.paste);
        if(nImages>0) selectWindow(getTitle));
</macrocode>

<button> Log last command
        label= Last Cmd
        icon= noicon
        action= run_macro_string
        arg= <macrocode>
        wn= call("ij.Prefs.get", "sessionlog.name","");
        if((wn=="")||(!isOpen(wn))) exit("Please set a session log window first");
        if(!isOpen("Recorder")) exit ("Recorder not available");
        selectWindow("Recorder");
        cmds=split(getInfo("window.contents"),"\n");
        if(cmds.length==0) showStatus('No commands on recorder');
        else print("["+wn+"]", cmds[cmds.length-1]);
        if(nImages>0) selectWindow(getTitle));
</macrocode>
</line>

// end of file
```

D.3 *Rename and Save ROI Sets*

```
// Toolset to quickly draw, rename and save ROIs
// It was thought for analyses of brain autoradiograms which typically require (tedious) manual
// contouring of multiple ROIs.
//
// Please note these macros will only run once saved in the'/macros/toolsets/' directory as
// 'Rename and Save ROISets.txt'.
//
// Detailed information is available at:
// http://rsb.info.nih.gov/ij/macros/toolsets/Rename%20and%20Save%20ROI%20Sets.txt

// Global variables:
var install =checkInstallation();
var version =requires139l();
var labels =getLabelList();
var groups =getGroupList();
var suffixs =getSuffixList();
var yy =startManager();
var aCmds =newMenu("Group *1* labeling Menu Tool", labels);
var bCmds =newMenu("Group *2* labeling Menu Tool", labels);
var cCmds =newMenu("Group *3* labeling Menu Tool", labels);
var cCmds =newMenu("Add suffix Menu Tool", suffixs);
var dCmds =newMenu("Settings Menu Tool", newArray("Define labels","Define groups",
                   "Define suffix tags","Select ROIset directory","-","Invert gray values","Paste Control...",
                   "Set Measurements...","-","Delete all selections","-","Help...","Reset settings"));
var pmCmds =newMenu("Popup Menu", newArray("Rectangle [1]","Ellipse [2]","Brush [3]",
                   "Polygon [4]","Freehand [5]","Refine selection [6]","-","Contralateral in X [F1]",
                   "Contralateral in Y [F2]","Highlight drawn [F3]","-","Enlarge...","Rotate...","-",
                   "Fit Spline","Fit Ellipse","-","Restore Selection","Undo"));

// Menus and Tools:
macro "Unused Tool - " {}

macro "Settings Menu Tool - C037D3eD4eD5eD6bD6cD6dD7aD89D98Da7Db6Dc6Dd6De4De5C037D2aD5dDa2Dd5C037C037D5
9D68D69D77D78D86D87D96C037D1aD1bD1cD29D2bD39D49D4bD4cD4dD58D67D76D85D92D93D94Da1Db1Db2Db4Dc1Dc4Dd4De3C037
D5aD6aD79D88D95D97Da5Da6C037D19D91C037D4aD5bDa4Db5C037D3aD5cDa3Dc5" {
        cmd = getArgument();
        if(cmd=="Define labels") createNewLabelList();
        else
        if(cmd=="Define groups") createNewGroupList();
        else
        if(cmd=="Define suffix tags") createNewSuffixList();
        else
        if(cmd=="Select ROIset directory") {
        dir = getDirectory(" Select or create a ROIset directory");
        call("ij.Prefs.set", "renameroisets.dir", dir);
        showStatus("ROIset directory's patth saved in IJ preferences");}
        else
        if(cmd=="Delete all selections") {
        showMessageWithCancel("Confirm clean Manager", "Are you sure you want to
        delete all ROIs?");
        roiManager("reset");}
        else
        if(cmd=="Reset settings") {
        showMessageWithCancel("Confirm reset settings","This will reset all labels, groups and suffix-
        tags.\nYou might need this if for e.g.:\n \n1) You typed nothing in one of the dialog choices;
        \n\n2) You typed '|' (used to concatenate strings);\n\n3) The IJ Prefs file has been modified;");
        call("ij.Prefs.set", "renameroisets.labels", "nolabels");
        call("ij.Prefs.set", "renameroisets.groups", "nogroups");
        call("ij.Prefs.set", "renameroisets.suffixes", "nosuffixes");
        checkInstallation();
        reInstall(); }
        else
        if (cmd!="-") run(cmd);
}
macro "Group *1* labeling Menu Tool - C037D10D1aD20D21D22D23D24D25D26D27D28D29D2aD30D3a" {
        cmd = getArgument();
```

```
        i =roiManager("index");
        a=call("ij.plugin.frame.RoiManager.getName", i);
        if (roiManager("count")==0) exit("ROI Manager is empty.");
        else
        if (isKeyDown("shift")) roiManager("Rename", a+":"+cmd);
        else
        roiManager("Rename",i+":"+cmd+":"+groups[0]);
        MoveToNext();
}
macro "Group *2* labeling Menu Tool -C037D10D1aD20D21D22D23D24D25D26D27D28D29D2aD30D3aD50D5aD60D61D62D63D6
4D65D66D67D68D69D6aD70D7a" {
        cmd = getArgument();
        i =roiManager("index");
        a=call("ij.plugin.frame.RoiManager.getName", i);
        if (roiManager("count")==0) exit("ROI Manager is empty.");
        else
        if (isKeyDown("shift")) roiManager("Rename", a+":"+cmd);
        else
        roiManager("Rename",i+":"+cmd+":"+groups[1]);
        MoveToNext();
}
macro "Group *3* labeling Menu Tool - C037D10D1aD20D21D22D23D24D25D26D27D28D29D2aD30D3aD50D5aD60D61D62D63D
64D65D66D67D68D69D6aD70D7aD90D9aDa0Da1Da2Da3Da4Da5Da6Da7Da8Da9DaaDb0Dba" {
        cmd = getArgument();
        i =roiManager("index");
        a=call("ij.plugin.frame.RoiManager.getName", i);
        if (roiManager("count")==0) exit("ROI Manager is empty.");
        else
        if (isKeyDown("shift")) roiManager("Rename", a+":"+cmd);
        else
        roiManager("Rename",i+":"+cmd+":"+groups[2]);
        MoveToNext();
}
macro "Add suffix Menu Tool - C037D10D11D12D13D14D15D16D17D18D19D1aD20D2aD30D35D3aD45D65D75D95Da0Da5DaaDb0
DbaDc0Dc1Dc2Dc3Dc4Dc5Dc6Dc7Dc8Dc9Dca" {
        cmd = getArgument();
        i =roiManager("index");
        a=call("ij.plugin.frame.RoiManager.getName", i);
        if (roiManager("count")==0) exit("ROI Manager is empty.");
        else
        if (isKeyDown("shift")) roiManager("Rename",i+":"+cmd);
        else
        roiManager("Rename", a+":"+cmd);
        MoveToNext();
}
macro "Selection cycler [shift+click: previous] [alt+click: first] Action Tool - C037D13D14D15D16D17D18D1
9D1aD1bD1cD44D45D46D47D48D49D4aD4bD55D56D57D58D59D5aD66D67D68D69D77D78D97D98Da6Da7Da8Da9Db5Db6Db7Db8Db9DbaDc
4Dc5Dc6Dc7Dc8Dc9DcaDcbDf3Df4Df5Df6Df7Df8Df9DfaDfbDfc"{
        if (roiManager("count")<=1) showStatus("Requires at least 2 ROIs in Manager");
        else
        if (isKeyDown("shift")) MoveToPrevious();
        else
        if (isKeyDown("alt")) roiManager("select", 0);
        else
        MoveToNext();
}
macro "Save All Regions Action Tool - CfffCeeeCdddCcccCbbbCaaaC999C888C777C666C555C444C333C222C111C037D2
aD2bD2cD2dD2eD3eD4eD58D5eD68D69D6eD71D72D73D74D75D76D77D78D79D7aD7eD81D82D83D84D85D86D87D88D89D8aD8bD8eD91
D92D93D94D95D96D97D98D99D9aD9bD9eDa1Da2Da3Da4Da5Da6Da7Da8Da9DaaDaeDb8Db9DbeDc8DceDdeDeeDfaDfbDfcDfdDfe"{
        if (roiManager("count")==0) showStatus("ROI Manager is empty. No ROIs to save.");
        else
        if (nImages==0 && roiManager("count")!=0) showStatus("This tool requires an open image.");
        else {
        dir= call("ij.Prefs.get",        "renameroisets.dir", "nodir");
        if (dir=="nodir") {
        lb="Other location";
        foot2="The 'ROIset directory' has not been defined yet";}
        else
        if(!File.isDirectory(dir)) {
        lb="Other Location";
        foot2="The 'ROIset folder' could not been found.\nMake sure it has not been moved or deleted";}
```

```
            else {
            if(File.exists(dir+getTitle+"-ROIset.zip")) {
            lb="ROIset directory (overwrite)";
            foot2="A ROIset.zip file for this image has been found\nin the 'ROIset folder'";}
            else {
            lb="ROIset directory";
            foot2= "No ROIset.zip file for this image found\nin the 'ROIset folder'";}
            }
            if (getDirectory("image")==""){
            options=newArray("Other location","",lb);
            foot =getTitle+" is either on a remote server or\nit has not been saved yet..."; }
            else
            if (File.exists(getDirectory("image")+getTitle+"-ROIset.zip")) {
            options=newArray("Image folder (overwrite)","",lb,"Other location");
            foot ="A ["+getTitle+"-ROIset.zip] file already exists in\n"+getDirectory("image"); }
            else {
            foot ="No ROIset.zip file found for "+getTitle+" in\n"+
            getDirectory("image");
            options=newArray("Image folder","",lb,"Other location"); }

            Dialog.create("Saving all ROIs");
            Dialog.addMessage(foot);
            Dialog.addMessage("\n"+foot2);
            Dialog.addChoice("Save set in",options);
            Dialog.show();
            target = Dialog.getChoice();
            if (startsWith(target, âĂIJImage folder")) roiManager("save",getDirectory("image")+getTitle+
            âĂIJ−ROIset.zip");
            else
            if (startsWith(target, âĂIJROIset directory")) roiManager("save",dir+getTitle+"-ROIset.zip");
            else
            if (target=="Other location") roiManager("save", getDirectory("Select a Directory")+getTitle+
            âĂIJ−ROIset.zip");
            showStatus("All ROIs in Manager have been saved...");
            beep();
            }
}

// Pop-up Menu:
macro "Popup Menu" {
            cmd = getArgument();
            if (cmd=="Rotate...") { ROIconverter();run(cmd); }
            else
            run(cmd);
}

// Macros:
macro "Rectangle [1]" {setTool("rectangle");}

macro "Ellipse [2]" {setTool("elliptical");}

macro "Brush [3]" {setTool("brush");}

macro "Polygon [4]" {setTool("polygon");}

macro "Freehand [5]" {setTool("freehand");}

macro "Refine selection [6]" {
            if (nImages==0) showStatus("'Refine selection mode' requires an open image");
            else {
            setTool("brush");
            while (true) {
            getCursorLoc(x, y, z, flags);
            if (flags&16!=0) {restorePreviousTool; exit;}
                        }
            }
}
macro "Select next [n]" {MoveToNext();}

macro "Select previous [p]" {MoveToPrevious();}
```

```
210 macro "Change selection color [q]" {
          a= newArray("red","green","blue","magenta","cyan","yellow","orange","black","white");
          b= "Selection color is now ";
          c= call("ij.gui.Roi.getColor");
          if(c=='java.awt.Color[r=255,g=0,b=0]') {run("Colors...", "selection="+a[1]);
          showStatus(b+a[1]);}
          else
          if(c=='java.awt.Color[r=0,g=255,b=0]') {run("Colors...", "selection="+a[2]);
          showStatus(b+a[2]);}
          else
220       if(c=='java.awt.Color[r=0,g=0,b=255]') {run("Colors...", "selection="+a[3]);
          showStatus(b+a[3]);}
          else
          if(c=='java.awt.Color[r=255,g=0,b=255]') {run("Colors...", "selection="+a[4]);
          showStatus(b+a[4]);}
          else
          if(c=='java.awt.Color[r=0,g=255,b=255]') {run("Colors...", "selection="+a[5]);
          showStatus(b+a[5]);}
          else
          if(c=='java.awt.Color[r=255,g=255,b=0]') {run("Colors...", "selection="+a[6]);
230       showStatus(b+a[6]);}
          else
          if(c=='java.awt.Color[r=255,g=200,b=0]') {run("Colors...", "selection="+a[7]);
          showStatus(b+a[7]);}
          else
          if(c=='java.awt.Color[r=0,g=0,b=0]') {run("Colors...", "selection="+a[8]);
          showStatus(b+a[8]);}
          else
          if(c=='java.awt.Color[r=255,g=255,b=255]') {run("Colors...", "selection="+a[0]);
          showStatus(b+a[0]);}
240       else {
          run("Colors...", "selection="+a[0]); showStatus(b+a[0]); }
    }
    macro "Contralateral in X [F1]" {
          fx=-1; fy=1;
          mirrorROI();
    }
    macro "Contralateral in Y [F2]" {
          fx=1; fy=-1;
          mirrorROI();
250 }
    macro "Highlight drawn [F3]" {
          while (true) {
          getCursorLoc(x, y, z, flags);
          if (flags&16!=0) {setOption("Show All", false); exit;}
          setOption("Show All", true);}
    }
    macro "Invert gray values" {
          if (selectionType()!=-1) {
          ROIconverter(); s=selectionType(); getSelectionCoordinates(x,y); x2= x; y2=y; }
260       else {s="line"; x2= newArray(0,0); y2=newArray(0,0);}
          if(bitDepth!=24) {
          if(is("Inverting LUT")==1)
          showMessageWithCancel("Warning", âĂIJImage is already using an inverting LUT.\n
          Invert image nevertheless?");
          run("Select None"); run("Invert"); run("Invert LUT");}
          if(bitDepth==24) {
          showMessageWithCancel("Warning", getTitle+" is a RGB Image.\nConvert to 8-bit
          and invert?");
          run("8-bit"); run("Select None"); run("Invert"); run("Invert LUT");}
270       makeSelection(s, x2, y2);
    }
    macro "Help..." {
          msg="Settings:\n"+"labels, groups, suffix-tags and a target directory to save\n"+"ROIsets can
          be defined in the settings menu\n \n"+"Shortcuts:\n"+"[1;2;3;4;5] Area selection tools\n"+"[6]
          Refine mode\n"+"[t] Add to Manager (IJ)\n"+"[E] Restore selection (IJ)\n"+"[n] Next ROI\n"+
          "[p] Previous ROI\n"+"[q] Change selection color\n"+"[f1] Contralateral in X\n"+"[f2]
          Contralateral in Y\n"+"[f3] Highlight drawn\n"+"Right-click on image to access most of these
          commands\n \n"+"Modifiers:\nShift in labeling menus: Label as suffix\n"+"Shift in add suffix
          menu: Suffix as label\n"+"Shift in cycler tool: Previous ROI\n"+"Alt in cycler tool: First ROI\n
```

```
        \n"+"Tags are displayed on result tables only if 'Display label'\n"+"from 'Set Measurements...'
        has been chosen";
        msg2="Please check for updates at:\nhttp://rsb.info.nih.gov/ij/macros/toolsets/"
        msg3="Open the toolset file (contains further information)";

        Dialog.create("Toolset to speed-up ROI measurements");
        Dialog.addMessage(msg);
        Dialog.addCheckbox(msg3, false);
        Dialog.addMessage(msg2);
        Dialog.show();
        Opfile =Dialog.getCheckbox();
        TSpath =getDirectory("macros")+"/toolsets/Rename and Save ROI Sets.txt";
        if (Opfile) open(TSpath);
}

// Functions:
function requires139l() {
        requires("1.39l"); return 0;
}
function startManager() {
        if (!isOpen("ROI Manager")) run("ROI Manager...");
        selectWindow("ROI Manager");
        return 0;
}
function checkInstallation() {
        TSpath =getDirectory("macros")+"/toolsets/Rename and Save ROI Sets.txt";
        labels =call("ij.Prefs.get",          "renameroisets.labels", "nolabels");
        groups =call("ij.Prefs.get",          "renameroisets.groups", "nogroups");
        suffixs =call("ij.Prefs.get",          "renameroisets.suffixes", "nosuffixes");
        spacer="|";
        text="'Rename and Save ROI Sets.txt' could not be found at the\nImageJ/macros/toolset folder.\n
        This toolset must be saved in this directory with the above\nname or it will not install...";

        if (!File.exists(TSpath)) exit(text);
        else {
        if (labels=="nolabels") {
        labels="C.Cortex"+spacer+"E.Cortex"+spacer+"DG"+spacer+"CA3"+spacer+"CA1"+spacer+
        "Subiculum"+spacer+"Striatum"+spacer+"C.Callosum"+spacer+"Thalamus"+spacer+
        "Hypothalamus"+spacer+"Amigdala"+spacer+"Raphe"+spacer+"-"+spacer+"Background";
        call("ij.Prefs.set", "renameroisets.labels", labels);}
        if(groups=="nogroups") {
        groups="WT"+spacer+"Het"+spacer+"KO";
        call("ij.Prefs.set", "renameroisets.groups", groups);}
        if(suffixs=="nosuffixes") {
        suffixs="Left"+spacer+"Right"+spacer+"-"+spacer+"Anterior"+spacer+"Posterior"+spacer+
        "-"+spacer+"Ventral"+spacer+"Medial"+spacer+"Dorsal"+spacer+"Lateral"+spacer+"-"+spacer+
        "Coronal"+spacer+âĂIJSagittal"+spacer+"Horizontal";
        call("ij.Prefs.set", "renameroisets.suffixes", suffixs);}
        }
        return 0;
}
function getLabelList() {
        labels = call("ij.Prefs.get", "renameroisets.labels", "nolabels");
        spacer="|";
        if(labels=="nolabels") checkInstallation();
        else labels=split(labels,spacer);
        return labels;
}
function getGroupList() {
        groups = call("ij.Prefs.get", "renameroisets.groups", "nogroups");
        spacer="|";
        if(groups=="nogroups") checkInstallation();
        groups=split(groups,spacer);
        return groups;
}
function getSuffixList() {
        suffixs = call("ij.Prefs.get", "renameroisets.suffixes", "nosuffixes");
        spacer="|";
        if(suffixs=="nosuffixes") checkInstallation();
        suffixs=split(suffixs,spacer);
```

```
350         return suffixs;
    }
    function createNewLabelList() {
         getLabelList();
         text="Fill in this list with the tags you will need to label\nyour selections.\nThese labels will
         be common to all groups.\n \n[shift+click] in any of the three labeling menus\nwill append
         these labels without the group−tag.\n \nLabels defined by one hyphen are ignored...";
         Dialog.create("Labels definition");
         Dialog.addMessage(text);
         Dialog.addString("Label 01",labels[0],15);Dialog.addString("Label 02",labels[1],15);
360      Dialog.addString("Label 03",labels[2],15);Dialog.addString("Label 04",labels[3],15);
         Dialog.addString("Label 05",labels[4],15);Dialog.addString("Label 06",labels[5],15);
         Dialog.addString("Label 07",labels[6],15);Dialog.addString("Label 08",labels[7],15);
         Dialog.addString("Label 09",labels[8],15);Dialog.addString("Label 10",labels[9],15);
         Dialog.addString("Label 11",labels[10],15);Dialog.addString("Label 12",labels[11],15);
         Dialog.addString("Label 13",labels[12],15);Dialog.addString("Label 14",labels[13],15);
         Dialog.show();
         spacer=""+"|";
         labels =""+Dialog.getString()+spacer+Dialog.getString()+spacer+Dialog.getString()+
         spacer+Dialog.getString()+spacer+Dialog.getString()+spacer+Dialog.getString()+spacer+
370      Dialog.getString()+spacer+Dialog.getString()+spacer+Dialog.getString()+spacer+
         Dialog.getString()+spacer+Dialog.getString()+spacer+Dialog.getString+spacer+
         Dialog.getString()+spacer+Dialog.getString();
         call("ij.Prefs.set", "renameroisets.labels", labels);
         showStatus("Labels saved in IJ.prefs file");
         reInstall();
    }
    function createNewGroupList() {
         getGroupList();
         text="These are your comparision/experimental groups.\nThese tags will be appended to
380      the labels previously\ndefined and assigned to the Labeling Menu Tools:";
         Dialog.create("Groups definition");
         Dialog.addMessage(text);
         Dialog.addString("Group *1* Labeling Menu",groups[0],14);
         Dialog.addString("Group *2* Labeling Menu",groups[1],14);
         Dialog.addString("Group *3* Labeling Menu",groups[2],14);
         Dialog.show();
         spacer=""+"|";
         groups =""+Dialog.getString()+spacer+Dialog.getString()+spacer+Dialog.getString();
         call("ij.Prefs.set", "renameroisets.groups", groups);
390      showStatus("Groups saved in IJ.prefs file");
         reInstall();
    }
    function createNewSuffixList() {
         getSuffixList();
         text="This list is installed under the [...] Menu.\n \nUse it to append extra notes to
         selections\n[simple click] or use [shift+click] to rename\nselections with these tags.
         \nLong strings may not display properly on the\nManager but will appear in the results
         table.";
         Dialog.create("Suffixes definition");
400      Dialog.addMessage(text);
         Dialog.addString("Suffix 01",suffixs[0],13); Dialog.addString("Suffix 02",suffixs[1],13);
         Dialog.addString("Suffix 03",suffixs[2],13); Dialog.addString("Suffix 04",suffixs[3],13);
         Dialog.addString("Suffix 05",suffixs[4],13); Dialog.addString("Suffix 06",suffixs[5],13);
         Dialog.addString("Suffix 07",suffixs[6],13); Dialog.addString("Suffix 08",suffixs[7],13);
         Dialog.addString("Suffix 09",suffixs[8],13); Dialog.addString("Suffix 10",suffixs[9],13);
         Dialog.addString("Suffix 11",suffixs[10],13); Dialog.addString("Suffix 12",suffixs[11],13);
         Dialog.addString("Suffix 13",suffixs[12],13); Dialog.addString("Suffix 14",suffixs[13],13);
         Dialog.show();
         spacer=""+"|";
410      suffixs =""+Dialog.getString()+spacer+Dialog.getString()+spacer+Dialog.getString()+
         spacer+Dialog.getString()+spacer+Dialog.getString()+spacer+Dialog.getString()+spacer+
         Dialog.getString()+spacer+Dialog.getString()+spacer+Dialog.getString()+spacer+
         Dialog.getString()+spacer+Dialog.getString()+spacer+Dialog.getString()+spacer+
         Dialog.getString()+spacer+Dialog.getString();
         call("ij.Prefs.set", "renameroisets.suffixes", suffixs);
         showStatus("Suffixes saved in IJ.prefs file");
         reInstall();
    }
    function reInstall(){
420      TSpath    =getDirectory("macros")+"/toolsets/Rename and Save ROI Sets.txt";
```

```
        text="'Rename and Save ROI Sets.txt' could not be found at the\nImageJ/macros/toolset
        folder.\nThis toolset must be saved in this directory with the above\nname or it will
        not install...";
        if (!File.exists(TSpath)) exit(text);
        else run("Install...", "install="+"["+TSpath+"]");
}
function ROIconverter() {
        run("Enlarge...", "enlarge=0");
}
function mirrorROI() {
        if (selectionType()==9) s="freehand"; else s=selectionType();
        ROIconverter();
        getSelectionBounds(x, y, width, height);
        originalX = x;
        originalY = y;
        getSelectionCoordinates(x,y);
        aX= newArray(x.length);
        aY= newArray(x.length);
        for (i=0; i<x.length; i++) {aX[i]= fx*x[i]; aY[i]= fy*y[i];}
        makeSelection(s, aX, aY);
        setSelectionLocation(originalX , originalY);
}
function MoveToNext() {
        n =roiManager("count");
        i =roiManager("index");
        if(n==i+1) roiManager("select", 0);
        else roiManager("select", i+1);
}
function MoveToPrevious() {
        n =roiManager("count");
        i =roiManager("index");
        if (i<=0) roiManager("select", n-1);
        else roiManager("select", i-1);
}

// end of file
```

D.4 *Toolset Creator*

```
/* Toolset Creator
 * http://rsb.info.nih.gov/ij/macros/toolsets/Toolset%20Creator.txt
 *
 * Makes tool sets of 'Menu Tools' listing commands of plugins subfolders
 *
 * The Menus will list all [".ijm",".js"] files (v1.41 and later) and [".class",".jar",
 * ".txt",".ijm",".js"] files that have at least one underscore in the filename);
 *
 * v .06
 *     Dropped support for macros subfolders listings (Wayne Rasband);
 *     With IJ 1.41n a macro moved to the plugins folder with the ".ijm" extension no longer
 *     requires a "_" in the name to be installed in the plugins menu.
 * v .05
 *     Added:      ijm and js support (Wayne Rasband);
 *     Added:      append Menus from different sources;
 * v .04
 *     Fixed:      macros subfolders not working properly;
 *     Added:      (macros): [List All], [Open/Install] with 'shift' and 'alt';
 * v .03
 *     Fixed:      cleaned code;
 *     Fixed:      subfolders containing hyphens;
 *     Added:      AutoRun;
 *     Added:      more icons choice;
 *     Added:      possibility for macros subfolders listing;
 *     Added:      acknowledge when no executable is found on subfolder;
 *
 * Icons based on other tools listed at http://rsb.info.nih.gov/ij/macros/tools/
 * or created with Jerome Mutterer's 'Image To Tool Icon' macro:
 * http://rsb.info.nih.gov/ij/macros/tools/Image_To_Tool_Icon.txt
 *
 */
var alphaindex= newArray("a","b","c","d","e","f","g","h");
var items= newArray(" -- None -- ","Bricks","Depth","Dump","Gear","Histogram","Hourglass","Image",
        "List (I)","List (II)","Measure","Movie","Reduce","Shuffle","Stacks","Tag","Tiles (filled)",
        "Tiles (frame)","Tool","Write");
var colors= newArray("Default","Black","Gray","Red","Green","Blue");
var icons= newArray("",
        "D00D03D06D09D0cD0fD10D13D16D19D1cD1fD20D21D22D23D26D27D28D29D2cD2dD2eD2fD30D33D36D39D3cD3
        fD40D43D46D49D4cD4fD50D53D54D55D56D59D5aD5bD5cD5fD60D63D66D69D6cD6fD70D73D76D79D7cD7fD80D8
        3D86D89D8cD8fD90D91D92D93D96D97D98D99D9cD9dD9eD9fDa0Da3Da6Da9Db0Db3Db6Db9Dc0Dc3Dc4Dc5Dc6Dc
        9DcaDcbDd0Dd3Dd6Dd9De0De3De6De9Df0Df3Df6Df9", // Bricks
        "D20D21D2bD2cD2dD30D3aD3dD40D49D4dD50D58D5dD60D67D6dD70D76D7dD80D85D8dD90D94D9dDa0Da3DadDb
        0Db1Db2DbcDbd", // Depth
        "D2aD2bD2cD2dD2eD3eD4eD58D5eD68D69D6eD71D72D73D74D75D76D77D78D79D7aD7eD81D82D83D84D85D86D8
        7D88D89D8aD8bD8eD91D92D93D94D95D96D97D98D99D9aD9bD9eDa1Da2Da3Da4Da5Da6Da7Da8Da9DaaDaeDb8Db
        9DbeDc8DceDdeDeeDfaDfbDfcDfdDfe", // Dump
        "D49D33D34D35D36D37D38D39D3aD43D44D45D46D47D48D4aD53D54D55D58D59D5aD63D64D69D6aD73D74D79D7
        aD83D84D85D89D8aD93D94D95D96D97D98D99D9aDa3Da5Da6Da7Da8Da9DaaD88Da4D26D62D6bDb6D27D72D7bDb
        7D16D61D6cDc6D23D2aD32D3bDa2DabDb3DbaD17D71D7cDc7CaaaD57D75D78D87CaaaD56D65D68D86CaaaCbbbC
        cccD24D29D42D4bD92D9bDb4Db9CcccD22D2bDb2CcccDbbCcccCdddCeeeD5bCeeeD25D28D52D82D8bDb5Db8Cee
        eCfffD0bD4cD77Db0Dc2DccDd7", // Gear
        "D1eD2dD1fD2eD3cD3dD4bD4cD5aD5bD6aD14D15D16D17D18D19D1aD1bD1cD1dD20D21D22D23D24D25D26D27D2
        8D29D2aD2bD2cD2fD33D34D35D36D37D38D39D3aD3bD3eD3fD47D48D49D4aD4dD4eD4fD5cD5dD5eD5fD6bD6cD6
        dD6eD6fD7dD7eD7fD8dD8eD8fD9dD9eD9fDaeDafDbeDbfDcfDdf", // Histogram
        "D10D1fD20D21D22D2dD2eD2fD30D33D3cD3fD40D44D4bD4fD50D55D5aD5fD60D66D67D68D69D6fD70D75D7aD7
        fD80D84D8bD8fD90D93D9cD9fDa0Da1Da2DadDaeDafDb0Dbf", // Hourglass
        "R01fbR2397", // Image
        "L00f0L03f3L06f6L09f9L0cfcL0fbf", // Continuous list
        "L00a0L03f3L06a6L09c9L0cfcL0fbf", // Indented list
        "L15f5L1519Lf5f9L8885L5855Lb8b5", // Measure
        "D00D01D02D03D04D05D06D07D08D09D0aD0bD0cD0dD0eD0fD12D17D1cD22D27D2cD30D31D32D33D34D35D36D3
        7D38D39D3aD3bD3cD3dD3eD3fD40D4bD50D5bD60D6bD70D7bD80D8bD90D9bDa0DabDb0Db1Db2Db3Db4Db5Db6Db
        7Db8Db9DbaDbbDbcDbdDbeDbfDc2Dc7DccDd2Dd7DdcDe0De1De2De3De4De5De6De7De8De9DeaDebDecDedDeeDe
        f", // Movie
        "D17D23D27D2bD33D34D37D3aD3bD40D41D42D43D44D45D47D49D4aD4bD4cD4dD4eD53D54D57D5aD5bD63D67D6
        bD77D83D87D8bD93D94D97D9aD9bDa0Da1Da2Da3Da4Da5Da7Da9DaaDabDacDadDaeDb3Db4Db7DbaDbbDc3Dc7Dc
        bDd7", // Reduce
```

```
            "D05D06D07D16D17D25D27D2aD34D3bD43D4cD52D5dD5fD6eD6fD7dD7eD7fD80D81D82D90D91Da0Da2DadDb3Db
            cDc4DcbDd5Dd8DdaDe8De9Df8Df9Dfa", // Shuffle
            "L00f0L01f1L04f4L05f5L08f8L09f9L0cbcL0dbd", // Stacks
            "D22D23D24D25D26D27D32D33D34D35D36D37D38D42D43D46D47D48D49D52D53D56D57D58D59D5aD62D63D64D6
            5D66D67D68D69D6aD6bD72D73D74D75D76D77D78D79D7aD7bD7cD83D84D85D86D87D88D89D8aD8bD8cD8dD94D9
            5D96D97D98D99D9aD9bD9cD9dD9eDa5Da6Da7Da8Da9DaaDabDacDadDaeDb6Db7Db8Db9DbaDbbDbcDbdDc7Dc8Dc
            9DcaDcbDccDd8Dd9DdaDdbDe9Dea", // Tag
            "F0077F9977F9077F0977", // Tiles (filled)
            "R0077R9077R9977R0977", // Tiles (frame)
            "D3eD4eD5eD6bD6cD6dD7aD89D98Da7Db6Dc6Dd6De4De5D2aD5dDa2Dd5D59D68D69D77D78D86D87D96D1aD1bD1
            cD29D2bD39D49D4bD4cD4dD58D67D76D85D92D93D94Da1Db1Db2Db4Dc1Dc4Dd4De3D5aD6aD79D88D95D97Da5Da
            6D19D91D4aD5bDa4Db5D3aD5cDa3Dc5", // Tool
            "D1dD2aD2bD2cD37D38D39D3aD3bD3eD43D44D45D46D47D48D49D4aD4dD4eD53D54D55D56D57D58D59D5cD5dD6
            3D64D65D66D67D68D6bD6cD6dD73D74D75D76D77D7aD7bD7cD7dD84D85D86D87D89D8aD8bD8cD92D93D95D96D9
            7D98D99D9aD9bD9cDa1Da2Da3Da4Da6Da7Da8Da9DaaDabDacDb2Db3Db4Db5Db7Db8Db9DbaDbbDbcDc3Dc4Dc5Dc
            6Dc8Dc9DcaDcbDccDd4Dd5Dd6De5De6" // Write
            );

showMessage("Toolset Creator...", "This macro must be installed before running.\n \n"+
              "For convenience, copy this file into the /macros/toolsets/ folder\n"+
              "and it will be accessible through the '>>' drop down menu.");

macro "Toolset Creator" {
     Dialog.create("Toolset Creator...");
     Dialog.addString("Toolset name (without extension)","",20);
     Dialog.addNumber("Containing how many tools? (1-7)",2);
     Dialog.show;
          n= Dialog.getNumber;
          name= Dialog.getString;
          parent= Dialog.getChoice;
     if(n<1||n>7) exit("The number of tools must be between 1 and 7");
     if(name==""||name==" ") showMessageWithCancel("Toolset Creator...",
                                  "Proceed without a name?\nThis file may not be recognized by your OS.");
          folders=listDirs(getDirectory("plugins"));
          path= getDirectory("macros");
     if(path=="") exit("could not find macros folder");
          path= getDirectory("macros")+"toolsets"+File.separator;
     if(!File.exists(path)) {File.makeDirectory(path); showStatus("Toolset folder created");}
          path= getDirectory("macros")+"toolsets"+File.separator+name+".txt";
     if(File.exists(path)) showMessageWithCancel("Toolset Creator",
                                "A file named "+name+".txt already exists.\nOverwrite?");
          f= File.open(path);
     printHeader();
     for (i=1; i<n+1; i++) promptForSettings();
     printFoot();
     print("Toolset '"+name+"' created");
     print("You can now install it by using the '>>' drop down menu");
     print("To edit list filters hold down 'shift' while clicking the menu");
     if(getVersion>='1.41l') run("Update Menus");
}

macro "AutoRun"{
     wait(10);
     run("Toolset Creator");
}

// Functions:
function listDirs(dir) {
     if (dir=="") exit ("Unable to find the"+dir+"directory");
          list= newArray("No subfolders found");
     if (!File.exists(dir)) return list;
          rawlist= getFileList(dir);
     if (rawlist.length==0) return list;
          count= 0;
     for (i=0; i< rawlist.length; i++) if (endsWith(rawlist[i], File.separator)) count++;
     if (count==0) return list;
          list= newArray(count); index =0;
     for (i=0; i< rawlist.length; i++) {
     if (endsWith(rawlist[i], File.separator))
          list[index++] = substring(rawlist[i], 0, lengthOf(rawlist[i])-1);
     }
```

```
    return list;
}
function printHeader() {
    getDateAndTime(year, month, week, day, hour, min, sec, msec);
    print(f,"/* File generated with the 'Toolset Creator' macro");
    print(f," * ");
    print(f," * Filename: '"+name+".txt'");
    print(f," * Created: "+year+"."+month+"."+day+" "+hour+":"+min+":"+sec);
    print(f," * ");
    print(f," * Edit the two lines below '// Settings:' to change which files");
    print(f," * should be listed (e.g. you can exclude .jar files implementing");
    print(f," * multiple commands via a plugins.config file)");
    print(f," * ");
    print(f," * For '.ijm' and '.js' files use key modifiers while selecting an");
    print(f," * item from the list: 'shift': opens the macro file;");
    print(f," * 'alt': installs the macro;");
    print(f," */");
    print(f,"");
    print(f,"// Settings:");
    print(f,"var AllowedFileExtensions= newArray('class','txt','ijm','jar','js');");
    print(f,"var IgnoreFilenamesContaining= newArray('$','//','//','//');");
    print(f,"");
    print(f,"");
    print(f,"// Macros:");
    print(f," macro 'Unused Tool -' {}");
    print(f,"");
}
function promptForSettings() {
    Dialog.create("Toolset Creator... Slot "+i+" of "+n);
    Dialog.addChoice("Folder to list",folders);
    Dialog.addChoice("Icon drawing",items,"- None -");
    Dialog.addChoice("Icon color",colors,"Gray")
    Dialog.addString("Icon text","(2-chr max.)",11);
    Dialog.addChoice("Text color",colors,"Default")
    Dialog.show();
        folder= Dialog.getChoice;
        idraw= Dialog.getChoice;
        idrawC= Dialog.getChoice;
        itext= Dialog.getString;
        itextC= Dialog.getChoice;
        j= alphaindex[i-1];
        idrawC= colorConverter(idrawC);
        itextC= colorConverter(itextC);
        icon= makeIcon(idraw, idrawC, itext,itextC);
        mcrname= replace(folder, "-", "");
    print(f,"  var "+j+"List= getPluginList('"+folder+"');");
    print(f,"  var "+j+"Cmds= newMenu('"+mcrname+" Menu Tool',"+j+"List);");
    print(f," macro '"+mcrname+" Menu Tool - "+icon+"' {");
    print(f,"  cmd = getArgument();");
    print(f,"  if (cmd!='-') run(cmd);");
    print(f," }");
    print(f,"");
}
function printFoot() {
    print(f,"");
    print(f,"// Functions:");
    print(f,"function getPluginList(subfolder) {");
    print(f,"  dir= getDirectory('plugins')+subfolder+File.separator;");
    print(f,"  list= newArray(''+subfolder+' not found','in the plugins directory...');");
    print(f,"  if (!File.exists(dir)) return list;");
    print(f,"  rawlist= getFileList(dir);");
    print(f,"  count= 0;");
    print(f,"  for (i=0; i< rawlist.length; i++) {");
    print(f,"  isMacro= (getVersion>='1.41n')&&(endsWith(rawlist[i],'.ijm')||endsWith(rawlist[i],'.js'));");
    print(f,"  if (indexOf(rawlist[i], '_')==-1&&!isMacro) rawlist[i]='-';");
    print(f,"  for (h=0; h<IgnoreFilenamesContaining.length; h++)");
    print(f,"  if (indexOf(rawlist[i], IgnoreFilenamesContaining[h])!=-1) rawlist[i]='-';');
    print(f," rawlist[i]=replace(rawlist[i],'_',' ');");
    print(f," for (j=0; j<AllowedFileExtensions.length; j++)");
    print(f," if (endsWith(rawlist[i],AllowedFileExtensions[j]))count++;");
    print(f," }");
```

```
210       print(f," if(count==0) list=newArray('No executable found','on '+''+subfolder);");
          print(f," else");
          print(f," list= newArray(count);");
          print(f," index= 0;");
          print(f," for (i=0; i< rawlist.length; i++) {");
          print(f," for (h=0; h< AllowedFileExtensions.length; h++) {");
          print(f," cmdlength=lengthOf(rawlist[i])-lengthOf(AllowedFileExtensions[h])-1;");
          print(f," if (endsWith(rawlist[i], AllowedFileExtensions[h]))");
          print(f," list[index++] = substring(rawlist[i], 0, cmdlength);");
          print(f," }");
220       print(f," }");
          print(f," return list;");
          print(f,"    ");
      }
      function colorConverter(color) {
          if(color=="Default") color ="C037";
          else if(color=="Black") color ="C000";
          else if(color=="Gray") color ="C555";
          else if(color=="Red") color ="C900";
          else if(color=="Green") color ="C090";
230       else if(color=="Blue") color ="C009";
          return color;
       }
      function makeIcon(idraw, idrawC, itext,itextC) {
          for (i=0; i< items.length; i++) if(idraw ==items[i]) idraw =icons[i];
          if(startsWith(itext, "(2)")) itext="          ";
          if(lengthOf(itext)==1) itext=itext+" ";
              itext1= substring(itext, 0, 1);
              itext2= substring(itext, 1, 2);
              idrawC= colorConverter(idrawC);
240           itextC= colorConverter(itextC);
              finalicon=""+itextC+"T1d13"+""+itext1+"T9d13"+""+itext2+""+idrawC+""+idraw;
          return finalicon;
       }

      // end of file
```

Bibliography

[1] J. P. Aggleton, D. J. Sanderson, and J. M. Pearce. Structural learning and the hippocampus. *Hippocampus*, 17(9):723–734, 2007.

[2] F. J. Ahmad, J. Hughey, T. Wittmann, A. Hyman, M. Greaser, and P. W. Baas. Motor proteins regulate force interactions between microtubules and microfilaments in the axon. *Nat Cell Biol*, 2(5):276–280, 2000 May.

[3] P. Albert, Q. Zhou, H. Van Tol, J. Bunzow, and O. Civelli. Cloning, functional expression, and mRNA tissue distribution of the rat 5-hydroxytryptamine1a receptor gene. *J Biol Chem*, 265:5825–5832, 1990.

[4] P. R. Albert and M. Tiberi. Receptor signaling and structure: insights from serotonin-1 receptors. *Trends Endocrinol Metab*, 12(10):453–60, Nov 2001.

[5] J. M. Aletta and L. A. Greene. Growth cone configuration and advance: a time-lapse study using video-enhanced differential interference contrast microscopy. *J Neurosci*, 8(4):1425–1435, 1988 Apr.

[6] P. Alifragis, J. G. Parnavelas, and B. Nadarajah. A novel method of labeling and characterizing migrating neurons in the developing central nervous system. *Exp Neurol*, 174(2):259–265, 2002 Apr.

[7] D. G. Amaral and M. P. Witter. The three-dimensional organization of the hippocampal formation: a review of anatomical data. *Neuroscience*, 31(3):571–91, Jan 1989.

[8] American Psychiatric Association. *Diagnostic and Statistical Manual of Mental Disorders*. Washington DC, Fourth edition, 1994.

[9] P. Andersen, R. Morris, D. Amaral, and J. O'Keefe. *The Hippocampus Book*. ISBN-13: 978 0 19 510027 3. Oxford University Press, First edition, Jan 2007.

[10] E. Audero, E. Coppi, B. Mlinar, T. Rossetti, A. Caprioli, M. Banchaabouchi, R. Corradetti, and C. Gross. Sporadic Autonomic Dysregulation and Death Associated with Excessive Serotonin Autoinhibition. *Science*, 321(5885):130–133, Jul 2008.

[11] G. Banker and K. Goslin. *Culturing Nerve Cells*. ISBN-13: 978 0 26 202438 9. MIT Press, Second edition, Jan 1998.

[12] D. M. Bannerman, M. Grubb, R. M. J. Deacon, B. K. Yee, J. Feldon, and J. N. P. Rawlins. Ventral hippocampal lesions affect anxiety but not spatial learning. *Behav Brain Res*, 139(1-2):197–213, Mar 2003.

[13] D. M. Bannerman, J. N. P. Rawlins, S. B. McHugh, R. M. J. Deacon, B. K. Yee, T. Bast, W.-N. Zhang, H. H. J. Pothuizen, and J. Feldon. Regional dissociations within the hippocampus–memory and anxiety. *Neuroscience and biobehavioral reviews*, 28(3):273–83, Jul 2004.

[14] N. J. Bannister and A. U. Larkman. Dendritic morphology of CA1 pyramidal neurones from the rat hippocampus: I. Branching patterns. *J Comp Neurol*, 360(1):150–60, Sep 1995.

[15] N. J. Bannister and A. U. Larkman. Dendritic morphology of CA1 pyramidal neurones from the rat hippocampus: II. Spine distributions. *J Comp Neurol*, 360(1):161–71, Sep 1995.

[16] R. Bartesaghi and L. Ravasi. Pyramidal neuron types in field CA2 of the guinea pig. *Brain Res. Bull.*, 50(4):263–73, Nov 1999.

[17] G. J. Bashaw, H. Hu, C. D. Nobes, and C. S. Goodman. A novel Dbl family RhoGEF promotes Rho-dependent axon attraction to the central nervous system midline in Drosophila and overcomes Robo repulsion. *J Cell Biol*, 155(7):1117–22, Jan 2002.

[18] G. J. Bassell, H. Zhang, A. L. Byrd, A. M. Femino, R. H. Singer, K. L. Taneja, L. M. Lifshitz, I. M. Herman, and K. S. Kosik. Sorting of beta-actin mrna and protein to neurites and growth cones in culture. *J Neurosci*, 18(1):251–265, 1998 Jan 1.

[19] S. J. Baudouin, J. Angibaud, G. Loussouarn, V. Bonnamain, A. Matsuura, M. Kinebuchi, P. Naveilhan, and H. Boudin. The signaling adaptor protein CD3ζ is a negative regulator of dendrite development in young neurons. *Mol Biol Cell*, 19(6):2444–56, Jun 2008.

[20] J.-C. Béïque, B. Campbell, P. Perring, M. W. Hamblin, P. Walker, L. Mladenovic, and R. Andrade. Serotonergic regulation of membrane potential in developing rat prefrontal cortex: coordinated expression of 5-hydroxytryptamine (5-HT)1A, 5-HT2A, and 5-HT7 receptors. *J Neurosci*, 24(20):4807–17, May 2004.

[21] D. L. Benson, P. J. Isackson, C. M. Gall, and E. G. Jones. Contrasting patterns in the localization of glutamic acid decarboxylase and ca2+/calmodulin protein kinase gene expression in the rat central nervous system. *Neuroscience*, 46(4):825–849, 1992.

[22] D. L. Benson, F. H. Watkins, O. Steward, and G. Banker. Characterization of GABAergic neurons in hippocampal cell cultures. *J Neurocytol*, 23(5):279–95, May 1994.

[23] L. M. Boulanger. MHC class I in activity-dependent structural and functional plasticity. *Neuron Glia Biol*, 1(3):283–9, Aug 2004.

[24] L. M. Boulanger, G. S. Huh, and C. J. Shatz. Neuronal plasticity and cellular immunity: shared molecular mechanisms. *Curr Opin Neurobiol*, 11(5):568–78, Oct 2001.

[25] F. Bradke and C. G. Dotti. The role of local actin instability in axon formation. *Science*, 283(5409):1931–4, Mar 1999.

[26] D. Bray. Surface movements during the growth of single explanted neurons. *Proc Natl Acad Sci U S A*, 65(4):905–10, Apr 1970.

[27] J. D. Bremner. Structural changes in the brain in depression and relationship to symptom recurrence. *CNS Spectr*, 7(2):129–130, 2002 Feb.

[28] J. D. Bremner, A. Horti, L. H. Staib, Y. Zea-Ponce, R. Soufer, D. S. Charney, and R. Baldwin. Kinetic modeling of benzodiazepine receptor binding with pet and high specific activity [(11)c]iomazenil in healthy human subjects. *Synapse*, 35(1):68–77, 2000 Jan.

[29] R. E. Brown, H. M. Schellinck, and J. Jagosh. Behavioural studies of MHC-congenic mice. *Genetica*, 104(3):249–57, Jan 1998.

[30] S. Bruening, E. Oh, A. Hetzenauer, S. Escobar-Alvarez, R. I. Westphalen, H. C. Hemmings, N. Singewald, T. Shippenberg, and M. Toth. The anxiety-like phenotype of 5-HT receptor null mice is associated with genetic background-specific perturbations in the prefrontal cortex GABA-glutamate system. *J. Neurochem.*, 99(3):892–9, Nov 2006.

[31] B. Bryan, V. Kumar, L. J. Stafford, Y. Cai, G. Wu, and M. Liu. GEFT, a Rho family guanine nucleotide exchange factor, regulates neurite outgrowth and dendritic spine formation. *J Biol Chem*, 279(44):45824–32, Aug 2004.

[32] M. Bunsey and H. Eichenbaum. Selective damage to the hippocampal region blocks long-term retention of a natural and nonspatial stimulus-stimulus association. *Hippocampus*, 5(6):546–56, Jan 1995.

[33] A. Caceres, G. Banker, O. Steward, L. Binder, and M. Payne. Map2 is localized to the dendrites of hippocampal neurons which develop in culture. *Brain Res*, 315(2):314–318, 1984 Apr.

[34] A. Caceres, G. A. Banker, and L. Binder. Immunocytochemical localization of tubulin and microtubule-associated protein 2 during the development of hippocampal neurons in culture. *J Neurosci*, 6(3):714–722, 1986 Mar.

[35] X. Cai, Z. Gu, P. Zhong, Y. Ren, and Z. Yan. Serotonin 5-HT1A receptors regulate AMPA receptor channels through inhibiting Ca^{2+}/calmodulin-dependent kinase II in prefrontal cortical pyramidal neurons. *J Biol Chem*, 277(39):36553–62, Aug 2002.

[36] V. Carola, G. Frazzetto, and C. Gross. Identifying interactions between genes and early environment in the mouse. *Genes Brain Behav*, 5(2):189–99, Mar 2006.

[37] B. J. Claiborne, D. G. Amaral, and W. M. Cowan. Quantitative, three-dimensional analysis of granule cell dendrites in the rat dentate gyrus. *J Comp Neurol*, 302(2):206–19, Dec 1990.

[38] H. T. Cline. Dendritic arbor development and synaptogenesis. *Curr Opin Neurobiol*, 11(1):118–26, Feb 2001.

[39] R. A. Corriveau, G. S. Huh, and C. J. Shatz. Regulation of class I MHC gene expression in the developing and mature CNS by neural activity. *Neuron*, 21(3):505–20, Sep 1998.

[40] R. A. Corriveau, C. J. Shatz, and E. Nedivi. Dynamic regulation of cpg15 during activity-dependent synaptic development in the mammalian visual system. *J Neurosci*, 19(18):7999–8008, Sep 1999.

[41] P. B. Crino and J. Eberwine. Molecular characterization of the dendritic growth cone: regulated mRNA transport and local protein synthesis. *Neuron*, 17(6):1173–87, Dec 1996.

[42] A. Cumbo, P. Mittaud, J. Ackermann, F. Magara, R. Hen, and J. Hornung. Changes in the dendritic arborisation of CA1 pyramidal neurons in absence of 5-HT1A receptors during development affect a specific intrahippocampal circuit in the mature hippocampus. In *FENS Abstr.*, volume 4, 142.4, 2008.

[43] M. E. Dailey and S. J. Smith. The dynamics of dendritic structure in developing hippocampal slices. *J Neurosci*, 16(9):2983–94, May 1996.

[44] U. Dannlowski, P. Ohrmann, J. Bauer, H. Kugel, B. T. Baune, C. Hohoff, A. Kersting, V. Arolt, W. Heindel, J. Deckert, and T. Suslow. Serotonergic genes modulate amygdala activity in major depression. *Genes Brain Behav*, 6(7):672–676, 2007 Oct.

[45] R. W. Davenport, P. Dou, L. R. Mills, and S. B. Kater. Distinct calcium signaling within neuronal growth cones and filopodia. *J Neurobiol*, 31(1):1–15, Sep 1996.

[46] K. L. Davis, D. Charney, J. T. Coyle, C. B. Nemeroff, and A. C. of Neuropsychopharmacology. *Neuropsychopharmacology: The Fifth Generation of Progress*. ISBN-13: 978 0 78 172837 9. Lippincott Williams & Wilkins, Fifth edition, 2002.

[47] L. de Hoz, J. Knox, and R. G. M. Morris. Longitudinal axis of the hippocampus: both septal and temporal poles of the hippocampus support water maze spatial learning depending on the training protocol. *Hippocampus*, 13(5):587–603, 2003.

[48] M. De Vivo and S. Maayani. Characterization of the 5-hydroxytryptamine1a receptor-mediated inhibition of forskolin-stimulated adenylate cyclase activity in guinea pig and rat hippocampal membranes. *J Pharmacol Exp Ther*, 238(1):248–253, 1986 Jul.

[49] E. W. Dent and F. B. Gertler. Cytoskeletal dynamics and transport in growth cone motility and axon guidance. *Neuron*, 40(2):209–27, Oct 2003.

[50] E. W. Dent and K. Kalil. Axon branching requires interactions between dynamic microtubules and actin filaments. *J Neurosci*, 21(24):9757–9769, 2001 Dec 15.

[51] A. M. Depino and C. Gross. Simultaneous assessment of autonomic function and anxiety-related behavior in BALB/c and C57BL/6 mice. *Behav Brain Res*, 177(2):254–60, Feb 2007.

[52] J. Deuchars and A. M. Thomson. Ca1 pyramid-pyramid connections in rat hippocampus in vitro: dual intracellular recordings with biocytin filling. *Neuroscience*, 74(4):1009–18, Oct 1996.

[53] A. Diefenbach and D. H. Raulet. Innate immune recognition by stimulatory immunoreceptors. *Curr Opin Immunol*, 15(1):37–44, Feb 2003.

[54] T. J. Diefenbach, B. D. Sloley, and J. I. Goldberg. Neurite branch development of an identified serotonergic neuron from embryonic Helisoma: evidence for autoregulation by serotonin. *Dev Biol*, 167(1):282–93, Jan 1995.

[55] C. G. Dotti, C. A. Sullivan, and G. Banker. The establishment of polarity by hippocampal neurons in culture. *J Neurosci*, 8(4):1454–68, Apr 1988.

[56] R. M. Drenan, R. Nashmi, P. Imoukhuede, H. Just, S. McKinney, and H. A. Lester. Subcellular trafficking, pentameric assembly, and subunit stoichiometry of neuronal nicotinic acetylcholine receptors containing fluorescently labeled alpha6 and beta3 subunits. *Mol Pharmacol*, 73(1):27–41, 2008 Jan.

[57] M. U. Ehrengruber, K. Lundstrom, C. Schweitzer, C. Heuss, S. Schlesinger, and B. H. Gähwiler. Recombinant semliki forest virus and sindbis virus efficiently infect neurons in hippocampal slice cultures. *Proc Natl Acad Sci U S A*, 96(12):7041–6, Jun 1999.

[58] E. Engin and D. Treit. The role of hippocampus in anxiety: intracerebral infusion studies. *Behavioural pharmacology*, 18(5-6):365–74, Sep 2007.

[59] J. Eyer and A. Peterson. Neurofilament-deficient axons and perikaryal aggregates in viable transgenic mice expressing a neurofilament-beta-galactosidase fusion protein. *Neuron*, 12(2):389–405, 1994 Feb.

[60] G. Feng, R. H. Mellor, M. Bernstein, C. Keller-Peck, Q. T. Nguyen, M. Wallace, J. M. Nerbonne, J. W. Lichtman, and J. R. Sanes. Imaging neuronal subsets in transgenic mice expressing multiple spectral variants of GFP. *Neuron*, 28(1):41–51, Nov 2000.

[61] I. Feoktistov, A. E. Goldstein, and I. Biaggioni. Cyclic AMP and protein kinase A stimulate Cdc42: role of A(2) adenosine receptors in human mast cells. *Mol Pharmacol*, 58(5):903–910, 2000 Nov.

[62] T. L. Fletcher, P. D. Camilli, and G. Banker. Synaptogenesis in hippocampal cultures: evidence indicating that axons and dendrites become competent to form synapses at different stages of neuronal development. *J Neurosci*, 14(11 Pt 1):6695–706, Nov 1994.

[63] C. A. Fornal, W. J. Litto, C. W. Metzler, F. Marrosu, K. Tada, and B. L. Jacobs. Single-unit responses of serotonergic dorsal raphe neurons to 5-HT1A agonist and antagonist drug administration in behaving cats. *J. Pharmacol. Exp. Ther.*, 270(3):1345–58, Sep 1994.

[64] T. M. Freiman, K. Gimbel, J. Honegger, B. Volk, J. Zentner, M. Frotscher, and T. Deller. Anterograde tracing of human hippocampus in vitro-a neuroanatomical tract tracing technique for the analysis of local fiber tracts in human brain. *J. Neurosci. Methods*, 120(1):95–103, Oct 2002.

[65] T. F. Freund and G. Buzsáki. Interneurons of the hippocampus. *Hippocampus*, 6(4):347–470, Jan 1996.

[66] A. D. Fricker, C. Rios, L. A. Devi, and I. Gomes. Serotonin receptor activation leads to neurite outgrowth and neuronal survival. *Brain Res Mol Brain Res*, 138(2):228–35, Jun 2005.

[67] T. Fujioka, A. Fujioka, and R. S. Duman. Activation of cAMP signaling facilitates the morphological maturation of newborn neurons in adult hippocampus. *J Neurosci*, 24(2):319–328, 2004 Jan 14.

[68] B. G. Galef, S. W. Wigmore, and D. J. Kennett. A failure to find socially mediated taste aversion learning in Norway rats (R. norvegicus). *Journal of Comparative Psychology (Washington, DC : 1983)*, 97(4):358–63, Dec 1983.

[69] W. B. Gan, D. L. Bishop, S. G. Turney, and J. W. Lichtman. Vital imaging and ultrastructural analysis of individual axon terminals labeled by iontophoretic application of lipophilic dye. *J Neurosci Methods*, 93(1):13–20, 1999 Oct 30.

[70] W.-B. Gan, J. Grutzendler, W. T. Wong, R. O. Wong, and J. W. Lichtman. Multicolor "DiOlistic" labeling of the nervous system using lipophilic dye combinations. *Neuron*, 27(2):219–25, Sep 2000.

[71] B. K. Garvalov, K. C. Flynn, D. Neukirchen, L. Meyn, N. Teusch, X. Wu, C. Brakebusch, J. R. Bamburg, and F. Bradke. Cdc42 regulates cofilin during the establishment of neuronal polarity. *J Neurosci*, 27(48):13117–29, Nov 2007.

[72] P. Gaspar, O. Cases, and L. Maroteaux. The developmental role of serotonin: news from mouse molecular genetics. *Nat Rev Neurosci*, 4(12):1002–12, Nov 2003.

[73] B. Gaudillière, Y. Konishi, N. de la Iglesia, G. lan Yao, and A. Bonni. A CaMKII-NeuroD signaling pathway specifies dendritic morphogenesis. *Neuron*, 41(2):229–41, Jan 2004.

[74] M. W. Gilbertson, M. E. Shenton, A. Ciszewski, K. Kasai, N. B. Lasko, S. P. Orr, and R. K. Pitman. Smaller hippocampal volume predicts pathologic vulnerability to psychological trauma. *Nat Neurosci*, 5(11):1242–1247, 2002 Nov.

[75] P. Godement. Specific guidance and modulation of growth cone motility during in vivo development. *J Physiol Paris*, 88(4):259–264, 1994.

[76] D. J. Goldberg and D. W. Burmeister. Stages in axon formation: observations of growth of aplysia axons in culture using video-enhanced contrast-differential interference contrast microscopy. *J Cell Biol*, 103(5):1921–1931, 1986 Nov.

[77] C. Golgi, M. Bentivoglio, and L. Swanson. On the fine structure of the pes hippocampi major (with plates XIII–XXIII). 1886. *Brain Res. Bull.*, 54(5):461–83, Mar 2001.

[78] E.-E. Govek, S. E. Newey, and L. V. Aelst. The role of the Rho GTPases in neuronal development. *Genes Dev*, 19(1):1–49, Jan 2005.

[79] E.-E. Govek, S. E. Newey, C. J. Akerman, J. R. Cross, L. V. der Veken, and L. V. Aelst. The X-linked mental retardation protein oligophrenin-1 is required for dendritic spine morphogenesis. *Nat Neurosci*, 7(4):364–72, Mar 2004.

[80] J. A. Gray and N. McNaughton. *The Neuropsychology of Anxiety: An Enquiry Into the Functions of the Septo-Hippocampal System*. ISBN-13: 978 0 19 852271 3. Jan 2003.

[81] C. Gross and R. Hen. The developmental origins of anxiety. *Nat. Rev. Neurosci.*, 5(7):545–52, Jul 2004.

[82] C. Gross, L. Santarelli, D. Brunner, X. Zhuang, and R. Hen. Altered fear circuits in 5-HT(1A) receptor KO mice. *Biol Psychiatry*, 48(12):1157–63, Jan 2001.

[83] C. Gross, X. Zhuang, K. Stark, S. Ramboz, R. Oosting, L. Kirby, L. Santarelli, S. G. Beck, and R. Hen. Serotonin1A receptor acts during development to establish normal anxiety-like behaviour in the adult. *Nature*, 416(6879):396–400, Mar 2002.

[84] J. Grutzendler, J. Tsai, and W.-B. Gan. Rapid labeling of neuronal populations by ballistic delivery of fluorescent dyes. *Methods*, 30(1):79–85, Apr 2003.

[85] L. Gutknecht, J. Waider, S. Kraft, C. Kriegebaum, B. Holtmann, A. Reif, A. Schmitt, and K.-P. Lesch. Deficiency of brain 5-HT synthesis but serotonergic neuron formation in tph2 knockout mice. *Journal of neural transmission*, 115(8):1127–32, Aug 2008.

[86] N. Haddjeri, C. Faure, G. Lucas, O. Mnie-Filali, G. Chouvet, B. Astier, B. Renaud, P. Blier, and G. Debonnel. In-vivo modulation of central 5-hydroxytryptamine (5-HT1A) receptor-mediated responses by the cholinergic system. *Int J Neuropsychopharmacol*, 7(4):391–9, Dec 2004.

[87] M. C. Halloran and K. Kalil. Dynamic behaviors of growth cones extending in the corpus callosum of living cortical brain slices observed with video microscopy. *J Neurosci*, 14(4):2161–2177, 1994 Apr.

[88] R. M. Harris. Morphology of physiologically identified thalamocortical relay neurons in the rat ventrobasal thalamus. *J Comp Neurol*, 251(4):491–505, Sep 1986.

[89] P. G. Haydon, D. P. McCobb, and S. B. Kater. Serotonin selectively inhibits growth cone motility and synaptogenesis of specific identified neurons. *Science*, 226(4674):561–4, Nov 1984.

[90] P. G. Haydon, D. P. McCobb, and S. B. Kater. The regulation of neurite outgrowth, growth cone motility, and electrical synaptogenesis by serotonin. *J Neurobiol*, 18(2):197–215, Mar 1987.

[91] L. K. Heisler, H. M. Chu, T. J. Brennan, J. A. Danao, P. Bajwa, L. H. Parsons, and L. H. Tecott. Elevated anxiety and antidepressant-like responses in serotonin 5-HT1A receptor mutant mice. *Proc Natl Acad Sci U S A*, 95(25):15049–54, Dec 1998.

[92] E. Hirsch, M. Pozzato, A. Vercelli, L. Barberis, O. Azzolino, C. Russo, C. Vanni, L. Silengo, A. Eva, and F. Altruda. Defective dendrite elongation but normal fertility in mice lacking the Rho-like GTPase activator Dbl. *Mol Cell Biol*, 22(9):3140–8, Apr 2002.

[93] G. S. Huh, L. M. Boulanger, H. Du, P. A. Riquelme, T. M. Brotz, and C. J. Shatz. Functional requirement for class I MHC in CNS development and plasticity. *Science*, 290(5499):2155–9, Dec 2000.

[94] L. L. Iacono and C. Gross. α-Ca^{2+}/Calmodulin-Dependent Protein Kinase II Contributes to the Developmental Programming of Anxiety in Serotonin Receptor 1A Knock-Out Mice. *Journal of Neuroscience*, 28(24):6250, Jun 2008.

[95] M. Ibrahim, A. Si-Ammour, M. R. Celio, F. Mauch, and P. Menoud. Construction and application of a microprojectile system for the transfection of organotypic brain slices. *J. Neurosci. Methods*, 101(2):171–9, Sep 2000.

[96] N. Ishizuka, W. M. Cowan, and D. G. Amaral. A quantitative analysis of the dendritic organization of pyramidal cells in the rat hippocampus. *J Comp Neurol*, 362(1):17–45, Nov 1995.

[97] E. A. Jares-Erijman and T. M. Jovin. FRET imaging. *Nat Biotechnol*, 21(11):1387–95, Nov 2003.

[98] X. Jian, H. Hidaka, and J. T. Schmidt. Kinase requirement for retinal growth cone motility. *J. Neurobiol.*, 25(10):1310–28, Oct 1994.

[99] S. Jin and J. H. Exton. Activation of RhoA by association of Galpha(13) with Dbl. *Biochem Biophys Res Commun*, 277(3):718–21, Nov 2000.

[100] X. Jin, H. Hu, P. H. Mathers, and A. Agmon. Brain-derived neurotrophic factor mediates activity-dependent dendritic growth in nonpyramidal neocortical interneurons in developing organotypic cultures. *J Neurosci*, 23(13):5662–73, Jul 2003.

[101] J. Johansen, M. E. Halpern, and H. Keshishian. Axonal guidance and the development of muscle fiber-specific innervation in drosophila embryos. *J Neurosci*, 9(12):4318–4332, 1989 Dec.

[102] S. Kaech and G. Banker. Culturing hippocampal neurons. *Nature protocols*, 1(5):2406–15, Jan 2006.

[103] K. Kalil. Growth cone behaviors during axon guidance in the developing cerebral cortex. *Prog Brain Res*, 108:31–40, 1996.

[104] P. Kettunen, J. Demas, C. Lohmann, N. Kasthuri, Y. Gong, R. O. L. Wong, and W.-B. Gan. Imaging calcium dynamics in the nervous system by means of ballistic delivery of indicators. *J. Neurosci. Methods*, 119(1):37–43, Sep 2002.

[105] K. Kjelstrup, F. Tuvnes, H. Steffenach, R. Murison, E. Moser, and M. Moser. Reduced fear expression after lesions of the ventral hippocampus. *Proc Natl Acad Sci U S A*, 99:10825–10830, 2002.

[106] K. Klemenhagen, A. Cumbo, J. Gordon, C. Denny, J. Richardson-Jones, C. O'Carroll, R. Meylan, E. Pralong, J. Monckton, L. L. Iacono, E. M. Boggio, M. Giustetto, C. Gross, R. Hen, and J.-P. Hornung. Increased dendritic branching of CA1 pyramidal neurons in mice lacking the 5-HT1A receptor correlates with the developmental appearance of anxiety-like behavior. *submitted*, 2009.

[107] K. C. Klemenhagen, J. A. Gordon, D. J. David, R. Hen, and C. Gross. Increased fear response to contextual cues in mice lacking the 5-HT1A receptor. *Neuropsychopharmacology*, 31(1):101–11, May 2005.

[108] L. Klimaschewski, W. Nindl, M. Pimpl, P. Waltinger, and K. Pfaller. Biolistic transfection and morphological analysis of cultured sympathetic neurons. *J Neurosci Methods*, 113(1):63–71, Dec 2001.

[109] B. K. Kobilka, T. Frielle, S. Collins, T. Yang-Feng, T. S. Kobilka, U. Francke, R. J. Lefkowitz, and M. G. Caron. An intronless gene encoding a potential member of the family of receptors coupled to guanine nucleotide regulatory proteins. *Nature*, 329(6134):75–79, 1987 Sep 3-9.

[110] J. H. Kogan, P. W. Frankland, J. A. Blendy, J. Coblentz, Z. Marowitz, G. Schütz, and A. J. Silva. Spaced training induces normal long-term memory in CREB mutant mice. *Curr Biol*, 7(1):1–11, Jan 1997.

[111] M. Kondoh, T. Shiga, and N. Okado. Regulation of dendrite formation of Purkinje cells by serotonin through serotonin1A and serotonin2A receptors in culture. *Neurosci Res*, 48(1):101–9, Jan 2004.

[112] J. Leemhuis, S. Boutillier, H. Barth, T. J. Feuerstein, C. Brock, B. Nürnberg, K. Aktories, and D. K. Meyer. Rho GTPases and phosphoinositide 3-kinase organize formation of branched dendrites. *J Biol Chem*, 279(1):585–96, Oct 2003.

[113] T. Leinders-Zufall, P. Brennan, P. Widmayer, P. C. S, A. Maul-Pavicic, M. Jäger, X.-H. Li, H. Breer, F. Zufall, and T. Boehm. MHC class I peptides as chemosensory signals in the vomeronasal organ. *Science*, 306(5698):1033–7, Nov 2004.

[114] S. Lemonde, G. Turecki, D. Bakish, L. Du, P. D. Hrdina, C. D. Bown, A. Sequeira, N. Kushwaha, S. J. Morris, A. Basak, X.-M. Ou, and P. R. Albert. Impaired repression at a 5-hydroxytryptamine 1a receptor gene polymorphism associated with major depression and suicide. *J Neurosci*, 23(25):8788–8799, 2003 Sep 24.

[115] W. Lerchner, C. Xiao, R. Nashmi, E. M. Slimko, L. van Trigt, H. A. Lester, and D. J. Anderson. Reversible silencing of neuronal excitability in behaving mice by a genetically targeted, ivermectin-gated Cl- channel. *Neuron*, 54(1):35–49, Apr 2007.

[116] Z. Li, L. V. Aelst, and H. T. Cline. Rho GTPases regulate distinct aspects of dendritic arbor growth in Xenopus central neurons in vivo. *Nat Neurosci*, 3(3):217–25, Mar 2000.

[117] Z. Li, C. D. Aizenman, and H. T. Cline. Regulation of rho GTPases by crosstalk and neuronal activity in vivo. *Neuron*, 33(5):741–50, Mar 2002.

[118] J. W. Lichtman, J. Livet, and J. R. Sanes. A technicolour approach to the connectome. *Nat Rev Neurosci*, 9(6):417–22, Jun 2008.

[119] V. Lieske, C. A. Bennett-Clarke, and R. W. Rhoades. Effects of serotonin on neurite outgrowth from thalamic neurons in vitro. *Neuroscience*, 90(3):967–74, Apr 1999.

[120] W. Lin and B. G. Szaro. Neurofilaments help maintain normal morphologies and support elongation of neurites in xenopus laevis cultured embryonic spinal cord neurons. *J Neurosci*, 15(12):8331–8344, 1995 Dec.

[121] W. L. Liu, M. M. Behbehani, and M. T. Shipley. Intracellular filling in fixed brain slices using miniruby, a fluorescent biocytin compound. *Brain Res.*, 608(1):78–86, Apr 1993.

[122] J. Livet, T. A. Weissman, H. Kang, R. W. Draft, J. Lu, R. A. Bennis, J. R. Sanes, and J. W. Lichtman. Transgenic strategies for combinatorial expression of fluorescent proteins in the nervous system. *Nature*, 450(7166):56–62, Nov 2007.

[123] B. Lotto, L. Upton, D. J. Price, and P. Gaspar. Serotonin receptor activation enhances neurite outgrowth of thalamic neurones in rodents. *Neurosci Lett*, 269(2):87–90, Aug 1999.

[124] P. E. Love, E. W. Shores, M. D. Johnson, M. L. Tremblay, E. J. Lee, A. Grinberg, S. P. Huang, A. Singer, and H. Westphal. T cell development in mice that lack the zeta chain of the T cell antigen receptor complex. *Science*, 261(5123):918–21, Aug 1993.

[125] L. Luo. Rho GTPases in neuronal morphogenesis. *Nat Rev Neurosci*, 1(3):173–80, Mar 2001.

[126] L. Luo. Actin cytoskeleton regulation in neuronal morphogenesis and structural plasticity. *Annu Rev Cell Dev Biol*, 18:601–35, Jul 2002.

[127] L. Luo, T. Hensch, L. Ackerman, S. Barbel, L. Jan, and Y. Jan. Differential effects of the rac gtpase on purkinje cell axons and dendritic trunks and spines. *Nature*, 379:837–840, 1996.

[128] C. Lüscher, L. Y. Jan, M. Stoffel, R. C. Malenka, and R. A. Nicoll. G protein-coupled inwardly rectifying K+ channels (GIRKs) mediate postsynaptic but not presynaptic transmitter actions in hippocampal neurons. *Neuron*, 19(3):687–95, Oct 1997.

[129] X.-M. Ma, J. Huang, Y. Wang, B. A. Eipper, and R. E. Mains. Kalirin, a multifunctional Rho guanine nucleotide exchange factor, is necessary for maintenance of hippocampal pyramidal neuron dendrites and dendritic spines. *J Neurosci*, 23(33):10593–603, Nov 2003.

[130] X.-M. Ma, J.-P. Huang, B. A. Eipper, and R. E. Mains. Expression of Trio, a member of the Dbl family of Rho GEFs in the developing rat brain. *J Comp Neurol*, 482(4):333–48, Jan 2005.

[131] T. Maeshima, F. Shutoh, S. Hamada, K. Senzaki, K. Hamaguchi-Hamada, R. Ito, and N. Okado. Serotonin2a receptor-like immunoreac tivity in rat cerebellar purkinje cells. *Neurosci Lett*, 252:72–74, 1998.

[132] J. E. Malberg, A. J. Eisch, E. J. Nestler, and R. S. Duman. Chronic antidepressant treatment increases neurogenesis in adult rat hippocampus. *J Neurosci*, 20(24):9104–9110, 2000 Dec 15.

[133] K. F. Martin, I. Phillips, M. Hearson, M. R. Prow, and D. J. Heal. Characterization of 8-OH-DPAT-induced hypothermia in mice as a 5-HT1A autoreceptor response and its evaluation as a model to selectively identify antidepressants. *Br J Pharmacol*, 107(1):15–21, 1992 Sep.

[134] T. A. Mathews, D. E. Fedele, F. M. Coppelli, A. M. Avila, D. L. Murphy, and A. M. Andrews. Gene dose-dependent alterations in extraneuronal serotonin but not dopamine in mice with reduced serotonin transporter expression. *J Neurosci Methods*, 140(1-2):169–81, Dec 2004.

[135] M. Mayford, M. E. Bach, Y. Y. Huang, L. Wang, R. D. Hawkins, and E. R. Kandel. Control of memory formation through regulated expression of a camkii transgene. *Science*, 274(5293):1678–1683, 1996 Dec 6.

[136] D. P. McCobb, C. S. Cohan, J. A. Connor, and S. B. Kater. Interactive effects of serotonin and acetylcholine on neurite elongation. *Neuron*, 1(5):377–85, Jul 1988.

[137] N. McNaughton. Cognitive dysfunction resulting from hippocampal hyperactivity–a possible cause of anxiety disorder? *Pharmacol Biochem Behav*, 56(4):603–11, Apr 1997.

[138] S. J. McRobbie and P. C. Newell. Changes in actin associated with the cytoskeleton following chemotactic stimulation of dictyostelium discoideum. *Biochem Biophys Res Commun*, 115(1):351–9, Aug 1983.

[139] M. Megías, Z. Emri, T. F. Freund, and A. I. Gulyás. Total number and distribution of inhibitory and excitatory synapses on hippocampal ca1 pyramidal cells. *Neuroscience*, 102(3):527–40, Jan 2001.

[140] E. Meijering, M. Jacob, J.-C. F. Sarria, P. Steiner, H. Hirling, and M. Unser. Design and validation of a tool for neurite tracing and analysis in fluorescence microscopy images. *Cytometry Part A : the journal of the International Society for Analytical Cytology*, 58(2):167–76, Apr 2004.

[141] J. Menard and D. Treit. Effects of centrally administered anxiolytic compounds in animal models of anxiety. *Neurosci Biobehav Rev*, 23(4):591–613, 1999 Mar.

[142] A. Mestek, J. H. Hurley, L. S. Bye, A. D. Campbell, Y. Chen, M. Tian, J. Liu, H. Schulman, and L. Yu. The human mu opioid receptor: modulation of functional desensitization by calcium/calmodulin-dependent protein kinase and protein kinase C. *J Neurosci*, 15(3 Pt 2):2396–406, Mar 1995.

[143] A. Meyer-Lindenberg and C. F. Zink. Imaging genetics for neuropsychiatric disorders. *Child Adolesc Psychiatr Clin N Am*, 16(3):581–597, 2007 Jul.

[144] F. D. Miller and D. R. Kaplan. Signaling mechanisms underlying dendrite formation. *Curr Opin Neurobiol*, 13(3):391–8, Jul 2003.

[145] J. B. Mitchell, L. J. Iny, and M. J. Meaney. The role of serotonin in the development and environmental regulation of type ii corticosteroid receptor binding in rat hippocampus. *Brain Res Dev Brain Res*, 55(2):231–235, 1990 Sep 1.

[146] J. Monckton, C. Gross, and R. Hen. Electrophysiological correlates of anxiety in serotonin 1a receptor knockout mice. In *Soc Neurosci Abstr.*, volume 28:550.1, 2002.

[147] D. L. Moolman, O. V. Vitolo, J.-P. G. Vonsattel, and M. L. Shelanski. Dendrite and dendritic spine alterations in Alzheimer models. *J Neurocytol*, 33(3):377–87, May 2004.

[148] R. Nashmi, M. E. Dickinson, S. McKinney, M. Jareb, C. Labarca, S. E. Fraser, and H. A. Lester. Assembly of alpha4beta2 nicotinic acetylcholine receptors assessed with functional fluorescently labeled subunits: effects of localization, trafficking, and nicotine-induced upregulation in clonal mammalian cells and in cultured midbrain neurons. *J Neurosci*, 23(37):11554–11567, 2003 Dec 17.

[149] T. Naumann. Retrograde tracing with fluoro-gold: different methods of tracer detection at the ultrastructural level and neurodegenerative changes of back-filled neurons in long-term studies. *J. Neurosci. Methods*, 103(1):11–21, Nov 2000.

[150] T. Neumann-Haefelin, F. Bosse, C. Redecker, H. W. Muller, and O. W. Witte. Upregulation of (GABA)A-receptor alpha1- and alpha2-subunit mRNAs following ischemic cortical lesions in rats. *Brain Res*, 816(1):234–237, 1999 Jan 16.

[151] A. Neumeister, E. Bain, A. C. Nugent, R. E. Carson, O. Bonne, D. A. Luckenbaugh, W. Eckelman, P. Herscovitch, D. S. Charney, and W. C. Drevets. Reduced serotonin type 1a receptor binding in panic disorder. *J Neurosci*, 24(3):589–591, 2004 Jan 21.

[152] M. Nikolic. The role of Rho GTPases and associated kinases in regulating neurite outgrowth. *Int J Biochem Cell Biol*, 34(7):731–45, Apr 2002.

[153] J. O'Brien and S. C. R. Lummis. Biolistic and diolistic transfection: using the gene gun to deliver DNA and lipophilic dyes into mammalian cells. *Methods*, 33(2):121–5, May 2004.

[154] D. Y. Okuhara and S. G. Beck. 5-HT1A receptor linked to inward-rectifying potassium current in hippocampal CA3 pyramidal cells. *J Neurophysiol*, 71(6):2161–2167, 1994 Jun.

[155] W. M. Oldham and H. E. Hamm. Heterotrimeric g protein activation by g-protein-coupled receptors. *Nat Rev Mol Cell Biol*, 9(1):60–71, Jan 2008.

[156] A. L. R. Oliveira, S. Thams, O. Lidman, F. Piehl, T. Hökfelt, K. Kärre, H. Lindå, and S. Cullheim. A role for MHC class Imolecules in synaptic plasticity and regeneration of neurons after axotomy. *Proc Natl Acad Sci U S A*, 101(51):17843–8, Dec 2004.

[157] D. Pantaloni, C. L. Clainche, and M. F. Carlier. Mechanism of actin-based motility. *Science*, 292(5521):1502–6, May 2001.

[158] C. L. Parks, P. S. Robinson, E. Sibille, T. Shenk, and M. Toth. Increased anxiety of mice lacking the serotonin 1A receptor. *Proc Natl Acad Sci U S A*, 95(18):10734–9, Sep 1998.

[159] J. F. Pasternak and T. A. Woolsey. On the "selectivity" of the Golgi-Cox method. *J. Comp. Neurol.*, 160(3):307–12, Apr 1975.

[160] T. Pattij, L. Groenink, T. H. Hijzen, R. S. Oosting, R. A. A. Maes, J. van der Gugten, and B. Olivier. Autonomic changes associated with enhanced anxiety in 5-HT(1A) receptor knockout mice. *Neuropsychopharmacology*, 27(3):380–90, Sep 2002.

[161] T. Pattij, L. Groenink, R. S. Oosting, J. van der Gugten, R. A. A. Maes, and B. Olivier. GABA(A)-benzodiazepine receptor complex sensitivity in 5-HT(1A) receptor knockout mice on a 129/Sv background. *Eur. J. Pharmacol.*, 447(1):67–74, Jun 2002.

[162] N. J. Penington, J. S. Kelly, and A. P. Fox. Whole-cell recordings of inwardly rectifying k+ currents activated by 5-ht1a receptors on dorsal raphe neurones of the adult rat. *J Physiol*, 469:387–405, 1993 Sep.

[163] D. L. Pettit, T. Koothan, D. Liao, and R. Malinow. Vaccinia virus transfection of hippocampal slice neurons. *Neuron*, 14(4):685–8, Apr 1995.

[164] J. Pokorný and T. Yamamoto. Postnatal ontogenesis of hippocampal CA1 area in rats. I. Development of dendritic arborisation in pyramidal neurons. *Brain Res Bull*, 7(2):113–20, Aug 1981.

[165] J. Pokorný and T. Yamamoto. Postnatal ontogenesis of hippocampal CA1 area in rats. II. Development of ultrastructure in stratum lacunosum and moleculare. *Brain Res Bull*, 7(2):121–30, Aug 1981.

[166] E. Ponimaskin, T. Voyno-Yasenetskaya, D. W. Richter, M. Schachner, and A. Dityatev. Morphogenic signaling in neurons via neurotransmitter receptors and small GTPases. *Mol Neurobiol*, 35(3):278–87, Jun 2007.

[167] G. Prusky and T. Arjannikova. Intracellular filling and reconstruction of identified neurons in fixed rat brain slices. *Brain Res Brain Res Protoc*, 3(3):313–9, Jan 1999.

[168] L. Prut and C. Belzung. The open field as a paradigm to measure the effects of drugs on anxiety-like behaviors: a review. *Eur J Pharmacol*, 463(1-3):3–33, Feb 2003.

[169] D. Purves, R. D. Hadley, and J. T. Voyvodic. Dynamic changes in the dendritic geometry of individual neurons visualized over periods of up to three months in the superior cervical ganglion of living mice. *J Neurosci*, 6(4):1051–60, Apr 1986.

[170] S. Ramboz, R. Oosting, D. A. Amara, H. F. Kung, P. Blier, M. Mendelsohn, J. J. Mann, D. Brunner, and R. Hen. Serotonin receptor 1A knockout: an animal model of anxiety-related disorder. *Proc Natl Acad Sci U S A*, 95(24):14476–81, Nov 1998.

[171] E. Ramon-Moliner. *The Golgi-Cox technique. In: Contemporary Research Methods in Neuroanatomy*. Berlin: Springer Verlag, 1970.

[172] S. Ramón y Cajal. *Histology of the Nervous System of Man and Vertebrates* (trans. N. Swanson and L. W. Swanson). ISBN-13: 978 0 19 507401 7. Oxford University Press, 1995.

[173] W. Rasband. ImageJ. *http://rsb.info.nih.gov/ij/*, U. S. National Institutes of Health, Bethesda, Maryland, USA, 1997–2008.

[174] J. R. Raymond, Y. V. Mukhin, A. Gelasco, J. Turner, G. Collinsworth, T. W. Gettys, J. S. Grewal, and M. N. Garnovskaya. Multiplicity of mechanisms of serotonin receptor signal transduction. *Pharmacol Ther*, 92(2-3):179–212, Mar 2002.

[175] J. R. Raymond, Y. V. Mukhin, T. W. Gettys, and M. N. Garnovskaya. The recombinant 5-HT1A receptor: G protein coupling and signalling pathways. *Br J Pharmacol*, 127(8):1751–64, Sep 1999.

[176] L. Redmond, A. H. Kashani, and A. Ghosh. Calcium regulation of dendritic growth via CaM kinase IV and CREB-mediated transcription. *Neuron*, 34(6):999–1010, Jun 2002.

[177] M. Riad, S. Garcia, K. C. Watkins, N. Jodoin, E. Doucet, X. Langlois, S. el Mestikawy, M. Hamon, and L. Descarries. Somatodendritic localization of 5-HT1A and preterminal axonal localization of 5-HT1B serotonin receptors in adult rat brain. *J Comp Neurol*, 417(2):181–94, Feb 2000.

[178] J. F. Rivera, S. Ahmad, M. W. Quick, E. R. Liman, and D. B. Arnold. An evolutionarily conserved dileucine motif in Shal K+ channels mediates dendritic targeting. *Nat Neurosci*, 6(3):243–50, Feb 2003.

[179] M. W. Rochlin, M. E. Dailey, and P. C. Bridgman. Polymerizing microtubules activate site-directed F-actin assembly in nerve growth cones. *Mol Biol Cell*, 10(7):2309–27, Jul 1999.

[180] A. Rodriguez, D. Ehlenberger, K. Kelliher, M. Einstein, S. C. Henderson, J. H. Morrison, P. R. Hof, and S. L. Wearne. Automated reconstruction of three-dimensional neuronal morphology from laser scanning microscopy images. *Methods*, 30(1):94–105, Apr 2003.

[181] K. L. Rossman, C. J. Der, and J. Sondek. GEF means go: turning on RHO GTPases with guanine nucleotide-exchange factors. *Nat Rev Mol Cell Biol*, 6(2):167–80, Feb 2005.

[182] U. Rudolph and H. Möhler. Analysis of $GABA_A$ receptor function and dissection of the pharmacology of benzodiazepines and general anesthetics through mouse genetics. *Annu Rev Pharmacol Toxicol*, 44:475–98, Jan 2004.

[183] L. Santarelli, M. Saxe, C. Gross, A. Surget, F. Battaglia, S. Dulawa, N. V. Weisstaub, J. Lee, R. Duman, O. Arancio, C. Belzung, and R. Hen. Requirement of hippocampal neurogenesis for the behavioral effects of antidepressants. *Science*, 301(5634):805–9, Aug 2003.

[184] K. V. Savelieva, S. Zhao, V. M. Pogorelov, I. Rajan, Q. Yang, E. Cullinan, and T. H. Lanthorn. Genetic disruption of both tryptophan hydroxylase genes dramatically reduces serotonin and affects behavior in models sensitive to antidepressants. *PLoS ONE*, 3(10):e3301, Jan 2008.

[185] A. W. Schaefer, N. Kabir, and P. Forscher. Filopodia and actin arcs guide the assembly and transport of two populations of microtubules with unique dynamic parameters in neuronal growth cones. *J Cell Biol*, 158(1):139–52, Jul 2002.

[186] L. Schiapparelli, J. Del Rio, and D. Frechilla. Serotonin 5-HT receptor blockade enhances Ca^{2+}/calmodulin-dependent protein kinase II function and membrane expression of AMPA receptor subunits in the rat hippocampus: implications for memory formation. *J Neurochem*, 94(4):884–895, 2005 Aug.

[187] A. R. Schlessinger, W. M. Cowan, and L. W. Swanson. The time of origin of neurons in ammon's horn and the associated retrohippocampal fields. *Anat. Embryol.*, 154(2):153–73, Aug 1978.

[188] D. Schmitz, R. Empson, and U. Heinemann. Serotonin reduces inhibition via 5-HT1A receptors in area CA1 of rat hippocampal slices in vitro. *J Neurosci*, 15:7217–7225., 1995.

[189] D. Schmitz, R. M. Empson, and U. Heinemann. Serotonin and 8-OH-DPAT reduce excitatory transmission in rat hippocampal area CA1 via reduction in presumed presynaptic Ca^{2+} entry. *Brain Res.*, 701(1-2):249–54, Dec 1995.

[190] M. Segal. Serotonin attenuates a slow inhibitory postsynaptic potential in rat hippocampal neurons. *Neuroscience*, 36:631–641, 1990.

[191] M. Segal and M. J. Gutnick. Effects of serotonin on extracellular potassium concentration in the rat hippocampal slice. *Brain Res*, 195(2):389–401, 1980 Aug 18.

[192] N. Shahani, S. Subramaniam, T. Wolf, C. Tackenberg, and R. Brandt. Tau aggregation and progressive neuronal degeneration in the absence of changes in spine density and morphology after targeted expression of alzheimer's disease-relevant tau constructs in organotypic hippocampal slices. *J Neurosci*, 26(22):6103–14, May 2006.

[193] K. Shen, M. N. Teruel, K. Subramanian, and T. Meyer. CaMKIIbeta functions as an F-actin targeting module that localizes CaMKIIalpha/beta heterooligomers to dendritic spines. *Neuron*, 21(3):593–606, Oct 1998.

[194] D. A. Sholl. Dendritic organization in the neurons of the visual and motor cortices of the cat. *J Anat*, 87(4):387–406, Oct 1953.

[195] E. Sibille, C. Pavlides, D. Benke, and M. Toth. Genetic inactivation of the Serotonin(1A) receptor in mice results in downregulation of major GABA(A) receptor alpha subunits, reduction of GABA(A) receptor binding, and benzodiazepine-resistant anxiety. *J Neurosci*, 20(8):2758–65, Feb 2001.

[196] S. Signorini, Y. Liao, S. Duncan, L. Jan, and M. Stoffel. Normal cerebellar development but susceptibility to seizures in mice lacking G protein- coupled, inwardly rectifying K+ channel GIRK2. *Proc Natl Acad Sci USA*, 94:923—927, 1997.

[197] L. Sikich, J. M. Hickok, and R. D. Todd. 5-HT1A receptors control neurite branching during development. *Brain Res Dev Brain Res*, 56(2):269–74, Nov 1990.

[198] E. M. Slimko, S. McKinney, D. J. Anderson, N. Davidson, and H. A. Lester. Selective electrical silencing of mammalian neurons in vitro by the use of invertebrate ligand-gated chloride channels. *J Neurosci*, 22(17):7373–9, Sep 2002.

[199] F. Solomon and M. Magendantz. Cytochalasin separates microtubule disassembly from loss of asymmetric morphology. *J Cell Biol*, 89(1):157–161, 1981 Apr.

[200] J. C. Sørensen, N. Tønder, and J. Zimmer. Biocytin pellets: an alternative technique for massive anterograde labeling of neuronal pathways in vivo and in vitro. *Brain Res.*, 608(2):338–44, Apr 1993.

[201] L. Stanford and R. E. Brown. MHC-congenic mice (C57BL/6J and B6-H-2K) show differences in speed but not accuracy in learning the Hebb-Williams Maze. *Behav Brain Res*, 144(1-2):187–97, Sep 2003.

[202] A. Strobel, L. Gutknecht, C. Rothe, A. Reif, R. Mössner, Y. Zeng, B. Brocke, and K.-P. Lesch. Allelic variation in 5-HT1A receptor expression is associated with anxiety- and depression-related personality traits. *Journal of neural transmission*, 110(12):1445–53, Dec 2003.

[203] J. Syken and C. J. Shatz. Expression of T cell receptor beta locus in central nervous system neurons. *Proc Natl Acad Sci U S A*, 100(22):13048–53, Oct 2003.

[204] N. Tamamaki. Organization of the entorhinal projection to the rat dentate gyrus revealed by dil anterograde labeling. *Exp Brain Res*, 116(2):250–8, Sep 1997.

[205] R. Threadgill, K. Bobb, and A. Ghosh. Regulation of dendritic growth and remodeling by Rho, Rac, and Cdc42. *Neuron*, 19(3):625–34, Oct 1997.

[206] G. Tredici, A. D. Francesco, A. Miani, and G. Pizzini. Real complete three-dimensional reconstruction of Golgi-impregnated neurons by means of a confocal laser scanning microscope. *Neuroimage*, 1(2):87–93, Sep 1993.

[207] T. Tsetsenis, X. Ma, L. L. Iacono, S. G. Beck, and C. Gross. Suppression of conditioning to ambiguous cues by pharmacogenetic inhibition of the dentate gyrus. *Nat Neurosci*, Jun 2007.

[208] P. Wahle, T. Gorba, M. J. Wirth, and K. Obst-Pernberg. Specification of neuropeptide Y phenotype in visual cortical neurons by leukemia inhibitory factor. *Development*, 127(9):1943–51, May 2000.

[209] S. Weiss, M. Sebben, D. E. Kemp, and J. Bockaert. Serotonin 5-HT1 receptors mediate inhibition of cyclic AMP production in neurons. *Eur. J. Pharmacol.*, 120(2):227–30, Jan 1986.

[210] J. M. Welch, J. Lu, R. M. Rodriguiz, N. C. Trotta, J. Peca, J.-D. Ding, C. Feliciano, M. Chen, J. P. Adams, J. Luo, S. M. Dudek, R. J. Weinberg, N. Calakos, W. C. Wetsel, and G. Feng. Cortico-striatal synaptic defects and OCD-like behaviours in Sapap3-mutant mice. *Nature*, 448(7156):894–900, Aug 2007.

[211] E. A. Welnhofer, L. Zhao, and C. S. Cohan. Actin dynamics and organization during growth cone morphogenesis in Helisoma neurons. *Cell Motil Cytoskeleton*, 37(1):54–71, Jan 1997.

[212] B. Wilkinson, J. S. Downey, and C. E. Rudd. T-cell signalling and immune system disorders. *Expert reviews in molecular medicine*, 7(29):1–29, Dec 2005.

[213] D. Wilkinson. Multiple roles of EPH receptors and ephrin in neural development. *Nat. Rev. Neurosci.*, 2 (2001)(155–164.), 2001.

[214] G. Winocur. Anterograde and retrograde amnesia in rats with dorsal hippocampal or dorsomedial thalamic lesions. *Behav Brain Res*, 38(2):145–54, May 1990.

[215] M. J. Wirth, A. Brun, J. Grabert, S. Patz, and P. Wahle. Accelerated dendritic development of rat cortical pyramidal cells and interneurons after biolistic transfection with BDNF and NT4/5. *Development*, 130(23):5827–38, Oct 2003.

[216] W. T. Wong, B. E. Faulkner-Jones, J. R. Sanes, and R. O. Wong. Rapid dendritic remodeling in the developing retina: dependence on neurotransmission and reciprocal regulation by Rac and Rho. *J Neurosci*, 20(13):5024–36, Jun 2000.

[217] W. Woodson, L. Nitecka, and Y. Ben-Ari. Organization of the GABAergic system in the rat hippocampal formation: a quantitative immunocytochemical study. *J. Comp. Neurol.*, 280(2):254–71, Feb 1989.

[218] F. S. Wouters, P. J. Verveer, and P. I. Bastiaens. Imaging biochemistry inside cells. *Trends Cell Biol*, 11(5):203–11, Apr 2001.

[219] C.-C. Wu, F. Chawla, D. Games, R. E. Rydel, S. Freedman, D. Schenk, W. G. Young, J. H. Morrison, and F. E. Bloom. Selective vulnerability of dentate granule cells prior to amyloid deposition in PDAPP mice: digital morphometric analyses. *Proc Natl Acad Sci U S A*, 101(18):7141–6, May 2004.

[220] C.-C. Wu, J. F. Reilly, W. G. Young, J. H. Morrison, and F. E. Bloom. High-throughput morphometric analysis of individual neurons. *Cereb Cortex*, 14(5):543–54, Apr 2004.

[221] G. Y. Wu and H. T. Cline. Stabilization of dendritic arbor structure in vivo by CaMKII. *Science*, 279(5348):222–6, Jan 1998.

[222] J. L. Yakel, X. M. Shao, and M. B. Jackson. The selectivity of the channel coupled to the 5-HT3 receptor. *Brain Res*, 533(1):46–52, 1990 Nov 12.

[223] R. X. Yamada, N. Matsuki, and Y. Ikegaya. cAMP differentially regulates axonal and dendritic development of dentate granule cells. *J. Biol. Chem.*, 280(45):38020–8, Nov 2005.

[224] W. Yan, C. C. Wilson, and J. H. Haring. 5-HT1a receptors mediate the neurotrophic effect of serotonin on developing dentate granule cells. *Brain Res Dev Brain Res*, 98(2):185–90, Feb 1997.

[225] W. Yan, C. C. Wilson, and J. H. Haring. Effects of neonatal serotonin depletion on the development of rat dentate granule cells. *Brain Res Dev Brain Res*, 98(2):177–84, Feb 1997.

[226] M. Yoshizawa, M. Sone, N. Matsuo, T. Nagase, O. Ohara, Y.-i. Nabeshima, and M. Hoshino. Dynamic and coordinated expression profile of dbl-family guanine nucleotide exchange factors in the developing mouse brain. *Gene Expr Patterns*, 3(3):375–81, Jun 2003.

[227] X. Yu and R. C. Malenka. β-catenin is critical for dendritic morphogenesis. *Nat Neurosci*, 6(11):1169–77, Oct 2003.

[228] E. Y. Yuen, Q. Jiang, P. Chen, Z. Gu, J. Feng, and Z. Yan. Serotonin 5-HT1A receptors regulate NMDA receptor channels through a microtubule-dependent mechanism. *J Neurosci*, 25(23):5488–501, Jun 2005.

[229] Y. Zheng. Dbl family guanine nucleotide exchange factors. *Trends Biochem Sci*, 26(12):724–32, Dec 2001.

[230] F. Q. Zhou and C. S. Cohan. Growth cone collapse through coincident loss of actin bundles and leading edge actin without actin depolymerization. *J Cell Biol*, 153(5):1071–84, May 2001.

[231] K. Zito, G. Knott, G. M. G. Shepherd, S. Shenolikar, and K. Svoboda. Induction of spine growth and synapse formation by regulation of the spine actin cytoskeleton. *Neuron*, 44(2):321–34, Oct 2004.